

Republic of Iraq
Ministry of Higher Education
and scientific Research
Al-Nahrain University
College of Science
Department of Physics



Studying the Effects of He-Ne Laser Beam and Gamma Radiation on CR-39 Detectors Irradiated by α -particles Using Some Spectroscopy Techniques

A Thesis

Submitted to the College of Science/Al-Nahrain University as a partial fulfillment of the requirements for the Degree of Master of Science in Physics.

By

Mohammed Muhsen Neamah

B.Sc. Physics / College Science / Al-Nahrain University

Supervised by

Dr. Nada F. Tawfiq

(Prof.)

بِسْمِ اللَّهِ الرَّحْمَنِ الرَّحِيمِ

﴿ قَالُوا سُبْحَانَكَ لَا عِلْمَ لَنَا إِلَّا مَا

عَلَّمْتَنَا إِنَّكَ ^طأَنْتَ الْعَلِيمُ الْحَكِيمُ ﴿٣٢﴾ ﴿

صَدَقَ اللَّهُ الْعَظِيمُ

سورة البقرة : آية (٣٢)

Supervisor Certification

I, certify that this thesis entitled "Studying the effects of He-Ne laser beam and gamma radiation on CR-39 detectors irradiated by α -particles using some spectroscopy techniques " was prepared by "Mohammed Muhsen Neamah" under our supervision at the College of Science/Al-Nahrain University as a partial fulfillment of the requirements for the Degree of Master of Science in physics.

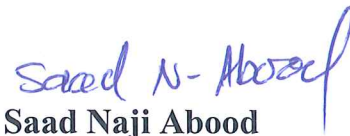
Signature: 

Name: **Dr. Nada F. Tawfiq**

Scientific Degree: Professor

Date: 5/4/2017

In view of the available recommendations, I forward this thesis for debate by the examining committee

Signature: 

Name: **Dr. Saad Naji Abood**

Scientific Degree: Professor

Title: Head of physics department

Date: 5/4/2017

Committee Certification

We, the examining committee certify that we have read this thesis entitled "Studying the effects of He-Ne laser beam and gamma radiation on CR-39 detectors irradiated by α -particles using some spectroscopy techniques" and examined the student "Mohammed Muhsen Neamah" in its contents and that in our opinion, it is accepted for the Degree of Master of Science in physics.

Signature: 

Name: **Dr. Khalid Hadi Mahdi**

Scientific Degree: Professor

Date: 6/4/2017

(Chairman)

Signature: 

Name: **Dr. Asia H. Al-Mashhadani**

Scientific Degree: Professor

Date: 6/4/2017

(Member)

Signature: 

Name: **Dr. Hussain Ali Al-Jobouri**

Scientific Degree: Assist Professor

Date: 5/4/2017

(Member)

Signature: 

Name: **Dr. Nada F. Tawfiq**

Scientific Degree: Professor

Date: 6/4/2017

(Member/ Supervised)

I, hereby certify upon the decision of the examining committee.

Signature:

Name: **Dr. Hadi M. A. Abood**

Scientific Degree: Professor

Title: Dean of College of Science

Date: / / 2017

Acknowledgement

Praise is to god “Allah” and peace and blessings on the Prophet Mohammed great of senders.

*I would like to express its sincere thanks and gratitude to my supervisor, **Prof. Dr. Nada F. Tawfiq** for proposed this project, encouragement, advice, valuable guidance in my research and insightful comments during the writing process.*

*And I wish to express my sincere thanks to the head of the physics department **Dr. Saad Naji abood** and dean of College of Sciences for their support to post graduate student.*

The nicest words of thanks express to my father, my mother, my brothers, my sisters, my best friends. Thanks to them for the incredible amount of patience that they have given me, especially throughout my thesis-writing period. I am deeply grateful to them.

Mohammed

Abstract

The aim of the present work was to study the effect of alpha-particles, gamma-rays and (He-Ne) laser beam on the track registration and optical properties of CR-39 detectors. Twenty-four detectors divided into five groups. First group: include nine detectors were exposed to different powers of (1, 5 and 10 mW) of laser beam at times (5, 10 and 15 min) and then irradiated to alpha-particles from ^{226}Ra source. Then it was measured following track parameters, track diameters-D, track density- ρ , and calculated the bulk etching rate- V_B , track etching rate- V_T , critical angle- Θ_c , etching efficiency- η , Sensitivity-S, etching ratio rate-V. The results show there was increased in the values of -D, ρ , V_B , V_T and Θ_c with increasing of the exposure times of laser beam at (1, 5 and 10 mW) powers, and decrease in the values of- η , S and V with increasing in the exposure time of laser beam at_1 mW power, while increasing within increase of exposed times of laser beam at (5 and 10 mW) powers. And found the appropriate etching time of CR-39 track detector at etching time of -4 h with NaOH etchant solution and-6.25 N at temperature 60 °C. Second group: includes un-irradiated detector as a control. Third group: include five detectors from CR-39 detector it was irradiated by gamma radiation from ^{60}Co source with doses (300, 500, 800, 1200 and 1600 kGy). Fourth group: include third groups where it was exposed to laser beam at 10 mW power for 15 min. Fifth group: include nine detectors were exposed to powers-1, 5 and 10 mW of laser beam at times (5, 10 and 15 min). The optical properties of detector were studied by using the UV-Vis. and FTIR spectroscopy. Where it was calculated the optical energy band gap and number of carbon atom to groups (Second, Third, Fourth and Fifth). The results of ultraviolet spectra show increasing in the absorbance-A of detector with increasing in the time exposure of laser beam at different powers and gamma doses, and also decreasing in the

optical energy band gap and increasing in the number of carbon atom with increasing in the exposure time of laser beam at different powers and gamma doses. As for the FTIR spectra show change in the peak position of the bands detector to groups (Third, Fourth and Fifth).

List of contents

Contents		
Abstract		II
List of contents		IV
List of figures		VIII
List of tables		XIII
List of symbols		XV
List of abbreviation		XVI
Chapter One “Introduction and Literature Review”		
1.1	Introduction	1
1.2	Types of radiation	2
1.2.1	Ionizing radiation	2
1.2.1.1	Gamma radiation	2
1.2.1.2	X-ray	3
1.2.1.3	Alpha particles	4
1.2.1.4	Beta particles	4
1.2.1.5	Neutron radiation	5
1.2.1.6	Ultraviolet radiation	5
1.2.2	Non-ionizing radiation	5
1.2.2.1	Radiowaves	6
1.2.2.2	Microwaves	6
1.2.2.3	Infrared	6
1.2.2.4	Visible light	7

1.2.2.5	Ultraviolet light	7
1.2.2.6	Laser	7
1.3	Literature review	8
1.4	Aim of project	15
Chapter Two “Theoretical part”		
2.1	Introduction	16
2.2	Historical review of solid state nuclear track detectors	16
2.3	Threshold of SSNTDs	17
2.4	Tracks formation in the SSNTDS	19
2.4.1	Tracks formation in inorganic materials	19
2.4.2	Tracks formation in organic materials	20
2.5	Types of SSNTDs	21
2.6	CR-39 track detectors	22
2.7	Chemical Etching	23
2.8	Track Affecting Parameters	24
2.8.1	Track Etch Rate- V_T	24
2.8.2	Bulk etch rate- V_B	25
2.9	Critical angle for etching- θ_c	26
2.10	Etching efficiency and sensitivity	28
2.11	Track etching geometry	29

2.12	Application of the SSNTDs	31
2.13	Analyses of UV-Vis spectra of SSNTDs	32
2.14	Measurement of energy gap	32
2.15	Number of carbon atoms measurement	33
2.16	Analyses of FTIR spectra of SSNTDs	34
Chapter three “Material and Method”		
3.1	Materials	36
3.1.1	CR-39 track detectors	36
3.1.2	Etchant solution	36
3.2	Irradiation sources	37
3.2.1	Gamma irradiation	37
3.2.2	Alpha irradiation	37
3.2.3	(He-Ne) laser beam	38
3.3	Materials analysis	38
3.3.1	FTIR-spectroscopy	38
3.3.2	UV-visible spectroscopy	39
3.4	Water Bath	40
3.5	Optical microscope	41
3.6	Methods	42
3.6.1	Sample irradiation	42

3.6.1.1	Gamma-ray irradiation	42
3.6.1.2	Alpha-particles irradiation	42
3.6.1.3	Laser exposure	43
Chapter Four “Results and discussion”		
4.1	Introduction	44
4.2	Effect of (He-Ne) laser and alpha-particles on CR-39 detectors	44
4.2.1	Track affect parameters measurement	44
4.3	Effect of (He-Ne) laser and Gamma-ray on CR-39 detectors	54
4.3.1	UV-Vis spectroscopy	54
4.3.2	Band gap energy measurement	58
4.3.4	FTIR spectroscopy	78
4.3.4.1	Effect of gamma radiation	79
4.3.4.2	Effect of (He-Ne) laser	83
4.3.4.2	Effect of gamma ray and (He-Ne) laser	92
4.4	Conclusion	96
4.5	Suggestion and future works	97
References		98

List of figures

Figure No.	Caption	Page No.
(1-1)	Illustration of the relative abilities of three different types of ionizing radiation to penetrate solid matter. Typical alpha particles (α) are stopped by a sheet of paper, while beta particles (β) are stopped by a plastic plate. Gamma radiation (γ) is dampened when it penetrates lead.	4
(2-1)	Primary ionization rate for various heavy ions versus particle velocity and track etch threshold for various materials [33].	18
(2-2)	Atomic character of a plastic track in a crystal [31].	19
(2-3)	Atomic character of a plastic track in polymer [31].	19
(2-4)	Molecular structure of CR-39 solid state nuclear track detector [10].	22
(2-5)	A track etching of a particle incident obliquely on the SSNTD: (a) track pit shape, its etching observed length and diameter depend on the two etch rates V_T and V_B (or their ratio V_T / V_B). (b) If the particle enters at very small angle from the surface such that the normal component of V_T is less than V_B , no etched track can be observed, as the surface is removed more rapidly than the track develops. (c) The critical value θ_c is obtained when the normal component $V_T \sin \theta$ is equal to $V_B = V_T \sin \theta_c$, $\theta_c = \sin^{-1} V_B / V_T$ [29, 30].	27
(2-6)	Track geometry for a particle penetrating a detector material normally [31,36].	30
(3 -1)	Gamma cell 900 system model by Bhabha Atomic Research Center-BHA, Trombay, Bombay, India.	37
(3-2)	CR-39 irradiated with (He-Ne) laser beam.	38

(3-3)	FTIR spectroscopy model Tensor 27 from Bruker company, Germany.	39
(3-4)	UV-Vis spectroscopy model SHIMADZU UV-1601PC UV-visible, Japan	40
(3-5)	Optical microscope	41
(4-1)	Diameter of track vs. Etching time for detector exposed to laser beam at 1 mW power, compared with irradiated with alpha particle detector.	45
(4-2)	Diameter of track vs. Etching time for detector exposed to laser beam at 5 mW power, compared with irradiated with alpha particle detector.	46
(4-3)	Diameter of track vs. Etching time for detector exposed to laser beam at 10 mW power, compared with irradiated with alpha particle detector.	46
(4-4)	Track density vs. Etching time for detector exposed to laser beam at 1 mW power, compared with irradiated with alpha particle detector.	47
(4-5)	Track density vs. Etching time for detector exposed to laser beam at 5 mW power, compared with irradiated with alpha particle detector.	47
(4-6)	Track density vs. Etching time for detector exposed to laser beam at 10 mW power, compared with irradiated with alpha particle detector.	48
(4-7)	Weight of detector vs. Etching time for detector exposed to laser beam at 1 mW power, compared with irradiated with alpha particle detector.	49
(4-8)	Weight of detector vs. Etching time for detector exposed to laser beam at 5 mW power, compared with irradiated with alpha particle detector.	49
(4-9)	Weight of detector vs. Etching time for detector exposed to laser beam at 10 mW power, compared with irradiated with	50

	alpha particle detector .	
(4-10)	Diameter etch rate vs. laser exposed time for detector exposed to laser beam at different powers.	51
(4-11)	Bulk etch rate vs. laser exposed time for detector exposed to laser beam at different powers.	52
(4-12)	Track etch rate vs. laser exposed time of He-Ne laser at different powers.	52
(4-13)	Etching rate ratio vs. laser exposed time for detector exposed to laser beam at different powers.	53
(4-14)	UV-Vis. at range (300-500 nm) for detector irradiated by laser beam at exposure times 5, 10 and 15 min at power 1 mW, comparted with un-irradiated detector control.	55
(4-15)	UV-Vis. at range (300-500 nm) for detector irradiated by laser beam at exposure times 5, 10 and 15 min at power 5 mW, comparted with un-irradiated detector control.	55
(4-16)	UV-Vis. at range (300-500 nm) for detector irradiated by laser beam at exposure times 5, 10 and 15 min at power 10 mW, comparted with un-irradiated detector control.	56
(4-17)	UV-Vis. at range (330-500 nm) for detector irradiated by gamma radiation at doses (300, 500, 800, 1200 and 1600 kGy), comparted with un-irradiated detector control.	57
(4-18)	UV-Vis. at range (330-500 nm) for detector irradiated with gamma ray for various dose (300, 500, 800, 1200 and 1600 kGy) then exposed for laser beam of 10 mW power at time 15 min, comparted with un-irradiated detector control.	58
(4-19)	Behavior of $(\alpha h\nu)^2$ and $(\alpha h\nu)^{0.5}$ vs. Photon energy ($h\nu$) for un-irradiated detector.	59

(4-20)	Behavior of $(\alpha hv)^2$ and $(\alpha hv)^{0.5}$ vs. photon energy (hv) for detector exposed to laser beam for 5 min at 1 mW power.	59
(4-21)	Behavior of $(\alpha hv)^2$ and $(\alpha hv)^{0.5}$ vs. photon energy (hv) for detector exposed to laser beam for 10 min at 1 mW power.	60
(4-22)	Behavior of $(\alpha hv)^2$ and $(\alpha hv)^{0.5}$ vs. photon energy (hv) for detector exposed to laser beam 15min at 1 mW power.	60
(4-23)	Behavior of $(\alpha hv)^2$ and $(\alpha hv)^{0.5}$ vs. photon energy (hv) for detector exposed to laser beam for 5 min at 5 mW power.	61
(4-24)	Behavior of $(\alpha hv)^2$ and $(\alpha hv)^{0.5}$ vs. photon energy (hv) for detector exposed to laser beam 10 min at 5 mW power.	61
(4-25)	Behavior of $(\alpha hv)^2$ and $(\alpha hv)^{0.5}$ vs. photon energy (hv) for detector exposed to laser beam 15 min at 5 mW power.	62
(4-26)	Behavior of $(\alpha hv)^2$ and $(\alpha hv)^{0.5}$ vs. photon energy (hv) for detector exposed to laser beam 5 min at 10 mW power.	62
(4-27)	Behavior of $(\alpha hv)^2$ and $(\alpha hv)^{0.5}$ vs. photon energy (hv) for detector exposed laser beam to 10 min at 10 mW power.	63
(4-28)	Behavior of $(\alpha hv)^2$ and $(\alpha hv)^{0.5}$ vs. photon energy (hv) for detector exposed to laser beam 15 min at 10 mW.	63
(4-29)	Behavior of $(\alpha hv)^2$ and $(\alpha hv)^{0.5}$ vs. photon energy (hv) for detector irradiated with gamma ray at 300 kGy dose.	64
(4-30)	Behavior of $(\alpha hv)^2$ and $(\alpha hv)^{0.5}$ vs. photon energy (hv) for detector irradiated with gamma ray at 500 kGy dose.	65
(4-31)	Behavior of $(\alpha hv)^2$ and $(\alpha hv)^{0.5}$ vs. photon energy (hv) for detector irradiated with gamma ray at 800 kGy dose.	65
(4-32)	Behavior of $(\alpha hv)^2$ and $(\alpha hv)^{0.5}$ vs. photon energy (hv) for detector irradiated with gamma ray at 1200 kGy dose.	66
(4-33)	Behavior of $(\alpha hv)^2$ and $(\alpha hv)^{0.5}$ vs. photon energy (hv) for detector irradiated with gamma ray at 1600 kGy dose.	66

(4-34)	Behavior of $(\alpha hv)^2$ and $(\alpha hv)^{0.5}$ vs. Photon energy (hv) for detector irradiated with gamma ray dose 300 kGy, then exposed to 15 min of laser beam at 10 mW power.	67
(4-35)	Behavior of $(\alpha hv)^2$ and $(\alpha hv)^{0.5}$ vs. Photon energy (hv) for detector irradiated with gamma ray dose 500 kGy, then exposed to 15 min of laser beam of 10 mW power.	68
(4-36)	Behavior of $(\alpha hv)^2$ and $(\alpha hv)^{0.5}$ vs. Photon energy (hv) for CR-39 detector irradiated with gamma ray dose 800 kGy and exposed to 15 min of laser beam of 10 mW power.	68
(4-37)	Behavior of $(\alpha hv)^2$ and $(\alpha hv)^{0.5}$ vs. Photon energy (hv) for detector irradiated with gamma ray dose 1200 kGy, then exposed to 15 min of laser beam of 10 mW power.	69
(4-38)	Behavior of $(\alpha hv)^2$ and $(\alpha hv)^{0.5}$ vs. Photon energy (hv) for detector irradiated with gamma ray dose 1600 kGy, then exposed to 15 min of laser beam of 10 mW power.	69
(4-39)	Indirect optical band gap energy vs. laser exposed time for detector exposed to laser beam at different powers.	70
(4-40)	Direct optical band gap energy vs. laser exposed time for detector exposed to laser beam at different powers.	70
(4-41)	Indirect optical band gap energy vs. dose of gamma ray for detector irradiated with various doses of gamma ray.	71
(4-42)	Direct optical band gap energy vs. dose of gamma ray for detector irradiated with various doses of gamma ray.	71
(4-43)	Indirect optical band gap energy vs. dose of gamma ray for detector irradiated with various doses of gamma ray, then exposed to laser beam for 15 min at 10 mW power.	72
(4-44)	Direct optical band gap energy vs. dose of gamma ray for detector irradiated with various doses of gamma ray, then exposed to laser beam for 15 min at 10 mW power.	72

(4-45)	Number of carbon atoms vs. laser exposed time for detector exposed to laser beam at different powers, for indirect transition.	73
(4-46)	Number of carbon atoms vs. laser exposed time for detector exposed to laser beam at different powers, for direct transition.	73
(4-47)	Number of carbon atoms vs. dose of gamma ray for detector irradiated with various doses of gamma ray, for indirect transition.	74
(4-48)	Number of carbon atoms vs. dose of gamma ray for detector irradiated with various doses of gamma ray, for direct transition.	74
(4-49)	Number of carbon atoms vs. dose of gamma ray for detector irradiated with various doses of gamma ray, then exposed to laser beam for 15 min at 10 mW power, for indirect transition.	75
(4-50)	Number of carbon atoms with dose of gamma ray and for detector irradiated with different doses of gamma ray, then exposed to laser beam for 15 min at 10 mW power, for direct transition.	75
(4-51)	FTIR spectra for detector un-irradiated (control).	78
(4-52)	FTIR spectra for detector un-irradiated and irradiated with various doses of gamma ray.	81
(4-53)	FTIR spectra at range (650-1250) for detector un-irradiated and irradiated with various doses of gamma ray.	82
(4-54)	FTIR spectra for detector un-irradiated and exposed to laser beam for different times at 1 mW power.	84
(4-55)	FTIR spectra at range (650-1250) for detector un-irradiated and exposed to laser beam for different times at 1 mW power.	85

(4-56)	FTIR spectra for detector un-irradiated and exposed to laser beam for different times at 5 mW power.	87
(4-57)	FTIR spectra at range (650-1250) for detector un-irradiated and exposed to laser beam for different times at 5 mW power.	88
(4-58)	FTIR spectra for detector un-irradiated and exposed to laser beam for different times at 10 mW power.	90
(4-59)	FTIR spectra at range (650-1250) for detector un-irradiated and exposed to laser beam for different times at 10 mW power.	91
(4-60)	FTIR spectra for detector un-irradiated and irradiated with various doses of gamma ray, then exposed to laser beam for 15 min at 10 mW power.	94
(4-61)	FTIR spectra at range (650-1250) for detector un-irradiated and irradiated with various doses of gamma ray, then exposed to laser beam for 15 min at 10 mW power.	95

List of tables

Table No.	Caption	Page No.
(2-1)	The wavenumbers of the more significant absorption peaks (transmission troughs) in the FTIR spectrum of CR-39 detector, and the corresponding assignment of the function groups and the modes of vibration [62].	35
(4-1)	Various track etching parameters for detector exposed to laser beam for (1, 5 and 10 mW) powers at different times.	55
(4-2)	Variations of the optical band gap energy and number of carbon atoms for detector un-irradiated and irradiated with various doses of gamma ray at range (300-1600 kGy).	77
(4-3)	Variations of the optical band gap energy and number of carbon atoms for detector irradiated with various doses of gamma ray, then exposed to laser beam for 15 min at 10 mW power.	78

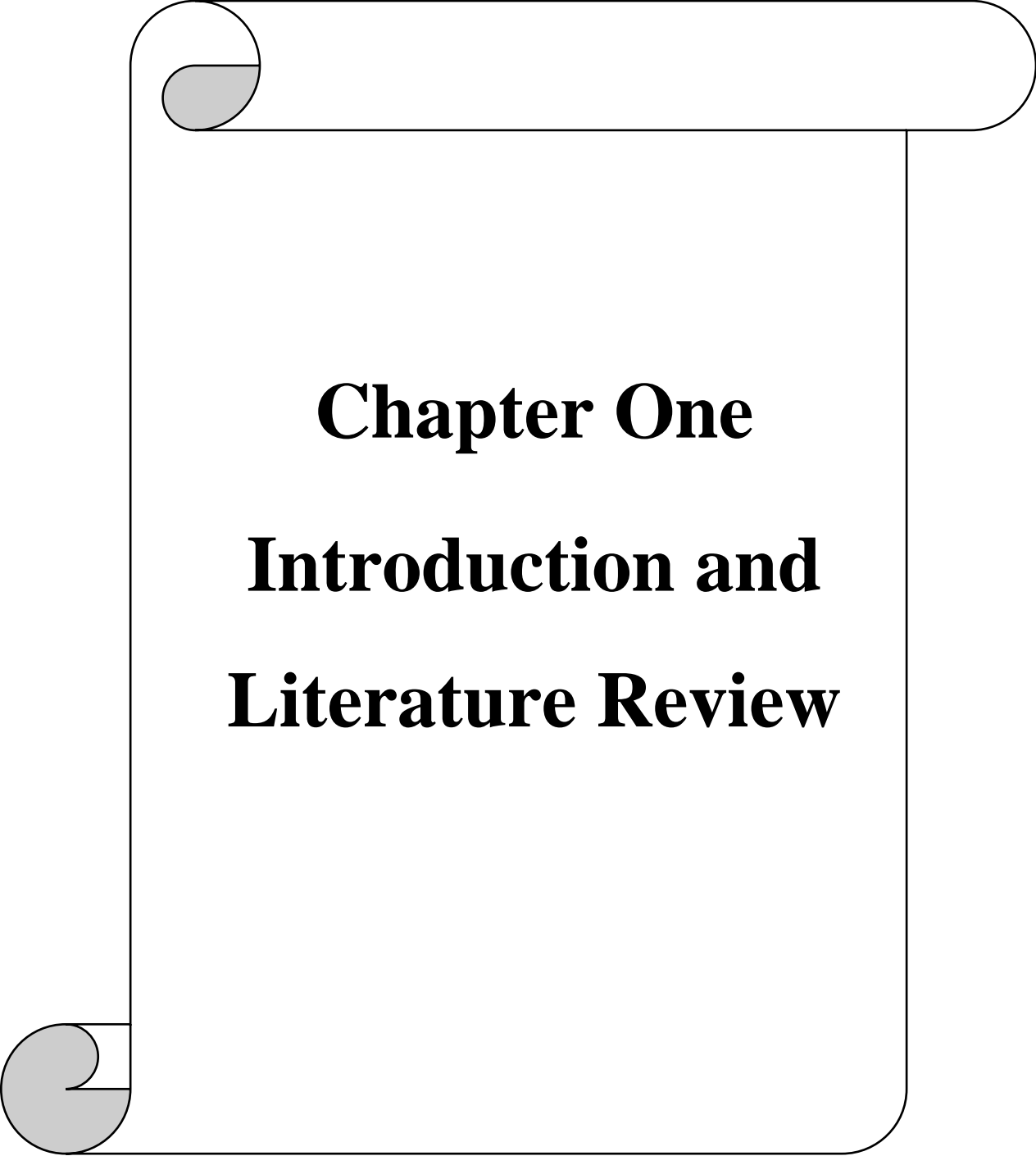
(4-4)	Variations of the optical band gap energy and number of carbon atoms for detector exposed to laser beam for 5, 10 and 15 min at different powers 1, 5 and 10 mW	78
(4-5)	Wavenumbers for detector un-irradiated and irradiated with various doses of gamma ray.	82
(4-6)	Wavenumbers for detector un-irradiated and exposed to laser beam for different times at 1 mW power.	85
(4-7)	Wavenumbers for detector un-irradiated and exposed to laser beam for different times at 5 mW power.	88
(4-8)	Wavenumbers for detector un-irradiated and exposed to laser beam for different times at 10 mW power.	91
(4-9)	Wavenumbers for detector un-irradiated and irradiated with various doses of gamma ray, then exposed to laser beam for 15 min at 10 mW power.	95

List of symbols

Symbol	Description
D	Track diameter.
ρ	Track Density.
L	Length of latent track.
N	Normality.
V_D	Diameter etch rate.
V_B	Bulk etch rate.
V_T	Track etch rate.
V	Etch rate ratio.
θ_C	Critical angle.
ϕ	Incident angle.
η	Etching efficiency.
S	Sensitivity.
μm	Micrometer.
λ	Wavelength.
A	Absorption.
α	Absorption coefficient.
E_g	Optical band gap energy.

List of abbreviations

Symbol	Description
He-Ne	Helium neon
NIR	Non ionizing radiation
SSNTDs	Solid State Nuclear Track Detectors.
TEM	Transmission Electron Microscopy.
LiF	Lithium fluoride.
HF	Hydrogen fluoride.
NaOH	Sodium Hydroxide.
UV-Vis	Ultraviolet-visible.
FTIR	Fourier transform infrared.
IAEA	International Atomic Energy Agency.
ICRP	International Commission of Radiation Protection.



Chapter One

Introduction and

Literature Review

Chapter One

Introduction and literature review

1.1 Introduction

Radiation is a fact of life. We live in a world in which radiation is naturally existing everywhere. Light and heat from nuclear reactions in the sun are necessary to our existence. Radioactive materials occur naturally throughout the environment, and our bodies contain radioactive materials such as carbon-14, potassium-40 and polonium-210 quite naturally. All life on Earth has evolved in the existence of this radiation. We can categorize radiation according to the effects it produces on matter, into ionizing and non-ionizing radiation. Ionizing radiation includes cosmic rays, X rays and the radiation from radioactive materials. Non-ionizing radiation includes ultraviolet light, radiant heat, radiowaves and microwaves [1]. Non-ionizing radiation is longer wavelength/lower frequency lower energy. While ionizing radiation is short wavelength/high frequency higher energy.

Both ionizing and non-ionizing radiation can be harmful effects to organisms and can result in changes to the natural environment. In general, however, ionizing radiation is more harmful to living organisms per unit of energy deposited than non-ionizing radiation, since the ions that are produced, even at low radiation powers, have the potential to cause DNA damage. By contrast, most non-ionizing radiation is harmful to organisms only in amount to the thermal energy deposited, and is conventionally considered harmless at low powers that do not produce a significant temperature increase. Ultraviolet radiation in some aspects occupies a middle ground, as it has some features of both ionizing and non-ionizing radiation [2].

1.2 Types of radiation

Most of the common types of radiation come from radioactive materials, but some types of radiation are produced in other ways. The most important example is that of x rays, therefore, comes from the metal atoms but, unlike radioactivity, it is not from the nucleus. Because of how they are produced, there is no half-life for an x ray, once the beam is switched off, the x rays disappear [1].

1.2.1 Ionizing radiation

Ionizing radiation is electromagnetic radiation that has sufficient energy to remove electrons from atoms. Ionization results in the production of negatively charged free electrons and positively charged ionized atoms. Ionizing radiation can be classified into two categories: photons (X-radiation and gamma radiation) and particles (alpha, beta particles and neutrons) [2].

1.2.1.1 Gamma radiation

Gamma radiation is a very high energy photon emitted from an unstable nucleus that is often emitting a beta particle at the same time. Gamma radiation causes ionization in atoms when it passes through matter, primarily due to interactions with electrons. It can be very penetrating and only a substantial thickness of dense materials such steel or lead can provide good shielding. Gamma radiation can therefore deliver significant doses to internal organs without inhalation or ingestion [3].

Gamma γ radiation consists of photons with a wavelength less than 3×10^{-11} m (greater than 10^{19} Hz and greater 100 keV) [4]. Gamma radiation emission is a nuclear process that occurs to rid the decaying nucleus of excess energy after it has emitted either alpha or beta radiation. Both alpha and beta particles have an electric charge and mass, and thus are quite likely to interact with other atoms in

their path. Gamma radiation, however, is composed of photons, which have neither mass nor electric charge and, as a result, penetrates much further through matter than either alpha or beta radiation [5].

1.2.1.2 X-ray

X-rays are electromagnetic waves with a wavelength less than about 10^{-9} m (3×10^{16} Hz up to the 3×10^{19} Hz Hz and 120 eV up to 100 keV). A smaller wavelength corresponds to a higher energy according to the equation [6]:

$$E = \frac{hc}{\lambda} \dots \dots \dots (1 - 1)$$

where:

E: Energy (J).

h: Planck's constant = 6.626×10^{-34} (J.s)

c: Speed of light = 299792458 (m/s)

λ : Wavelength (m)

A "packet" of electromagnetic waves is called a photon.

X-rays high-energy photons, like gamma radiation, and are produced artificially by the rapid slowing down of an electron beam. x rays are similarly penetrating and, in the absence of shielding by dense materials, can deliver significant doses to internal organs.

1.2.1.3 Alpha particles

Alpha-particles are a positively charged like helium nucleus ${}^4\text{He}$ (two protons and two neutrons) emitted by a larger unstable nucleus. It is a relatively massive particle, due to their relatively large mass and charge, they have an extremely limited ability to penetrate matter [4], it only has a short range in air (1–2 cm) and can be absorbed completely by paper or skin. Alpha radiation can, however, be hazardous if it enters the body by inhalation or ingestion, because large exposures can result in nearby tissues, such as the lining of the lung or stomach [1].

1.2.1.4 Beta particles

Beta-particles are an electron emitted by an unstable nucleus. Beta particles are much smaller than alpha particles and can penetrate further into materials or tissue. Beta particles can be absorbed completely by sheets of plastic, glass, or metal as shown in figure (1-1). It does not normally penetrate beyond the top layer of skin. However large exposures to high-energy beta emitters can cause skin burns. Such emitters can also be hazardous if inhaled or ingested [1].

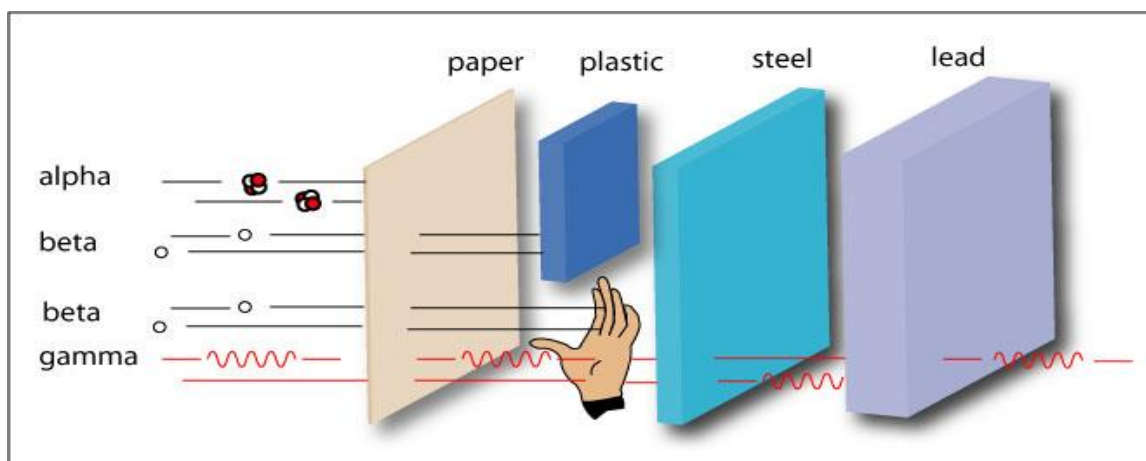


Figure (1-1) The relative abilities of three different types of ionizing radiation to penetrate solid matter. Typical alpha particles (α) are stopped by a sheet of paper, while beta particles (β) are stopped by a plastic plate. Gamma radiation (γ) is dampened when it penetrates lead [1].

1.2.1.5 Neutron radiation

Neutron is emitted by an unstable nucleus, in particular during atomic fission and nuclear fusion. Apart from a component in cosmic rays, neutrons are usually produced artificially. Because they are electrically neutral particles, neutrons can be very penetrating and when they interact with matter or tissue, they cause the emission of beta and gamma radiation [1].

1.2.1.6 Ultraviolet radiation

Ultraviolet of ionizing wavelengths from 200×10^{-9} m to 286×10^{-9} m ionizes air molecules, and this interaction causes it to be strongly absorbed by air. Ionizing UV therefore does not penetrate Earth's atmosphere to a significant degree, and is therefore sometimes referred to as vacuum ultraviolet [2].

1.2.2 Non-ionizing radiation

Non-Ionizing radiation NIR refers to radiative energy that, instead of producing charged ions when passing through matter, has sufficient energy only for excitation. Never the less it is known to cause biological effects. Non-ionizing radiations NIR encompass the long wavelength (> 100 nm), low photon energy (< 12.4 eV) portion of the electromagnetic spectrum, from 1 Hz to 3×10^{15} Hz. Except for the narrow visible region, NIR cannot be perceived by any of the human senses unless its intensity is so great that it is felt as heat. The ability of NIR to penetrate the human body, the sites of absorption, and the subsequent health effects are very much frequency dependent [2].

Non-Ionizing radiation originates from various sources: Natural origin (such as sunlight or lightning discharges etc.) and man-made (seen in wireless communications, industrial, scientific and medical applications). The NIR spectrum is divided into two main regions: optical radiations and electromagnetic radiation.

1.2.2.1 Radiowaves

Radiowaves are a type of electromagnetic radiation; radiowaves have the longest wavelengths in the EM spectrum, ranging from about 0.1 m to more than 10 m. They also have the lowest frequencies, from about 3×10^7 Hz up to about 3×10^9 Hz [2].

The best-known use of radiowaves is for communication; television, cellphones and radios all receive radiowaves and convert them to mechanical vibrations in the speaker to create sound waves that can be heard.

1.2.2.2 Microwaves

Microwaves are electromagnetic waves, as are radiowaves. Microwaves have frequencies ranging from about 3×10^9 Hz up to about 3×10^{11} Hz and wavelengths of about 10^{-3} m up to 0.1 m, although these values are not definitive. Microwaves have a range of applications, including communications, radar and, perhaps best known by most people, cooking [2].

1.2.2.3 Infrared

Infrared radiation IR is a type of electromagnetic radiation, as are radio waves, and microwaves. It is invisible to human eyes, but people can feel it as heat. IR radiation is one of the three ways heat is transferred from one place to another, the other two being convection and conduction. Everything with a temperature above about 5 degrees Kelvin emits IR radiation. The sun gives off half of its total energy as IR, and much of its visible light is absorbed and re-emitted as IR. It has frequencies from about 3×10^{11} Hz up to about 4×10^{14} Hz and wavelengths of about 700×10^{-9} m to 10^{-3} m [2].

1.2.2.4 Visible light

Light, or visible light, is a very narrow range of electromagnetic radiation of a wavelength that is visible to the human eye. It has wavelength from about 700×10^{-9} to 400×10^{-9} m, which equates to a frequency range of 4×10^{14} to 7×10^{14} Hz [2].

1.2.2.5 Ultraviolet light

As noted above, the lower part of the spectrum of ultraviolet, from 3 eV to about 10 eV. It has wavelength from about 10^{-8} to 700×10^{-9} m which equates to a frequency range of 10^{14} to 10^{16} Hz, is non-ionizing. However, the effects of non-ionizing ultraviolet on chemistry and the damage to biological systems exposed to it (including oxidation, mutation, and cancer) are such that even this part of ultraviolet is often compared with ionizing radiation [2].

1.2.2.6 Laser

Laser is an acronym for light amplification by stimulated emission of radiation. The term light is used in a broad sense to include radiation at frequencies in the infrared, visible or ultraviolet regions of the electromagnetic wave spectrum. In common parlance the term laser refers more to a device based on this principle than to the principle itself. The term laser action is often used when referring to the process. Lasers are different from the other light source they coherent light [7].

The physical principle (stimulated emission) responsible for laser action was introduced by Albert Einstein in 1916. A device called MASER (microwave amplification by stimulated emission of radiation) based on this principle was first operated in the microwave regime. The laser is an extension of this principle to the visible part of the electromagnetic spectrum [7].

Light produced from the lasers have several valuable characteristics not shown by light obtained from other conventional light sources, which make them suitable for a variety of scientific and technological applications. Their monochromaticity, directionality, laser line width, brightness, and coherence of laser light make them highly important for various materials processing and characterization applications. These properties are discussed separately in the following subsections [8].

Radiation from lasers is different from conventional optical light, like microwave radiation, because it is approximately monochromatic. Although each laser has its own fine spectral distribution and noise properties, the electric and magnetic fields from lasers are considered to have precise phase and amplitude variations in the first-order approximation [9].

Depending on the nature of the active media, lasers are classified into three main categories, (solid, liquid, and gas). Scientists and researchers have investigated a wide variety of laser materials as active media in each category since 1958, when lasing action was observed in ruby crystal. It is inconvenient to discuss all lasers having these materials as active media [8].

1.3 Literature review

Many studies have been found to study the effects of ionizing radiation and non-ionizing radiation track detectors using several techniques. Below we give a summary of some of these studies, according to the irradiation dose used and other types of radiation.

- Sinha et. al., (1997) [10] had studied the effect of gamma radiation in CR-39 detectors and studied in the dose range of 1 - 10⁶ Gy. Some of the properties like bulk-etch rate, track-etch rate, activation energy for bulk and track-etching have been found out for different gamma doses from ⁶⁰Co Source in CR-39.

- Sinha et. al., (2001) [11] used the Cr-39 detector that were exposed to different doses of gamma radiation ranging from 10 to 10^6 Gy from a ^{60}Co source. The effect of gamma doses on etch-rates were studied. Etch-rate values were found to increase at the dose of 10^6 Gy for all samples of Cr-39 detector. The influence of gamma exposure on sensitivity and etching efficiency of these detectors was also determined.
- Ahmed , (2006) [12] measured the energy gap of some glassy polymers –PC, PS and PMMA, he studied the effect of gamma-ray and UV light radiation on the energy gap of these polymers and then the effect of dyes (anthracene) on the energy gap for these materials for exposure times (0 to 34 h). He found that the energy gap of pure polymers and doped polymers measurement was changed depending on the gamma and UV dose and the mechanism of interaction between molecules of polymers and dye. It was found that the addition of anthracene to polymers leads to a reduction in the energy gap generally.
- Zaki (2008) [13], effect of gamma irradiation on optical absorption of nuclear track detectors like CR-39 was studied in different absorbed doses using ultraviolet-visible (UV-VIS) spectroscopy. The existence of the peaks, their shifting and broadening as a result of gamma irradiation has been discussed. The width of the tail of localized states in the band gap (E_u) was evaluate using the Urbach edge method. Finally, the indirect and direct band gap in pristine and gamma irradiated CR-39 have been determined. The values of indirectly band gap have been found to be lower than the corresponding values of direct band gap. A decrease in the optical energy gap with increasing the gamma absorbed dose can be discussed on the basis of gamma-irradiation-induced defects in the CR-39. The correlation between optical band gap and the number of carbon atoms in a cluster with modified Tauc's equation has been discussed in case of CR-39.

- Kalsi et. al., (2008) [14] determined the bulk-etch rates of a newly developed track detector called poly-[N-allyloxycarbonyl diethanolamine-bis allyl carbonate] (PNADAC) homopolymer at different temperatures to deduce its activation energy. The effects of gamma irradiation on this new detector in the dose range of 4.7–14.5 Mrad have also been studied using UV–Vis spectroscopic technique. The optical band gaps of the un-irradiated and the gamma-irradiated detectors determined from the UV–Vis spectra were found to decrease with the increase in gamma dose.
- Jyotsna et. al., (2009) [15] obtained the effects of gamma irradiation in the dose range of 1.0 – 20.0Mrad on the etching and optical characteristics of Tuffak polycarbonate ($C_{16}H_{14}O_3$)n nuclear track detector that have been studied by using etching and UV–Vis spectroscopic techniques. The result showed that bulk etch rates increase and the activation energies for bulk etching decrease with the increase in gamma dose. The optical band gaps determined from the UV–Vis spectra were found to decrease with the increase in gamma dose. These results have been explained on the basis of scission of the detector due to gamma irradiation.
- Amer, (2009) [16] works show, the effect of 514nm argon laser radiation on the alpha particles tracks diameters, tracks growth velocity and the tracks appearing time in LR-115 nuclear track detector has been studied. Increasing the exposure time of laser radiation were found to improve the above mentioned parameters up to 7min of exposure time, then it was decrease gradually with exposure time and become near data of standard sample of detector at 15 min.

- Mostafa (2011) [17], the optical properties of CR-39 polymer track detectors which irradiated by alpha particle at different energies and constant fluence were investigated. The optical properties were studied with ultraviolet-visible (UV-Vis.) spectroscopy. The track properties were verified using etching technique. Moreover, the optical energy band gap was calculated at different etching times (1.50, 3.00 and 6.00 h). The optical properties studies for the samples and track diameter measurements showed a fair agreement in which a scission occurred in CR-39 polymer chains etched at times 1.50 and 3.00 h when alpha particle irradiation 2.17 MeV. The etching time at 1.50 h was the optimum condition as a method to determine the alpha particle energies by the corresponding optical properties of CR-39.
- Kumara et. al., (2011) [18], the thermal behavior of pristine and γ -irradiated CR-39 polymer (up to a maximum dose of 1800 kGy) has been studied. The changes in degradation activation energy, frequency factor, entropy of activation, free energy of decomposition and rate coefficient have been analyzed as a consequence of γ -irradiation. The results clearly indicate the lowering of thermal stability of CR-39 as an effect of γ -irradiation. Such a reduction in thermal stability has been tried to be correlated with the induced structural changes as revealed by FTIR spectroscopy.
- Zaki (2012) [19], was studied the effects of He-Ne laser on the optical characteristics of Cellulose nitrate, CN-85, and Poly allyl diglycole carbonate(CR-39) nuclear track detector using photoluminescence (PL) and UV-visible spectroscopic techniques. The polymers irradiated with alpha particles with close contact to ^{241}Am and then exposed to (He-Ne) laser with different doses. The laser energy intensities ranged between 0 and 217 J/cm². The

change in the PL spectra may be explained by chain conformational disorders as well as chain scission. From the UV-visible spectra, it is found that a shift in the absorption edge towards a longer wavelength with increasing laser doses can be readily observed. The absorption peak with increasing dose is seen to change into a broad one. The optical band gaps determined from the UV-visible spectra were found to decrease with the increase of energy intensities of He-Ne laser. These results have been explained on the basis of scission of the polymers due to laser irradiation. The UV absorption tail formation in both polymers was related to the diminution of optical band gap.

- Abdel Raouf, (2013) [20] studied the CR-39 irradiated with γ -rays, x-rays and alpha particles by FTIR spectroscopy. He made a comparison between the effect of many types of radiation on the sensitivity of CR-39 detector by using the FTIR spectrometer. It was found that, investigated CR-39 is so sensitive for all types of radiation used that was used as a dosimeter for these types of radiation. In this work the optical density of the detector was calculated and then it is used to determine α -range.
- Ashok, et. al., (2014) [21], FTIR spectra of bare CR-39, CR-39 Cf + UV (pre exposed) and CR-39 UV + Cf (post exposed) at 160 nm were study, he found that transmittance increases for the pre exposed sample and decreases for post exposed sample. Sharp increase is observed in every peak (about 8%) for pre exposed sample and transmittance reduces (about 5%) for post exposed samples. And that pre and post exposure of UV radiations results significant change in bulk and track etch rates. Activation energy for bulk etch rates for alpha, alpha+UV and UV+alpha irradiated CR-39 is calculated and found to be (0.61 ± 0.52) eV, (0.58 ± 0.22) eV and (0.62 ± 0.47) eV resp. The activation energy for track etching

for alpha, UV+ alpha and alpha + UV irradiated CR-39 is (0.52 ± 0.04) eV, (0.58 ± 0.61) eV and (0.60 ± 0.61) eV resp.

- Emad, et. al., (2014) [22], the effects of α -particles on the physical properties (optical properties, electrical properties and the structure) of CR-39 polymer were investigated. The irradiations were performed by using ^{241}Am at constant alpha particle energy 4.86 MeV at normal incident for different irradiation times (6-96) hours. A variation in the optical energy band gap- E_g values was appeared.
- M. Choudhary et. al., (2014) [23], they study the structural changes in CR-39 polycarbonate irradiated to gamma radiations at different doses varying from 1 kGy to 125 kGy. The intensity of many functional groups has been found to decrease with increased dose indicating a release of some gases due to irradiation except at 5 kGy dose. The G-values corresponding to some specific species have been calculated to study the reaction mechanism of polymer modifications and the water content has been increased.
- Abdul-Kader et. al., (2014) [24], the effect of gamma ray irradiations on the optical and electrical, properties of CR-39 were investigated. The obtained results showed a decrease in the optical energy gap with increasing the gamma dose. Increase in the numbers of carbon atoms (N) in a formed cluster with increasing the irradiation dose was observed.
- Fala et. al., (2014) [25], she study effect of the radiation dose assessment of gamma rays and ultraviolet radiation on nuclear track detector-NTDs types

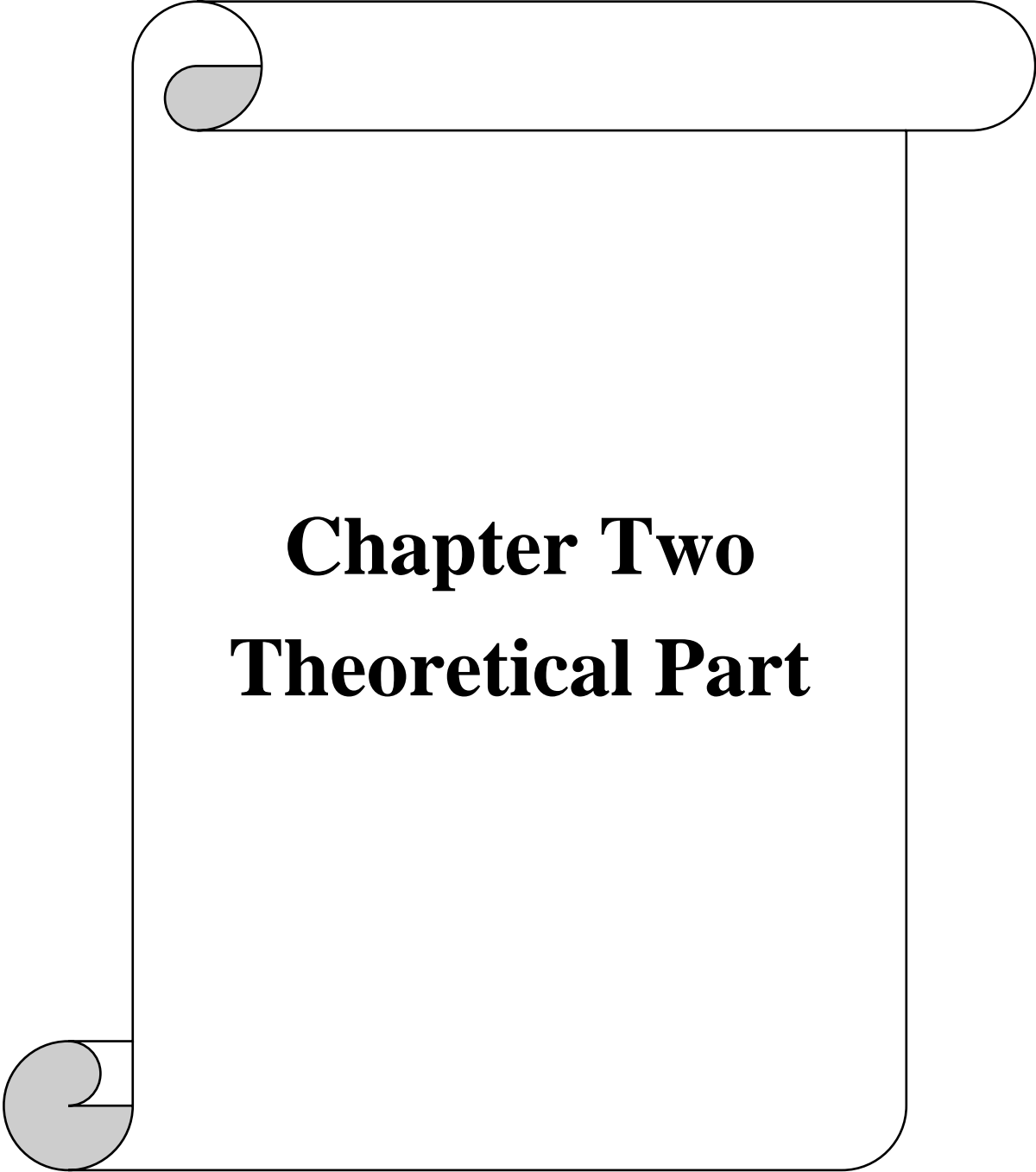
CR-39 , Lexan and LR-115 through measuring the absorbance-A by using UV-visible spectroscopy technique and measuring the spectral deviation of Fourier transform infrared- FTIR technique .

- Ahmed, et al., (2016) [26], he studied the effect of Nd: YAG laser of wavelength (532 nm), laser power 150 MW on the CR-39 polymer. Alpha track diameters, bulk etching velocity- V_B , track etching velocity- V_T , etching efficiency- η , etching ratio- V were determined. The activation energies of bulk etch- E_B and track etch- E_T for unexposed, post- exposed and pre-exposed are found to be equal to 1.10, 0.92, 0.82 eV and 1.07, 0.86, 0.79 eV respectively.

1.4 Aims of the project

The main objective of the research was to:

1. Study the Effect of (He-Ne) laser beam and gamma radiation on optical properties of nuclear track detectors CR-39 in different absorbed doses using FTIR and ultraviolet-visible (UV-Vis) spectroscopy, and determine the direct and indirect band gap energy.
2. Clarification of the etching properties (V_B , V_T , V , θ_C , η and S) of CR-39 track detector irradiated by alpha particles (^{226}Ra source) and (He-Ne) laser beam.



Chapter Two
Theoretical Part

Chapter Two

Theoretical Part

2.1 Introduction

Nuclear track detector technique has over the last few decades, become a popular and well established method of measurement in a large number of fields involving different aspect of radioactivity or nuclear interactions. It has grown to such an extent that now there is hardly a branch of science and technology where it does not have actual or potential applications. In this chapter we will introduce and review some concepts of this technique [19].

2.2 Historical review of solid state nuclear track detectors

The field of Solid State Nuclear Track Detectors_SSNTDs had its foundation in the year 1958 when first observations were reported by D.A. Young at AERE Harwell. He noticed that when lithium fluoride crystals (LiF), held 1 mm away from uranium oxide film, were irradiated with thermal neutrons, the crystal surface revealed a number of low etch pits after treatment with a chemical reagent ($\text{HF} + \text{CH}_3\text{COOH}$). Further the number of these pits (as seen under the optical and electron microscope) had a one to one correspondence with the theoretically estimated number of fission fragments recoiling into the crystal from the uranium foil. It seemed that each pit was formed around the site of solid-state damage produced by the fission fragments [27].

In 1959 E.C.Silk and R. S. Barnes at AERE Harwell, show the direct observation of these damaged regions, produced by fission fragments, in thin sheets of mica, using transmission electron microscope_TEM to observe the latent tracks [28]. In 1962 R.L. Fleischer, P. B. Price and R. M. Walker

development of a new particle detector, they extended the etching technique of Young to mica and eventually to a variety of other materials such as glasses, plastics and various mineral crystals [29,30]. Since then, the field has grown to such an extent that now there is hardly a field of science and technology where it does not have an actual or potential application.

Solid State Nuclear Track Detectors (SSNTDs) are insulating solids both naturally occurring and man-made. There are several types of these detectors including inorganic crystals, glasses and plastics. When a heavily ionizing charged particle passes through such insulating solids, it leaves a narrow trail of damage about 50 Å in diameter along its path. This is called 'Latent Track' as it cannot be seen with the human eyes. It is possible to view this latent track with an electron microscope. The exact nature of the physical and chemical changes occurring at the damage site depends on the charge Z and velocity ($\beta = v/c$, where v is the particle velocity and c is the velocity of light) of the particle, on the chemical structure of the detector pressure. These latent tracks can be distended / developed so that they can be viewed under an optical microscope by etching with some chemicals such as sodium hydroxide (NaOH) and hydrofluoric acid (HF) [31].

The first detector used for recording alpha tracks was cellulose nitrate. It has low sensitivity and is now replaced by a more sensitive detector called CR-39. Polycarbonate detectors such as Lexan are generally used for recording fission fragment tracks. Each detector is characterized by a critical value of energy loss rate by the charged particle. Only those charged particles which give up energy exceeding the critical value alone can produce etchable tracks [31].

2.3 Threshold of SSNTDs

Track formation related to the production of dense regions of ionization by charged particle and to a first approximation, track formation are regarded as

occurring when the number of ions exceeds a certain threshold value; this threshold varies from one type of material to another. The threshold for track registration can be defined, as the minimum primary ionization energy required occurring track able for chemical etching [32].

The track formation should be related to the number of different parameters, such as total energy loss rate, primary ionization, restricted energy loss, type and energy of the ionized charge particle and depend on the chemical structure of detector material. The track formation criterion, that takes the form of a statement are formed in a medium when, the chosen parameter exceeds some critical value [33].

These track formation criteria can be tested by irradiating a given solid with a number of ions at various energies and recording those cases for which etchable tracks are formed on diagram, the theoretical curves of the relative damage caused by different ions as a function of their velocities are shown in Figure (2-1) [34].

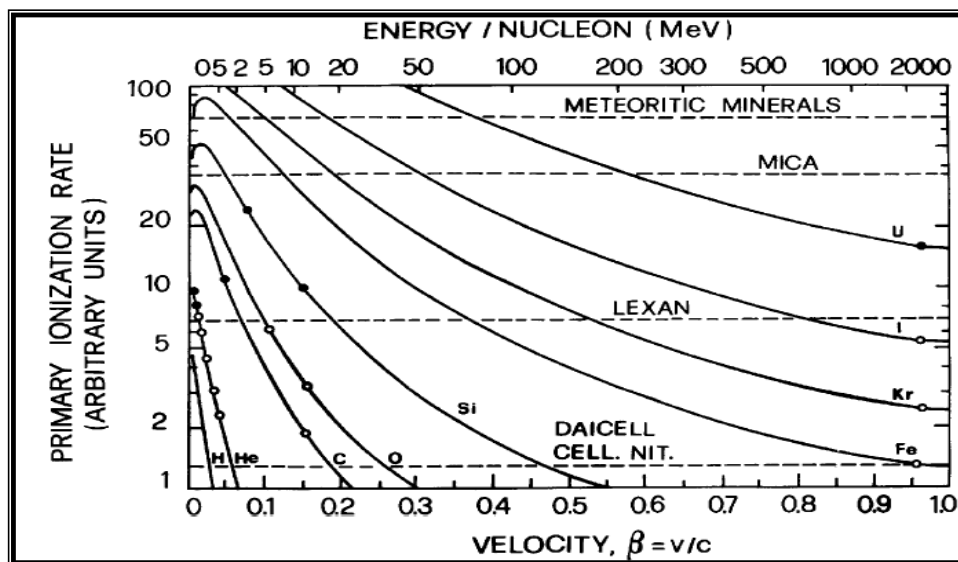


Figure (2-1) Primary ionization rate for various heavy ions versus particle velocity and track etch threshold for various materials [34].

2.4 Tracks formation in the SSNTDs

The radiation damage in the (SSNTDs) takes two types: Inorganic material such as crystal and organic material such as polymer [35].

2.4.1 Tracks formation in inorganic materials

There are two important major factors in damage production; the primary and the secondary ionization by electrons. It obviously appears that the damage caused by interaction with the electrons. This proposal postulates that the passage of a heavily-ionizing particle leaves a narrow region containing a high concentration of positive ions (burst ionization) in its wake [35]. These arrays of adjacent ions are electro statistically unstable and according to coulomb interaction, following ionization, an array of interstitial ions and vacant lattice sites are produced by coulomb energy, subsequent processes include neutralization of the positive ions and elastic relaxation of the local stresses by spreading the strain more widely around the track path as shown in Figure (2-2). In the final stage, the long strain makes possible the direct observation of un-etched tracks in crystals by (TEM) or etches tracks by optical microscope [32].

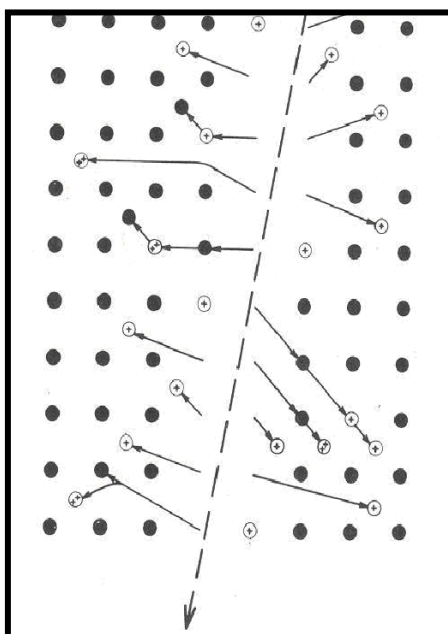


Figure (2-2) Atomic character of a plastic track in a crystal [32].

2.4.2 Tracks formation in organic materials

The favorable theory for track formation in organic materials is that based on the radiochemical damage mechanism. The etched tracks are formed by the breaking of the long polymer chains to short chains when irradiated. The result is new chain ends, i.e., chemically reactive sites are formed. The polymer is a chemical compound of large molecules, which consist of small repeated units called monomers; the monomer is a collection of atoms connected by covalent bonds [32].

The passage of ionizing particles e.g. (proton, deuteron, and alpha particles) through the polymer will excite and ionize the polymer molecules, some excited molecules may in their turn, de excite through the emission of radiation or through non-radioactive transitions. Excitation energy can also transfer from one molecule to another.

Both ions and excited molecular chains along its path form a complex array of stable molecules, free radicals, ionized molecules and radical ions. Further reactions among these ions, free radicals and molecules will take place as shown in Figure (2-3). However, these free ions is relatively small, only free radicals react among them or with other molecules.

The net effect on the plastic will be the production of many broken molecular chains, leading to reduction in the average molecular weight of the substance. Therefore, the rate of chemical etching attack on a plastic increases as the molecular weight decreases. It is likely that the damage region is more etch able than the bulk material which leads to the etching along the track and is greater in rate than that of the bulk material [32].

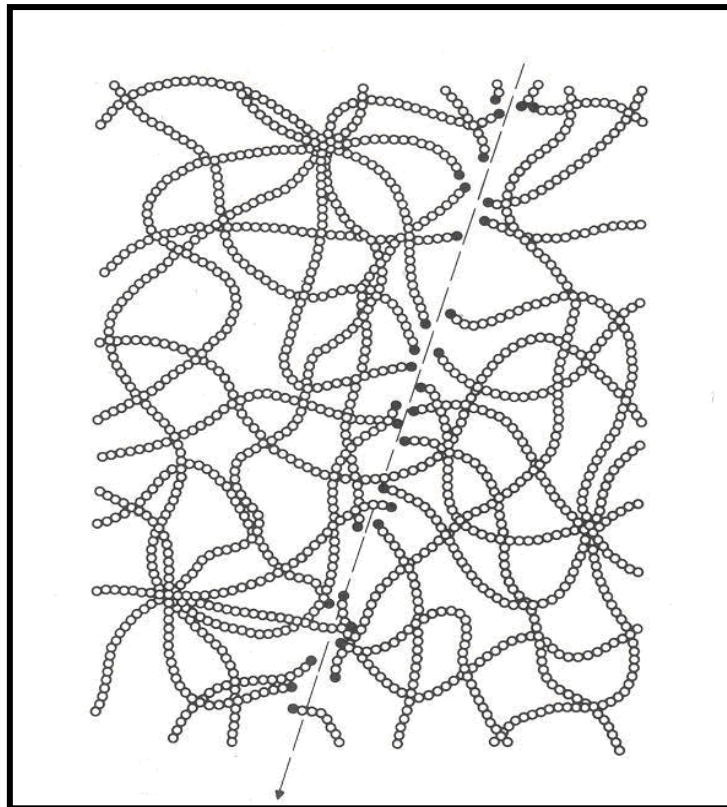


Figure (2-3) Atomic character of a plastic track in polymer [32].

2.5 Types of SSNTDs

Solid state nuclear track detectors-SSNTD's can be classified into three several types:

1. Crystals most of the natural and man-made crystalline solids can be used as solid state nuclear track detectors. Crystalline solids widely exist in the earth crust as mineral compositions of rocks, soils, and dust. Large-sized muscovite mica and quartz are examples of pure track detectors. The main compositions of granite are mica, feldspar, and quartz. All of them are transparent crystalline minerals and can be used as nuclear track detector materials. Many kinds of accessory minerals, such as apatite, zircon, and sphene, are also contained in granite [36].

2. Glasses, as nuclear track detectors, are a type of amorphous non-crystalline inorganic solid. It can be divided into natural glasses and man-made glasses. Natural glasses include terrestrial glasses and extraterrestrial glasses [36].
3. Polymers since the discovery that polymers-plastics can record etch able tracks of heavy charged particles, more than 30 types of polymer detectors have been successfully etched to reveal tracks. Compared with inorganic crystalline solids and glasses, plastic track detectors are more sensitive to heavy charged particles, such as the charge as low as $Z = 1$ (proton). The sensitivities of different polymers are different. CR-39 (poly allyl diglycol carbonate (PADC)) is the most sensitive detector in common use (the recordable charge $Z \geq 1$); amber is the most insensitive plastic detector (the lowest recordable charge is fission fragments, $Z > 30$) [29].

2.6 CR-39 track detectors

CR-39, or poly allyl diglycol carbonate -PADC has the high sensitive and high charge resolution detector of the nuclear track recording polymer (plastics). This plastic detector is made by polymerization of the 1-ethanediyl, oxydi-2, di-2-propenyl ester of carbonic acid. It contains two of monomer ally functional groups $[\text{CH}_2 = \text{CH} - \text{CH}_2 -]$. The chemical composition of CR-39 is $\text{C}_{12}\text{H}_{18}\text{O}_7$, with its molecular weight being 274.2707 g/mol, and has the following molecular structure:

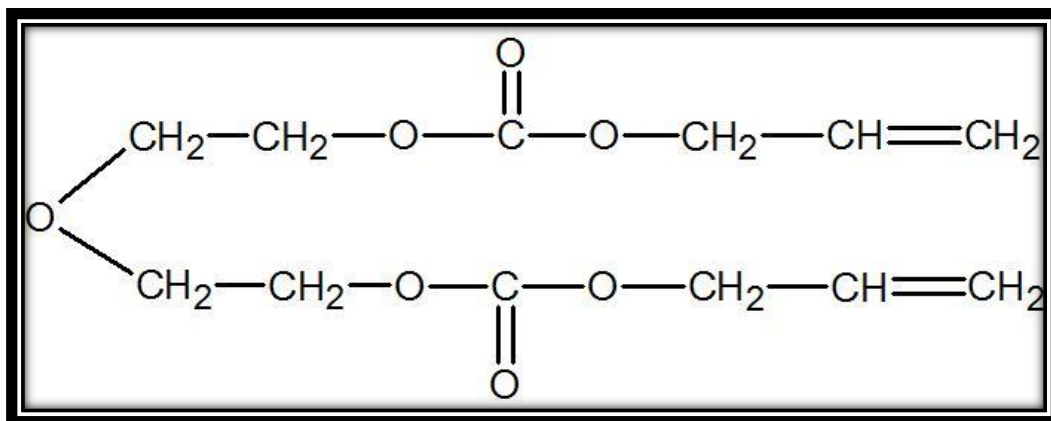


Figure (2-4) Molecular structure of CR-39 solid state nuclear track detector [12].

In general, chainlike structures are more sensitive to radiation than the other structures, such as a benzene ring in polycarbonate. It is thus reasonable why CR-39 is more sensitive than polycarbonate [37].

CR-39 density is 1.32 g/cm^3 , refractive index $n = 1.504$, $A/Z = 1.877$, and its mean ionization potential $I = 70.2 \text{ eV}$ [37]. CR-39 detector can not only record track number N , positions (X, Y, Z), directions (zenith angle θ , azimuth angle Ψ), but also derive particle charge Z , mass M , and energy E from the track parameters. It is the most widely used solid-state nuclear track detector.

CR-39 detectors are the most sensitive and popular detector for recording α -particles. Its energy window for recording α -particles is from ~ 0.1 to $>20 \text{ MeV}$, or approximately from zero to infinite [38].

Even though CR-39 is sensitive to low Z heavy charged particles, it can be used safely to detect fission fragments induced by high-energy projectiles. At very high energies over several hundreds of MeV/amu , CR-39 can identify the charges of projectiles and distinguish the tracks of projectiles and fission fragments.

2.7 Chemical etching

Chemical etching is the basic technique used to get nuclear particle tracks in solids. An etchant is a particular chemical formulation which preferentially reacts with the damaged materials in the particle track resulting from the passage of a heavy charged particle in the solid state nuclear track detector. The etching conditions include three aspects [39]:

- (a) Compositions of the chemicals used as etchant.
- (b) Temperature during etching.

(c) Duration of the etching.

The etchant is particular for each detector material type. Selection of the wrong etchant will certainly not reveal tracks. Usually, a higher temperature and higher etchant concentration will etch tracks more rapidly; longer etching times will make the etched track larger in diameter.

The etching conditions are optimized experimentally for each detector types [40]. In general, etchants for polymeric detectors are often solutions of alkali hydroxides such as KOH or NaOH with (1-12 N) at (40 – 60 °C) [41,42]. For glasses and minerals, crystals such as quartz, mica, and certain pyroxenes are etched in aqueous solutions of acids such as HF with ~ 48% concentration at (20 °C) [43,44].

Times of etching can vary from few seconds to many hours. It varies according to the exact etching conditions; the concentration of the etchant and the temperature [45].

2.8 Track affecting parameters

There are two essential factors that affect the appearance of a track; the bulk etch rate V_B and the track etches rate V_T .

2.8.1 Track etch rate- V_T

The track etch rate is the ratio of dissolution of a detector along the line of the track [46]. Its value depends on the type of detector, etching conditions, the particle velocity and its energy. Experiments prove that $-V_T$ increased with increasing the rate of ionization for different organic and inorganic detectors [47,48].

The relation between V_T and the temperature of the etching solution is [31]:

$$V_T = V_B \left[\frac{1 + V_D^2 / V_B^2}{1 - V_D^2 / V_B^2} \right] \dots \dots \dots (2 - 1)$$

where:

V_T = track etch rate ($\mu\text{m/h}$).

V_D = diameter etch rate ($\mu\text{m/h}$).

V_B = bulk etch rate ($\mu\text{m/h}$).

and:

$$V_D = \frac{\Delta D}{\Delta t} \dots \dots \dots (2 - 2)$$

2.8.2 Bulk etch rate- V_B

The bulk etch rate can define as the rate of dissolution of the stored detector normal to the surface and energy remote from any track [49]. It is an important parameter for determining the sensitivity of track of $-(SSNTD)$ [50]. It depends on the construction of the plastic, the constituents of the etching solution, its temperature and concentration [51]. It is found that for a given homogenous and isotropic solid, the bulk etch rate velocity V_B increases exponentially with etching temperature and concentration of the etching solution [37]. The bulk etch rate is found by using the following relation [52]:

$$V_B = \frac{1}{2 \rho A} \frac{\Delta m}{\Delta t} \dots \dots \dots (2 - 3)$$

where:

V_B = bulk etch rate ($\mu\text{m/h}$).

A = area of samples (cm²).

ρ = density of nuclear track detectors (g/cm³).

m = mass of the nuclear track detectors (g).

t = etching time (h).

2.9 Critical angle for etching- θ_c

For every SSNTDs etched under a given condition, there is found to exist certain minimum angle called the critical angle- θ_c , measured from the detector surface show in Figure (2-5) which if the particle enters the detector surface, its tracks cannot be observed after etching because in that case the surface etches faster than the track is formed [32]. this limitation is due to the geometry of track etching.

From the geometry of track etching figure (2-5), one can find for constant V_B and V_T that [31]:

$$\theta_c = \sin^{-1} \frac{V_B}{V_T} \dots \dots \dots (2 - 4)$$

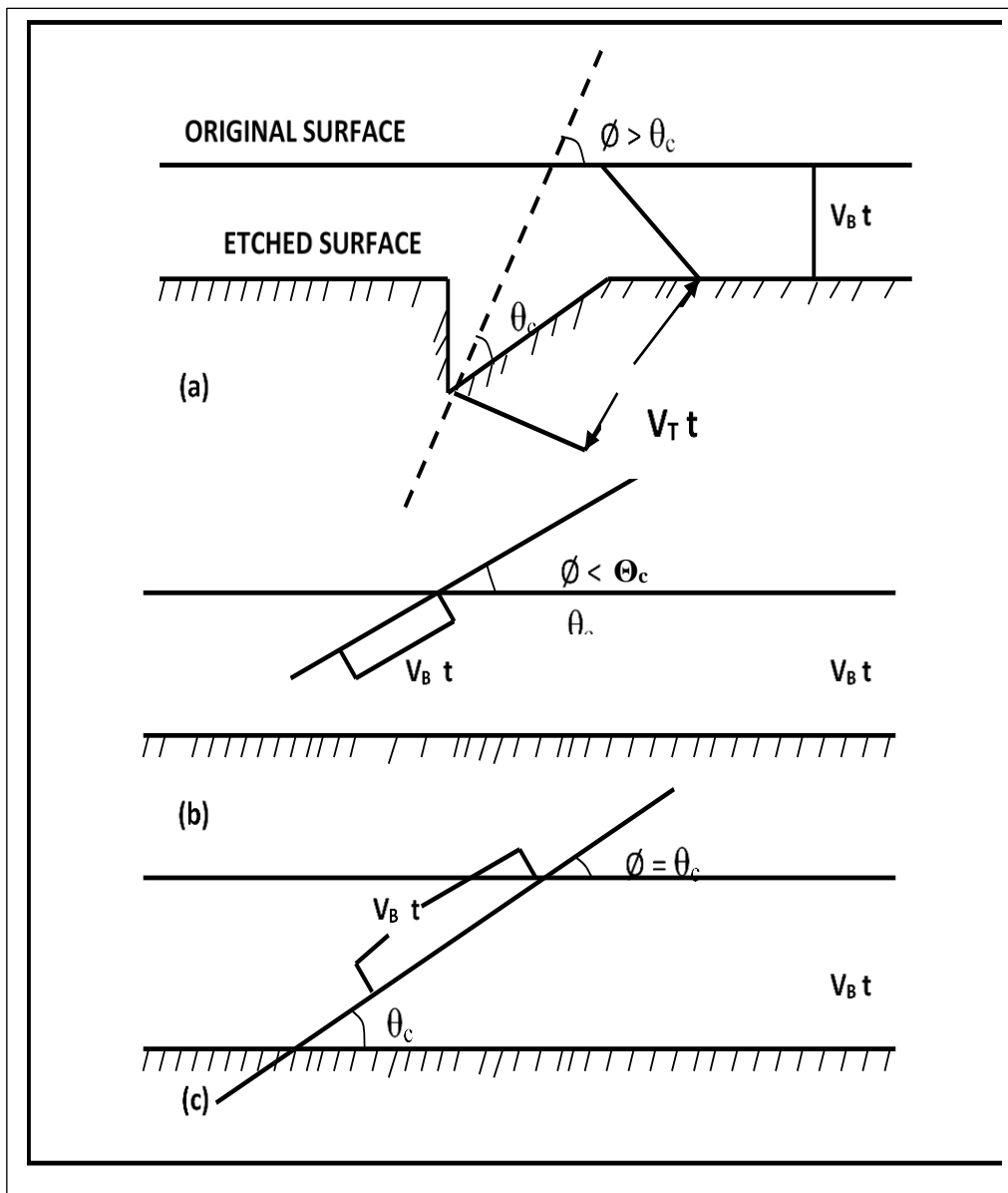


Figure (2-5) A track etching of a particle incident obliquely on the SSNTD: (a) track pit shape, its etching observed length and diameter depend on the two etch rates V_T and V_B (or their ratio V_T / V_B). (b) If the particle enters at very small angle from the surface such that the normal component of V_T is less than V_B , no etched track can be observed, as the surface is removed more rapidly than the track develops. (c) The critical value θ_c is obtained when the normal component $V_T \sin \theta$ is equal to $V_B = V_T \sin \theta_c$, $\theta_c = \sin^{-1} V_B / V_T$ [32,36].

2.10 Etching efficiency and sensitivity

The etching efficiency is defined as the ratio of the counted tracks and the number of particles incident on the detector surface [51].

$$\text{efficiency} - \eta = \frac{\text{no. of etched tracks}}{\text{no. of incident particles}}$$

The efficiency (η) depends on the track etched rate $-V_T$ and the bulk etched rate $-V_B$ as present in equation (2-5) [45]:

$$\eta = 1 - \frac{V_B}{V_T} \dots \dots \dots (2 - 5)$$

or:

$$\eta = 1 - \sin \theta_c \dots \dots \dots (2 - 6)$$

Etching sensitivity can be given by the following relationship:

$$S = V - 1 \dots \dots \dots (2 - 7)$$

And can get it from the critical angle:

$$S = \frac{1}{\sin \theta_c} - 1 \dots \dots \dots (2 - 8)$$

2.11 Track etching geometry

The track etching geometry depends on the angle of incident particle which it makes with the surface detector. However, we cannot record the tracks when the angle of incident particle θ (placed between the particle passage and detector surface) is less than the critical angle [37].

The etching process includes two types of chemical reactions: etchant with damaged material and etchant with bulk material of the detector. The first proceeds with velocity $-V_T$ along the trajectory, called track-etch rate. The second proceeds perpendicularly to the surface of the detector with velocity $-V_B$ called bulk etch rate. The etching process is a combined reaction of $-V_T$ and V_B [36].

We can see the track when $-V_T$ is greater than V_B , i.e. $(V_T / V_B) > 1$ [29]. The incident particles on the track detector can be identified by the charge Z or effective charge $-Z_{\text{eff}}$, the mass M and the energy E or relativistic velocity ($\beta = v/c$). The difference in these parameters of the incident particles produce changes in the track etching parameters, a total range of the particle through the detector material R (track length), the track etching velocity $-V_T$ and the variation of $-V_T$ with position along the track. The etched track has a conical shape and the easily measurable parameters are the conical etched-out length $-L_e$ and the diameter $-D$ of the etch pit opening [33].

The etched track formation process can be envisioned as the incident particle parameters (charge Z , mass M and energy E) representing the input parameters, while the etched track parameters (track length L_e , axes, profile and contour) represent the output parameters. The all processes in-between the above-mentioned parameters represent the damage formation and the etching principle [39]. In the simple instance is a particle penetrating a detector material to its original surface as shown in figure (2-6).

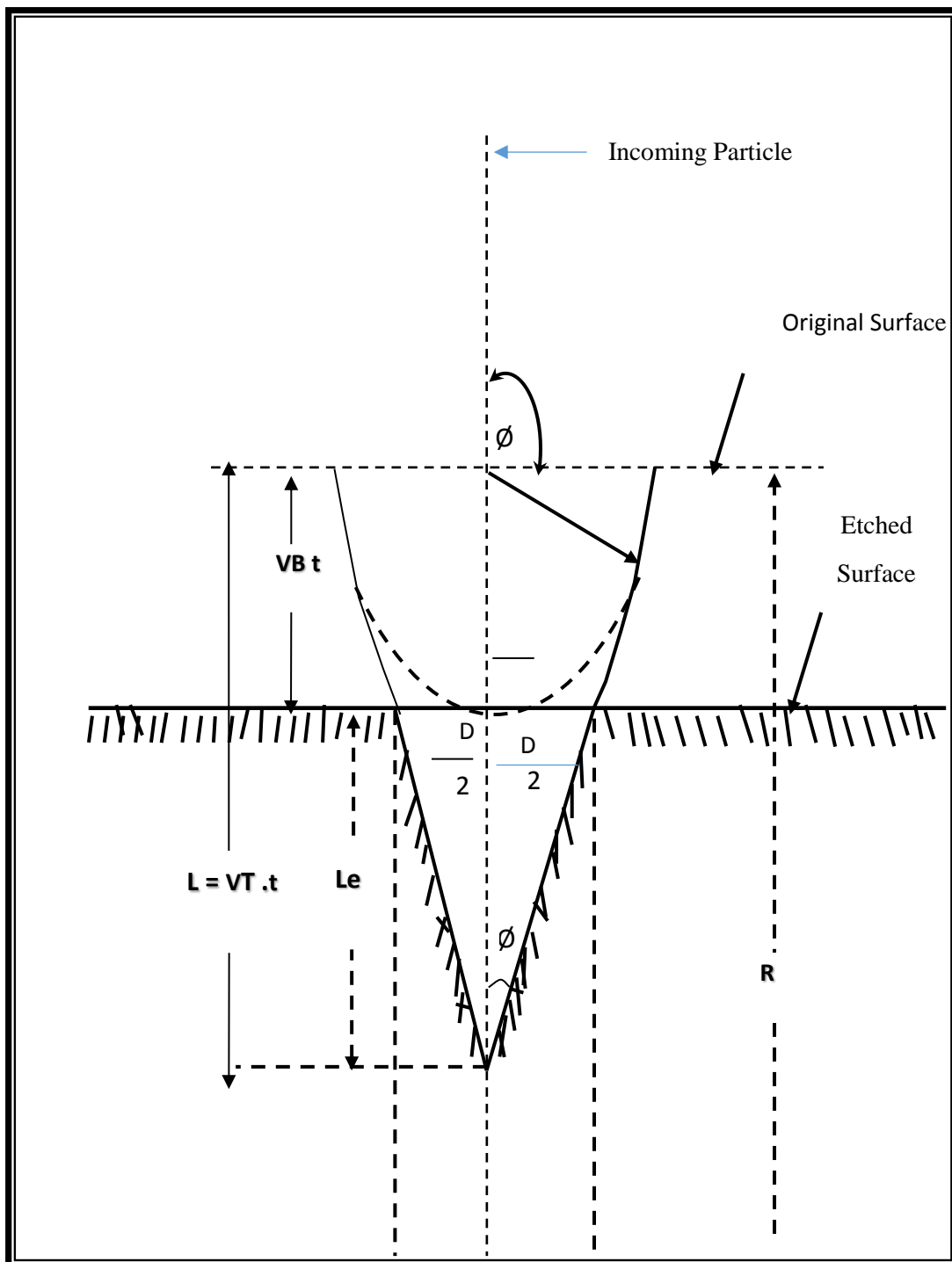


Figure (2-6) Track geometry for a particle penetrating a detector material normally [31,36].

The etching rate ratio is represented in this equation:

$$V = \frac{V_T}{V_B} \dots \dots \dots (2 - 9)$$

Where:

V = etch rate ratio

It is clear from the equations that, the track diameter d depend essentially on the competitive effects of V_T and V_B . When $V_B = V_T$, D vanish, then no track is produced [33].

2.12 Application of the SSNTDs

Solid state nuclear track detectors-SSNTD's, has grown to such an extent, that now there is hardly a branch of science and technology where it does not have actual or potential applications. Fields where well-established applications of this technique already exist, it went on to say include [36]:

- 1) Physical sciences including low and high energy physics, astrophysics, cosmic-ray physics, plasma physics, nuclear reactor physics, and elemental analysis [37].
- 2) Earth and planetary sciences including fission track dating, geothermal chronology, meteorite studies, lunar and solar particles, uranium and petroleum exploration, and earthquake prediction.
- 3) Life and environmental sciences, which include radiation protection dosimetry, radon and thoron monitoring, neutron dosimetry, and radioactive contamination.

4) Nanotechnology and material sciences.

2.13 Analyses of UV-Vis spectra of SSNTDs

UV-Vis was an optical spectrometer records the wavelengths at which absorption occurs, together with the degree of absorption at each wavelength. The resulting spectrum is presented as a graph of absorbance-A versus wavelength. CR-39 detector has a sharp decrease in absorption with increasing wavelength up to certain value [19]. The region of wavelength of spectrum at the range (200-800nm). This behavior is generally interpreted as caused by the formation of extended systems of conjugate bonds, i.e. possible formation of carbon clusters and/or defects. The absorption bands in the investigated range of wavelength are associated to the $\pi-\pi^*$ electronic transitions [53-54]. This type of transitions occurs in the unsaturated centers of the molecules, i.e. in compounds containing double or triple bonds and also in aromatics. The excitation of π electron requires smaller energy and hence, transition of this type occurs at longer wavelengths [19].

2.14 Measurement of energy gap

The optical absorption technique can provide information about the band structure and energy gap in crystalline and non-crystalline materials [55]. The optical gap (E_g) of the CR-39 detectors, could be found by Tauc's relation [56]:

$$\alpha(h\nu) = \frac{\beta(h\nu - E_g)^n}{h\nu} \dots \dots \dots (2 - 10)$$

where α is the absorption coefficient, $(h\nu)$ is the energy of the incident photons, (E_g) is the value of the optical energy gap between the valence band and the

conduction band, and n is integer, which characterizes the electronic transition, whether it is direct or indirect during the absorption process in the K -space. Specially, n is $1/2$, $3/2$, 2 and 3 for direct allowed, direct forbidden, indirect allowed and indirect forbidden transitions, respectively. The factor β depends on the transition probability and can be assumed to be constant within the optical frequency range. The usual method for the determination of the value of E_g involves plotting $(\alpha h\nu)^{1/n}$ against $(h\nu)$. In the present study the most satisfactory fit is obtained by plotting $(\alpha h\nu)^{1/2}$ and $(\alpha h\nu)^2$ as a function of photon energy $(h\nu)$, taking into account the linear portion of the fundamental absorption edge of the UV–visible spectra [22].

The absorbance coefficient (α) could be obtaining from the following relation:

$$\alpha = 2.323 \frac{A}{d} \dots \dots \dots (2 - 11)$$

where A is the absorption and d is a thickness of the samples.

2.15 Number of carbon atoms measurement

The carbon atoms number per conjugated length $-N$ for a linear structure is given by Robertson relation [57]:

$$E_g = \frac{2\beta\pi}{\sqrt{N}} \dots \dots \dots (2 - 12)$$

where N is the number of carbon atoms per conjugated length, 2β gives the band structure energy of a pair of adjacent π sites. The value of β is taken to be ~ 2.9 eV as it is associated with π - π^* optical transition in the $-C=C-$ structure. From

the Robertson's relation cluster size can be calculated and then the following relation can be used to calculate the number of carbon atoms per band [58]:

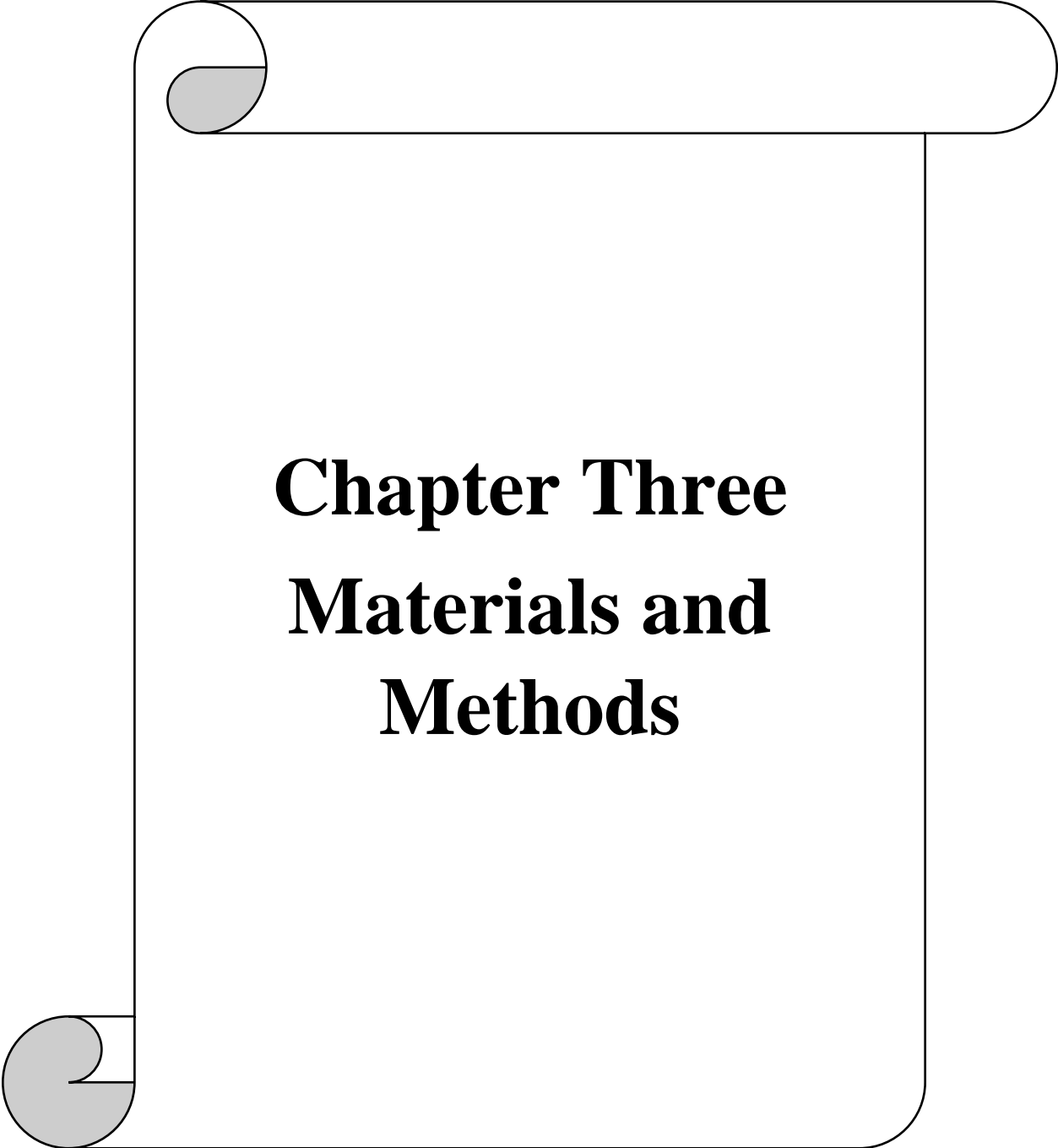
$$E_g = \frac{34.3}{\sqrt{M}} \dots \dots \dots (2 - 13)$$

2.16 Analyses of FTIR spectra of SSNTDs

FTIR was an optical spectroscopy records the wavenumber at which absorption or transmission occurs, together with the degree of absorption or transmission at each wavenumber. The resulting spectrum is presented as a graph of absorbance-A or Transmission-T % versus wavenumber. CR-39 detector is a highly cross linked thermoset fabricated by polymerization of the allyl diglycol carbonate monomer [59]. IR spectroscopy allows the identification of different absorption bands decreased when the thickness of the CR-39 detector decreases, so these are characteristic of the CR-39 detector. The wave numbers corresponding to these absorptions (transmission troughs), and the corresponding assignment of the functional groups and the modes of vibration are summarized in table (2.1) [60,61].

Table (2.1) The wavenumbers of the more significant absorption peaks (transmission troughs) in the FTIR spectrum for 5 μm CR-39 detector (film), and the corresponding assignment of the function groups and the modes of vibration [62].

Position of the peak (cm^{-1})	Functional Groups/modes of vibration
3636	OH asymmetric stretching vibrations
3549	OH symmetric stretching vibrations
3470	First overtone of C=O stretching vibration of ester
3385	OH stretching vibrations
2958, 2911	CH ₂ asymmetric stretching vibrations
2875	CH ₂ symmetric stretching vibrations
1744	C=O stretching vibrations of carbonate group
1650	C=C stretching vibrations of vinyl group
1456, 1405, 1360, 1228	CH ₂ deformation vibrations
1260	C-O-C asymmetric stretching vibrations of carbonate
1137	C-O-C asymmetric stretching vibrations of ether
1096	C-O-C symmetric stretching vibrations of carbonate
1026	C-O-C symmetric stretching vibrations of ether
910	C=C deformation vibrations
877	CH ₂ deformation vibration of $-\text{CH}=\text{CH}_2$ group



Chapter Three
Materials and
Methods

Chapter Three

Material and Method

3.1 Materials

3.1.1 CR-39 track detectors

CR-39, or poly allyl diglycol carbonate-PADC were used in the present work. CR-39 is a polymer organic solid state nuclear track detectors in the sheets form (plastic detector), with thickness about-250 μm made by pershore moulding LTD company, England. Its chemical formula $\text{C}_{12}\text{H}_{18}\text{O}_7$ with density about 1.32 g/cm^3 and molecular weight equal to 274 a.m.u.. These sheets were cut into small pieces each with area- $1.5 \text{ cm} \times 1.5 \text{ cm}$.

3.1.2 The etchant solution

Sodium hydroxide solution-NaOH with 6.25 N normality has been used for the etching process, prepared as:

$$W = W_{\text{eq}} \times N \times V \dots \dots \dots (3 - 1)$$

where:

W: The weight of NaOH needed to prepare the given normality.

W_{eq} : Equivalent weight of NaOH ≈ 40 .

N: Normality = 6.25 N.

V : Volume of distilled water.

The etchant compartment has a volume of about 250 ml. This apparatus is a closed assembly, except for small aperture at the bottom of the condenser tube, which avoids any change of etchant normality (concentration) during the experiment due to evaporation. The etching was performed at 60 °C while the etching time was (1.5, 2, 3, 4, 5, 6, and 7 hours).

3.2 Irradiation sources

In this research we used three type of radiation sources, two was ionizing radiation gamma ray and alpha particle and third was non-ionizing radiation He-Ne laser beam for the irradiation of samples as shown in the follow sections:

3.2.1 Gamma irradiation

Source of gamma ray that used in this research to irradiate the CR-39 detector was ^{60}Co gamma cell 900 in the department of physics, college of science, Baghdad university. The activity of the source was-5.41274 Ci with energy-1.1732 and 1.3325 MeV and dose rate-71.745 Gy/h.



Figure (3 -1) Gamma cell 900 system model by Bhabha Atomic Research Center-BHA, Trombay, Bombay, India

3.2.2 Alpha irradiation

The irradiation of α -particle that used in this study was carried out by the source of α -particle ^{226}Ra with activity-10.54 μCi .

3.2.3 (He-Ne) laser beam

The (He-Ne) laser beam was used in this study, by gas laser types, which irradiate with powers (1, 5, 10 mW) at times (5, 10, 15 min). The distance between the source and the detectors was-5 cm with a wavelength of-632.8 nm.



Figure (3-2) CR-39 irradiated with (He-Ne) laser beam.

3.3 Materials analysis

3.3.1 FTIR-spectroscopy

FTIR-spectroscopy, or fourier transform infrared spectroscopy is one of the most important analytical techniques. One of the advantages of infrared spectroscopy is that almost any sample in virtually any state may be studied. Liquids, solutions, pastes, powders, films, fibres, gases and surfaces can all be

studied with a choice of sampling technique transmission, emission, photoconductivity or Raman scattering.

FTIR-spectroscopy used in this study was FTIR-model Tensor 27 made by Bruker company, Germany. The system was located in the Ibn al-Bitar Company / Ministry of Industry and Minerals. The wavenumber range used in this study was (400-4000 cm^{-1}) mid-infrared. All the CR-39 detector samples measured by FTIR-spectroscopy were adjusted directly in sample unit in the space of cavity cell.



Figure (3- 3) FTIR spectroscopy model Tensor 27 from Bruker company, Germany.

3.3.2 UV-Visible spectroscopy

UV-Vis spectroscopy, its refers to reflection spectroscopy or absorption spectroscopy in the ultraviolet-visible spectral region. Its uses the light in the ranges of near-UV, near-IR and visible. The reflection or absorption in the visible range directly affects the perceived color of the chemicals involved.

Ultraviolet-visible spectroscopy is located in the department of physics the college of science - Al-Nahrain university, model was (SHIMADZU UV-1601PC UV-visible, Japan). The wavelength range used in this study was (200-800 nm). All the samples of CR-39 measured in UV-Vis spectroscopy were adjusted directly in sample unit in the space of Cavity cell.



Figure (3-4) UV-Vis spectroscopy model SHIMADZU UV-1601PC UV-visible, Japan

3.4 Water Bath

Water bath of the type (Labsco, Germany) was have used in this study. It involved a thermostat, which could be worked over a range of 20 °C to 110 °C. However, in this study the chemical etching was carried out at 70 °C, and filtered water was used as the bath liquid. The accuracy of regulation of temperature for the bath used was better than ± 0.1 °C.

3.5 Optical microscope

The optical microscope type is (Motic, Malaysia). It is capable of giving magnifications of 40X and eye piece 10X to measure number of tracks and calculating the track density from the following equation:

$$\text{Track density}_{\rho} = \frac{\text{average of total track}}{\text{area of field view}} \dots \dots \dots (3 - 2)$$



Figure (3-5) Optical microscope

3.6 Methods

3.6.1 Sample irradiation

3.6.1.1 Gamma-ray irradiation

The condition of the irradiate the samples with gamma-ray irradiation were:

- The distance between gamma cell ^{60}Co and samples was 6cm.
- The irradiation of the gamma cell was at room temperature in air.
 - The dose rate of the gamma cell ^{60}Co was -71.745 Gy/h at time period (2015-2016).
- The range of gamma irradiation was 300-1600 kGy.
- The dose rate was calculated using the equation below:

$$D = \frac{Y \times 3.7 \times 10^7 \times (E_i \times \mu_m) 3600}{4\pi R^2 \times 6.25 \times 10^9} \dots \dots \dots (3 - 3)$$

Where:

D : dose rate (Gy/h).

Γ : gamma constant.

Y : activity of the source.

E_i : energy of gamma source (1.1732 and 1.3325 MeV).

μ_m : mass absorption coefficient (cm^2/g).

R : distance from gamma source to the detector (cm).

3.6.1.2 Alpha-particles irradiation

The condition of the irradiated the CR-39 track detectors with Alpha-particle irradiation were:

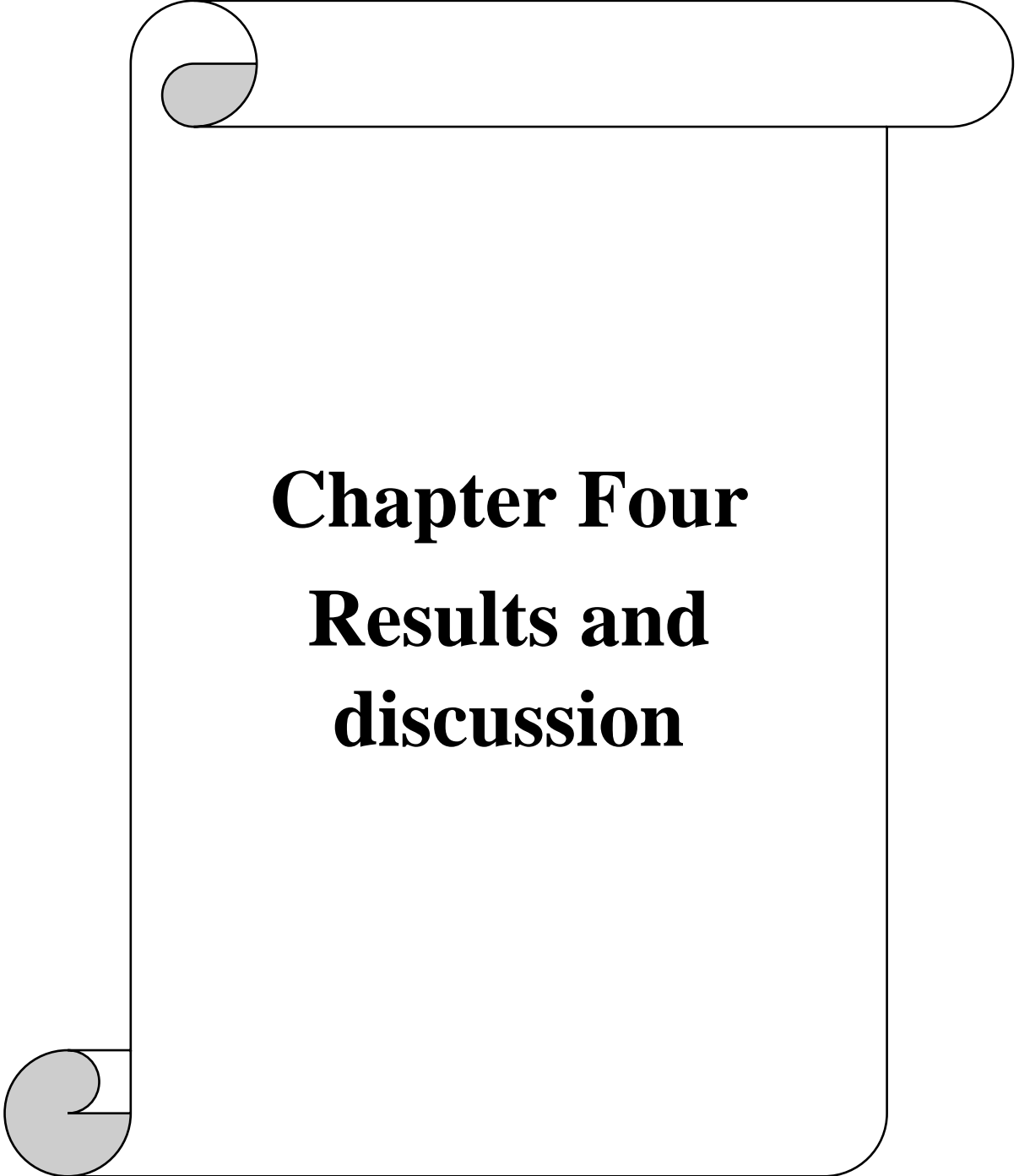
- CR-39 track detector was irradiated with Alpha-particle source ^{226}Ra at 2π geometry.

- The irradiation of the alpha-particle was at room temperature in air.
- The activity of the alpha-particle source ^{226}Ra was $-10.54 \mu\text{Ci}$.
- The time of irradiation of the alpha-particle source ^{226}Ra was 3 minute.

3.6.1.3 Laser exposure

(He-Ne) laser was used in this study, the condition of the irradiate the samples with He-Ne laser beam were:

- The distance between the laser source and the samples was 5 cm
- The irradiation of the He-Ne laser was at room temperature in air.
- The power of the laser that use were (1, 5 and 10 mW) and with irradiation time (5, 10 and 15 min).



Chapter Four
Results and
discussion

Chapter Four

Results and discussion

4.1 Introduction

In this chapter we present the results which have been obtained from the effects of both types of radiation, non-ionizing radiation (He-Ne laser beam) and ionizing radiation (gamma-ray and alpha-particles) on CR-39 nuclear track detectors by using UV-Vis spectrometer and FTIR spectroscopic techniques.

4.2 Effect of (He-Ne) laser and alpha-particles on CR-39 detectors

4.2.1 Track affect parameters measurement

The relation between the track diameter and track density at different etching time for three groups (α +He-Ne) (1, 5 and 10 mW) powers of CR-39 detector were shown in figures (4-1) to (4-6). Each group contains three detectors exposed to laser at different times (5, 10 and 15 min) and different powers (1, 5 and 10 mW) and irradiated with alpha particle, the results show that increasing in the track diameter and track density response to increase in the etching time, and at high etching time show decrease in the track density and this interpretation that increase in time of etching lead to increase in the thickness of removed layer that responsible of track appearing and reach the minimum value due to increase in the track diameter at high etching time, also figures show that the density and diameter of track increase response to increase in the exposure time of laser at different power, because laser increase in elasticity of detector and get the decomposition in molecular chains main of detectors which cause new molecular chains, this chains have free radicals repulsive among themselves, and construct

a new number from the free radicals as results of lost alpha-particles for its energies when it passed through the detectors, and when the etchant solution process the etchant will begins to attack the free radicals leading to remove it from molecule of detectors, and thus free radicals repulsive away from the center of track and made a track with large diameter.

From figures (4-4) to (4-6) show that the etching time for all groups using the NaOH solution were (4 h). At (4 h) etching time shown that the maximum of track density increase with increase in the time exposed of laser at each case of power, the track density has the maximum value at -10 mw laser power, the reason of increase was because increase in elasticity of detector at increase of time exposure and laser power.

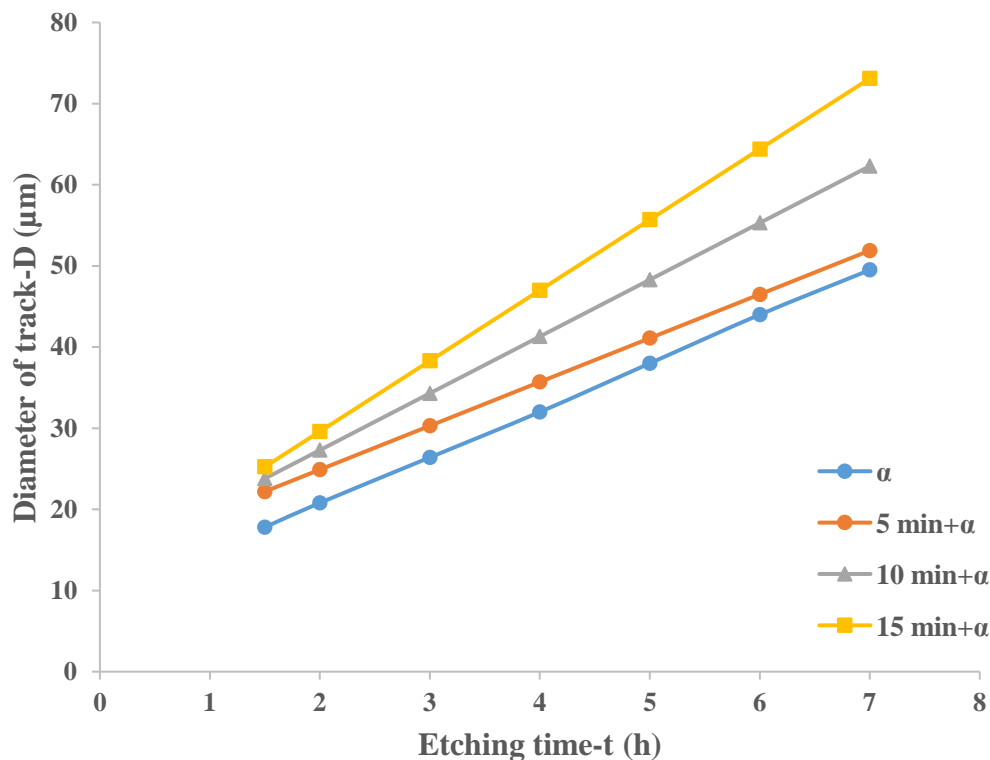


Figure (4-1) Diameter of track vs. Etching time for detector exposed to laser beam at 1 mW power, compared with detector irradiated with alpha particle.

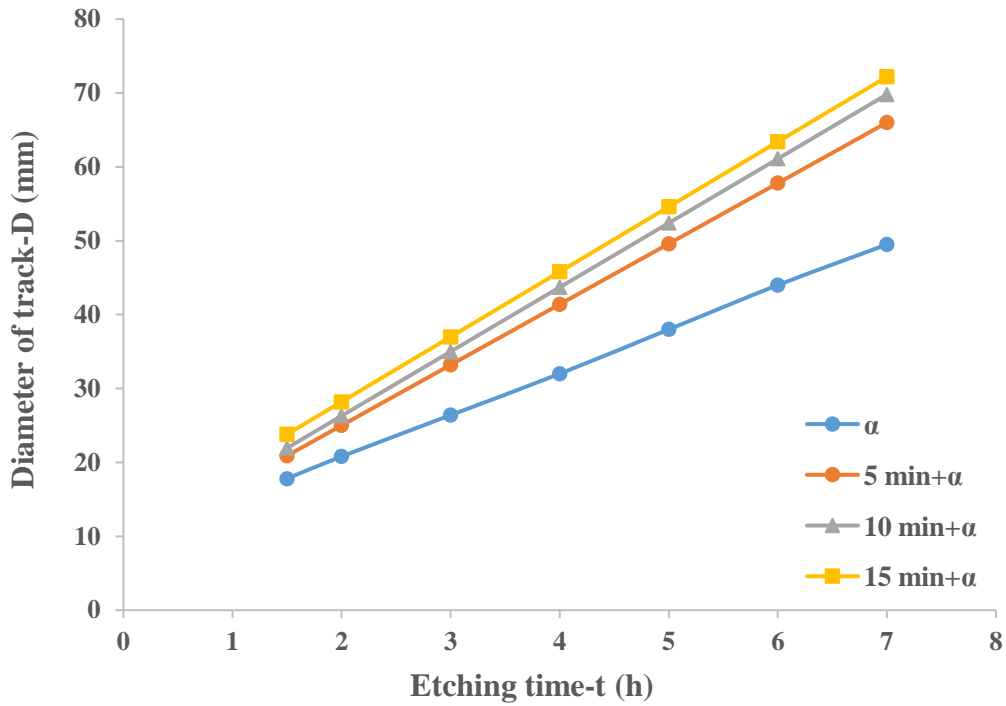


Figure (4-2) Diameter of track vs. Etching time for detector exposed to laser beam at 5 mW power, compared with detector irradiated with alpha particle.

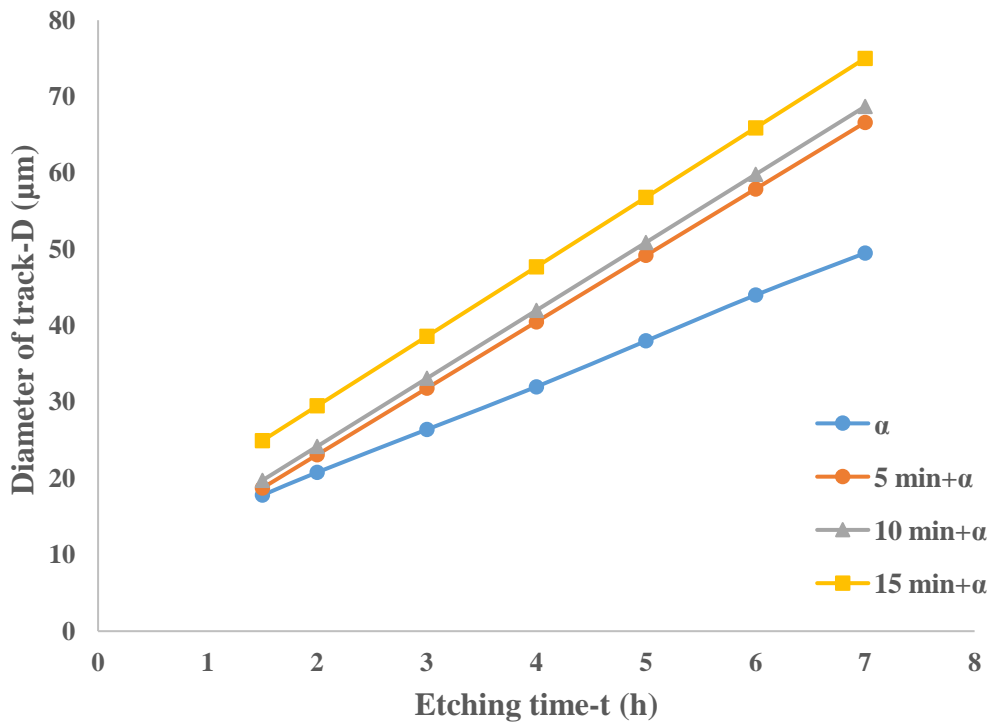


Figure (4-3) Diameter of track vs. Etching time for detector exposed to laser beam at 10 mW power, compared with detector irradiated with alpha particle.

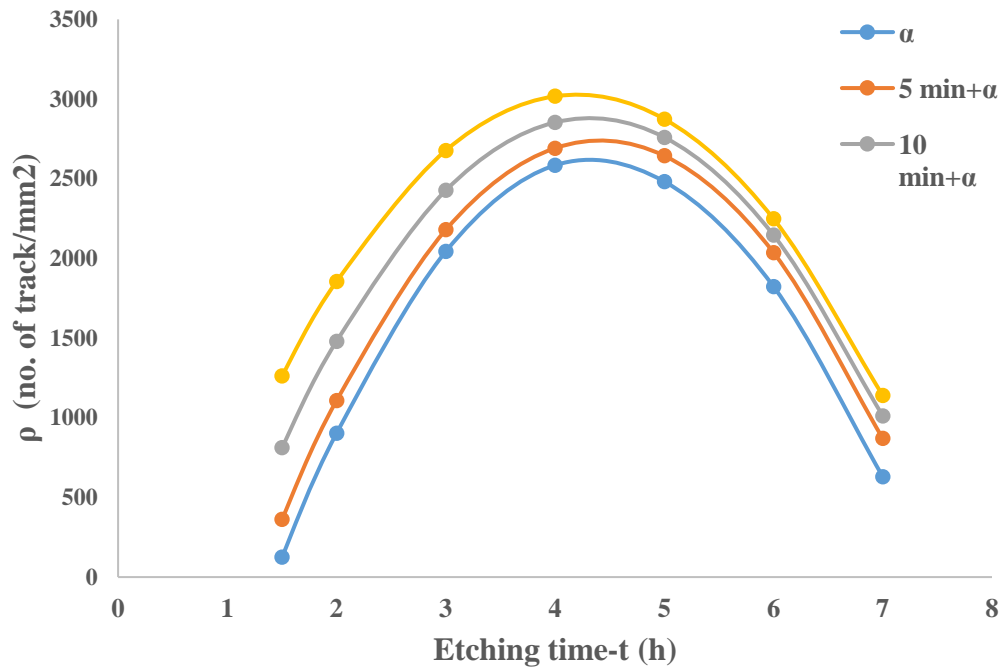


Figure (4-4) Track density vs. Etching time for detector exposed to laser beam at 1 mW power, compared with detector irradiated with alpha particle.

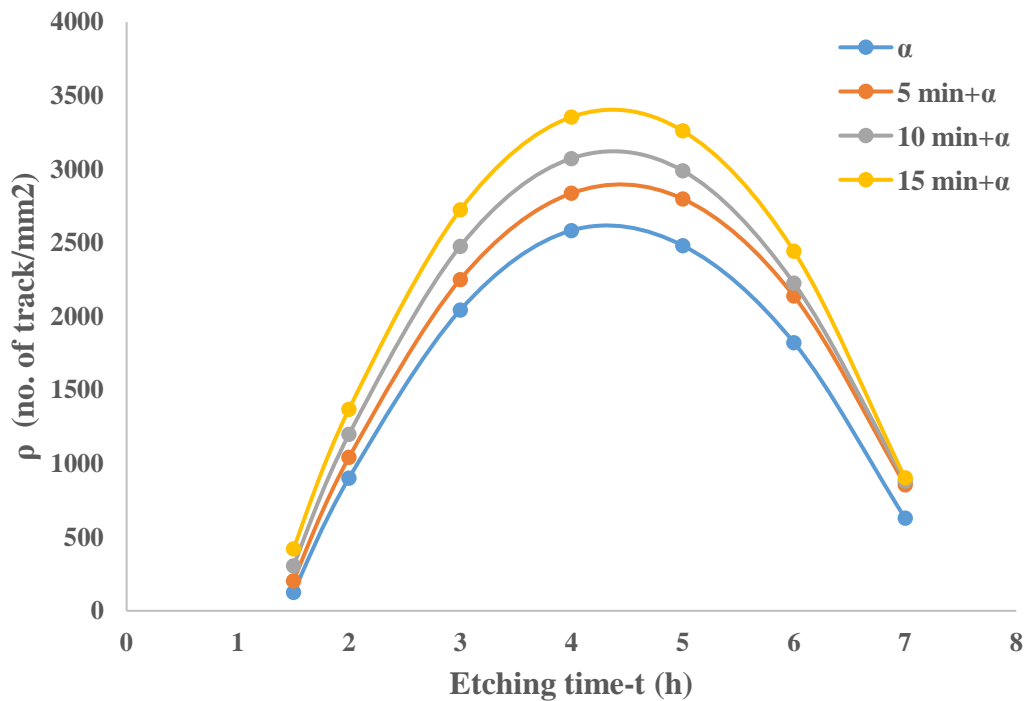


Figure (4-5) Track density vs. Etching time for detector exposed to laser beam at 5 mW power, compared with detector irradiated with alpha particle.

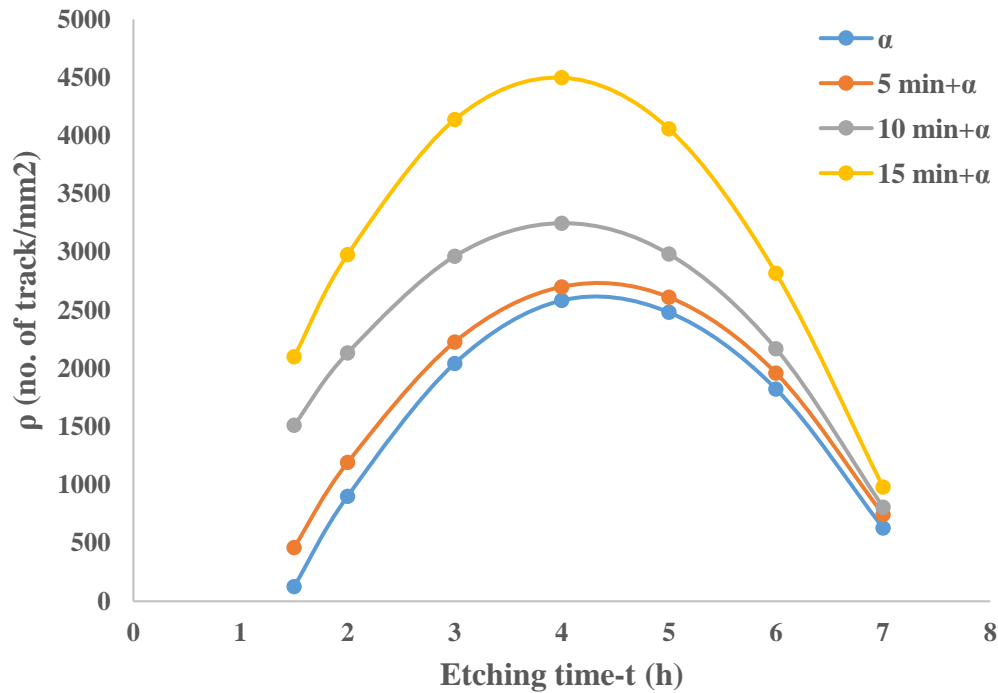


Figure (4-6) Track density vs. Etching time for detector exposed to laser beam at 10 mW power, compared with detector irradiated with alpha particle.

The relation between detectors weight and etching time for detector exposed to laser beam at different power were shown in figures (4-7) to (4-9), these figures show that increasing in the exposure time of laser at different power cause to decrease in the weight of detectors after etching, because of increase in the thickness of remove layers from the detectors. The bulk etch rate- V_B calculated using equation (2-3) for detector at different powers of laser beam and different times exposure.

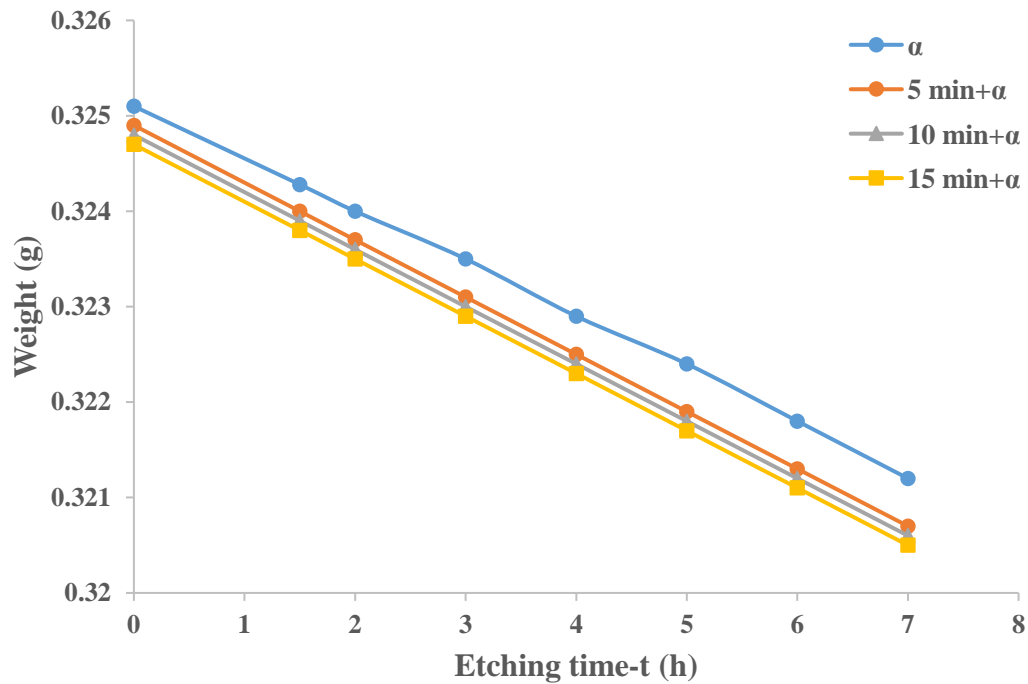


Figure (4-7) Weight of detector vs. Etching time for detector exposed to laser beam at 1 mW power, compared with detector irradiated with alpha particle.

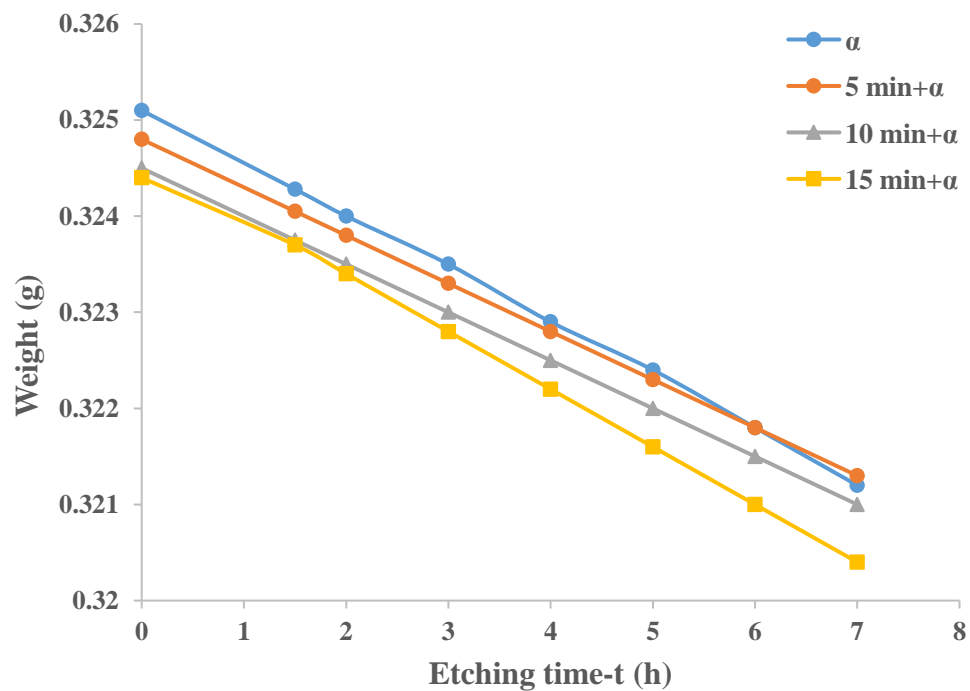


Figure (4-8) Weight of detector vs. Etching time for detector exposed to laser beam at 5 mW power, compared with detector irradiated with alpha particle.

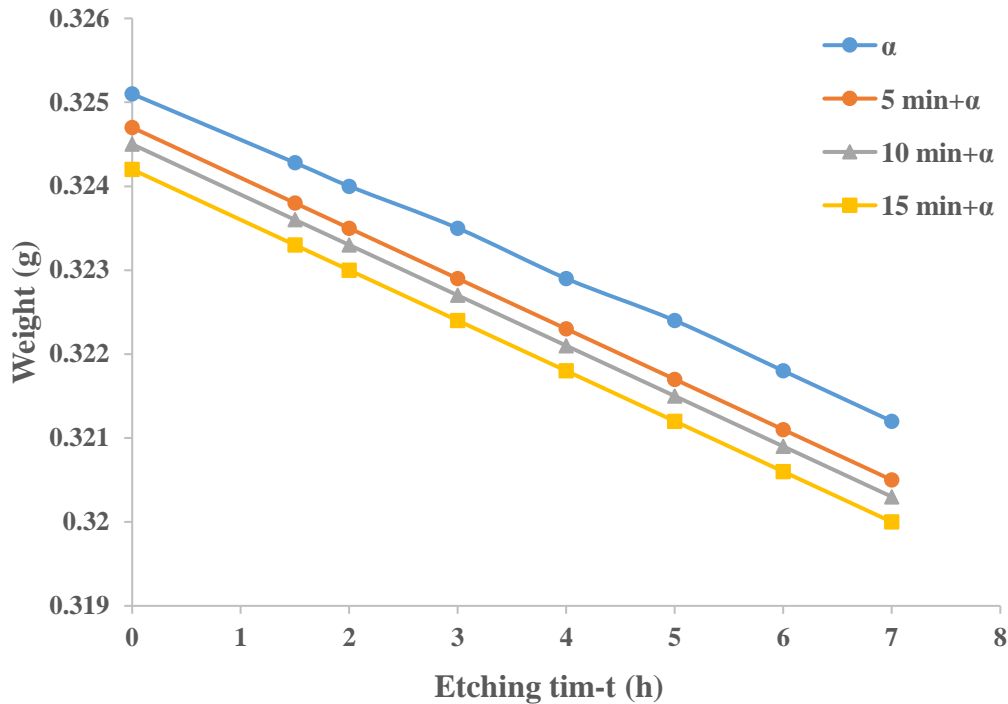


Figure (4-9) Weight of detector vs. Etching time for detector exposed to laser beam at 10 mW power, compared with detector irradiated with alpha particle.

The diameter etch rate- V_D and track etch rate- V_T were calculated using equations (2-1) and (2-2).

The relation between the etch rates (V_D , V_B and V_T) and the laser exposed time- t for detector exposed to laser beam at (1, 5 and 10 mW) powers were shown in figures (4-10) to (4-12), they show that increasing in exposure time of laser light for each power values lead to increase in the values of etch rates. The relation between the etch ratio- V and exposure time to laser light at different power were shown in figure (4-13), it shows that at-1 mW power the etch ratio decrease at increases the exposure time of laser while for (5, 10 mW) power it shows that increasing in the etch ratio values at increase of exposure time of laser.

The critical angle- Θ_c and efficiency- η were calculated using equations (2-4) and (2-5).

The values of critical angle- Θ_c and efficiency- η at different exposure time of laser light for laser power (1,5 and 10 mW) were shown in table (4-1), and we conclude that increasing in the exposure time of laser for each case of power lead to increase critical angle value because of increasing in the values of the etch rates (V_B and V_T) and this lead to increase values of critical angle, while the efficiency of etching decrease at increase in the exposure time of laser for all power the reason was that the increasing in the values of etch rates (V_B and V_T) lead to increasing in values of (V_B/V_T) and thus to decrease in the efficiency of etching.

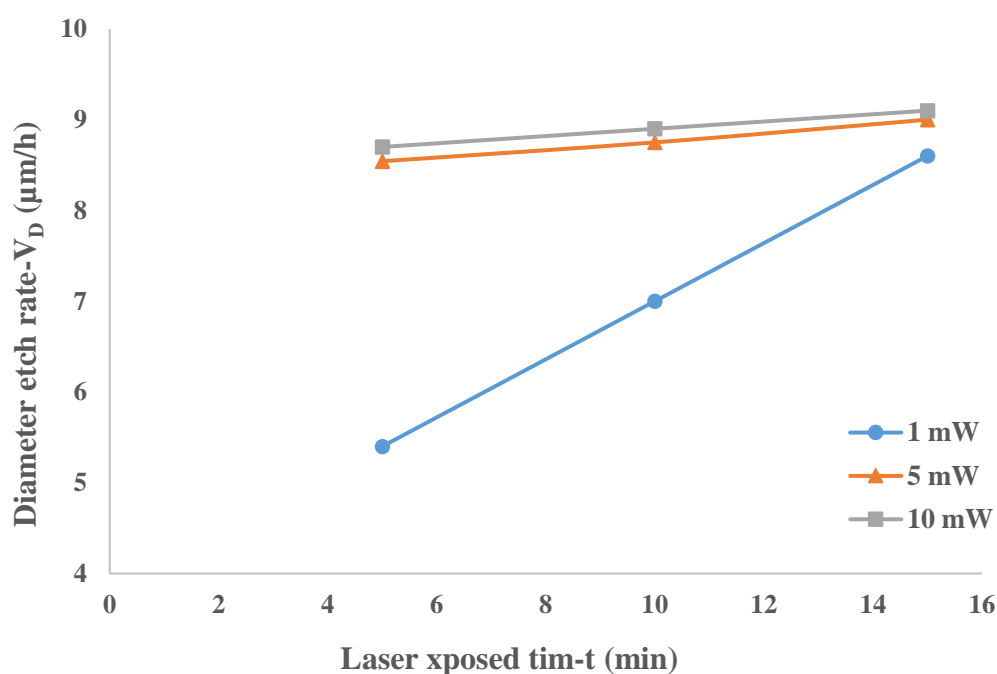


Figure (4-10) Diameter etch rate vs. laser exposed time for detector exposed to laser beam at different powers.

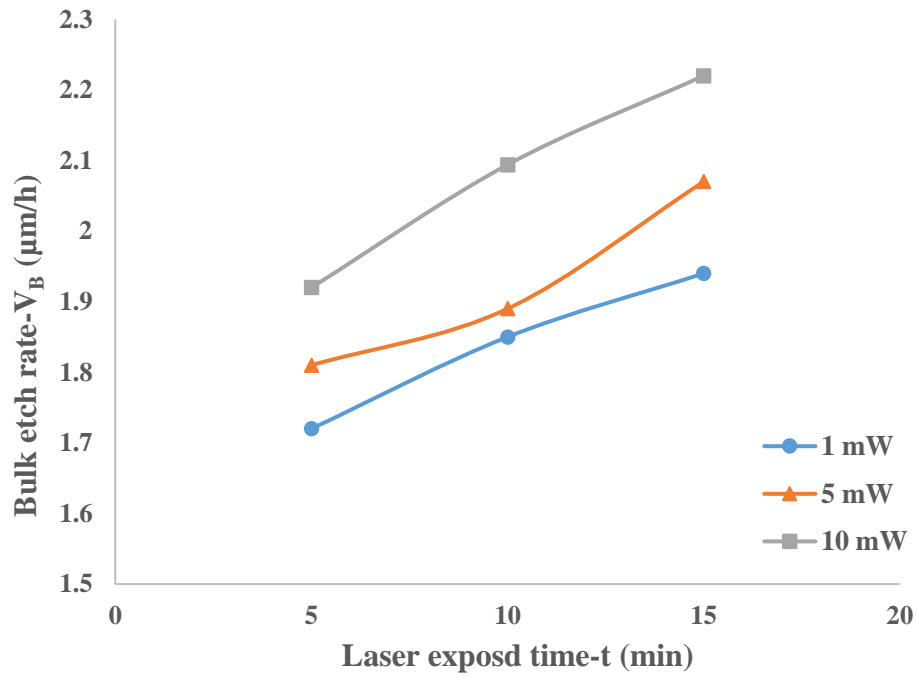


Figure (4-11) Bulk etch rate vs. laser exposed time for detector exposed to laser beam at different powers.

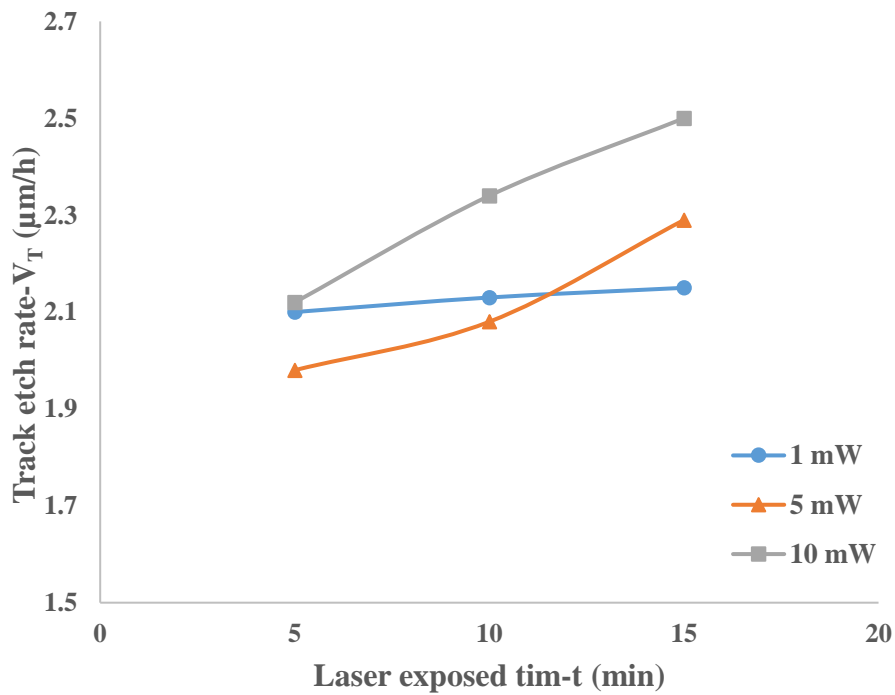


Figure (4-12) Track etch rate vs. laser exposed time of He-Ne laser at different powers.

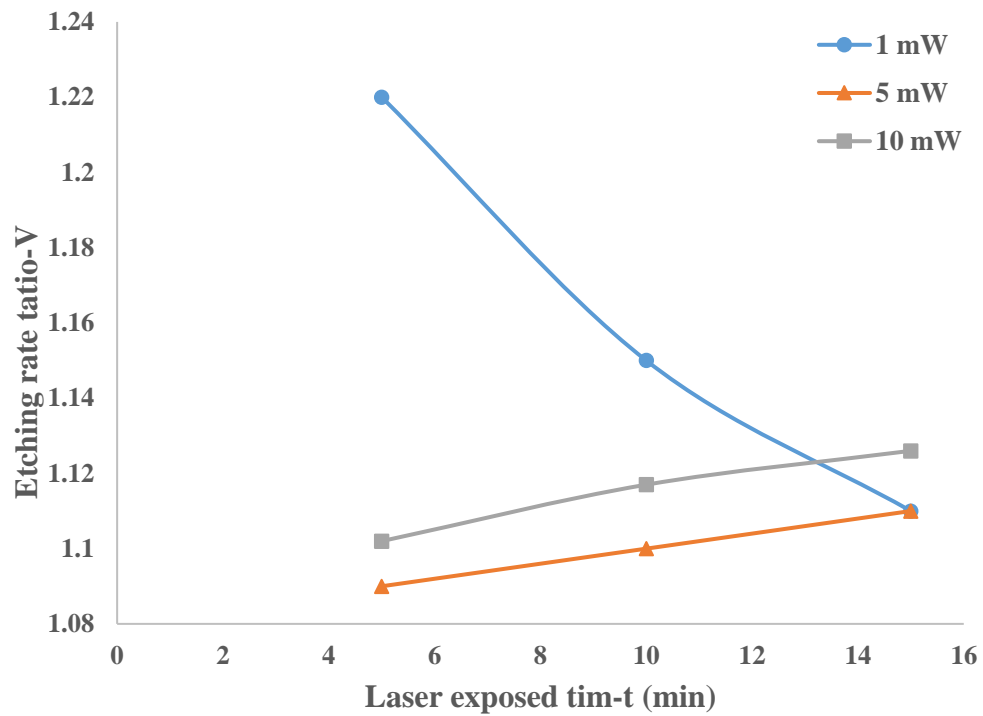


Figure (4-13) Etching rate ratio vs. laser exposed time for detector exposed to laser beam at different powers.

Table (4 -1) Various track etching parameters for detector exposed to laser beam for (1, 5 and 10 mW) powers at different times.

P (mW)	t (min)	V _D (μm/h)	V _B (μm/h)	V _T (μm/h)	V	Θ _C	η	S
1	5	5.4	1.72	2.1	1.22	54.78	0.183	0.22
	10	7	1.85	2.13	1.15	60.32	0.131	0.15
	15	8.6	1.95	2.15	1.1	64.49	0.097	0.1
5	5	8.549	1.81	1.984	1.094	66.07	0.086	0.094
	10	8.7	1.89	2.08	1.099	65.49	0.09	0.099
	15	9	2.07	2.297	1.111	64.16	0.1001	0.111
10	5	8.7	1.92	2.116	1.102	65.15	0.093	0.102
	10	8.9	2.09	2.34	1.117	63.54	0.105	0.117
	15	9.1	2.22	2.503	1.127	62.53	0.112	0.127

4.3 Effect of gamma ray and (He-Ne) laser on CR-39 detectors

4.3.1 UV-VIS spectroscopy

The relation between the absorbance and the wavelength at range (300-500 nm) using UV-Vis spectroscopy for detector un-irradiated (Control) and exposed to laser beam for power (1,5 and 10 mW) at different times were shown in figures from (4-14) to (4-16), the results show that the absorbance increased with the decreases in the wavelength and increasing in exposure time of laser for each case of laser power.

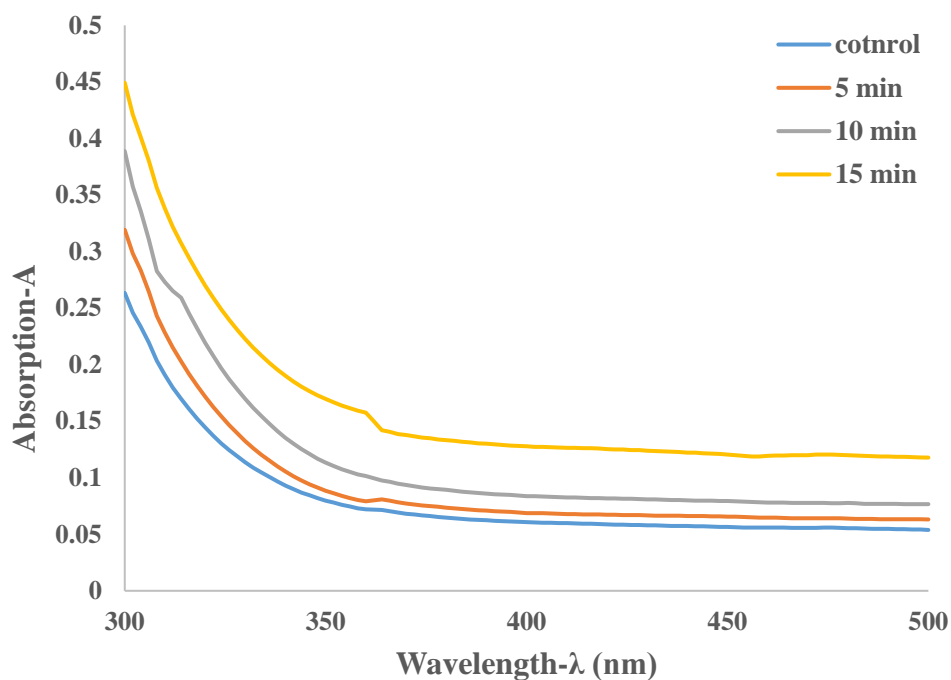


Figure (4-14) UV-Vis. at range (300-500 nm) for detector irradiated by laser beam at exposure times 5, 10 and 15 min at power 1 mW, compared with un-irradiated detector control.

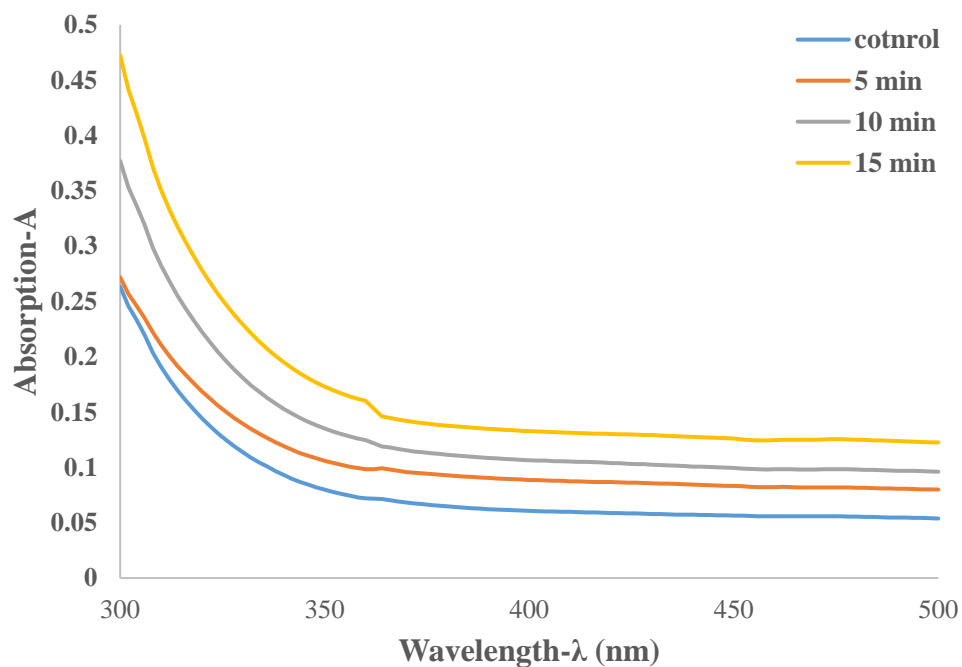


Figure (4-15) UV-Vis. at range (300-500 nm) for detector irradiated by laser beam at exposure times 5, 10 and 15 min at power 5 mW, compared with un-irradiated detector control.

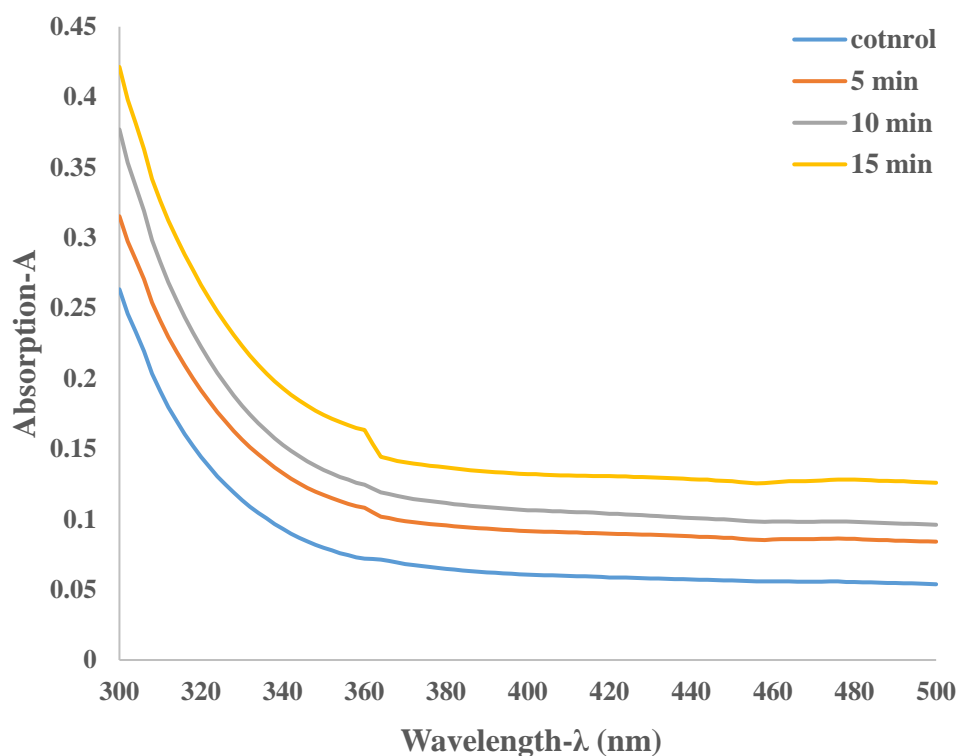


Figure (4-16) UV-Vis. at range (300-500 nm) for detector irradiated by laser beam at exposure times 5, 10 and 15 min at power 10 mW, compared with un-irradiated detector control.

The relation between the absorbance and the wavelength at range (330-500 nm) for detector un-irradiated (control) and irradiated with gamma ray at different doses (300, 500, 800, 1200 and 1600 kGy) were shown in figure (4-17), the results show that increased in the absorbance values with the increase in the gamma ray dose.

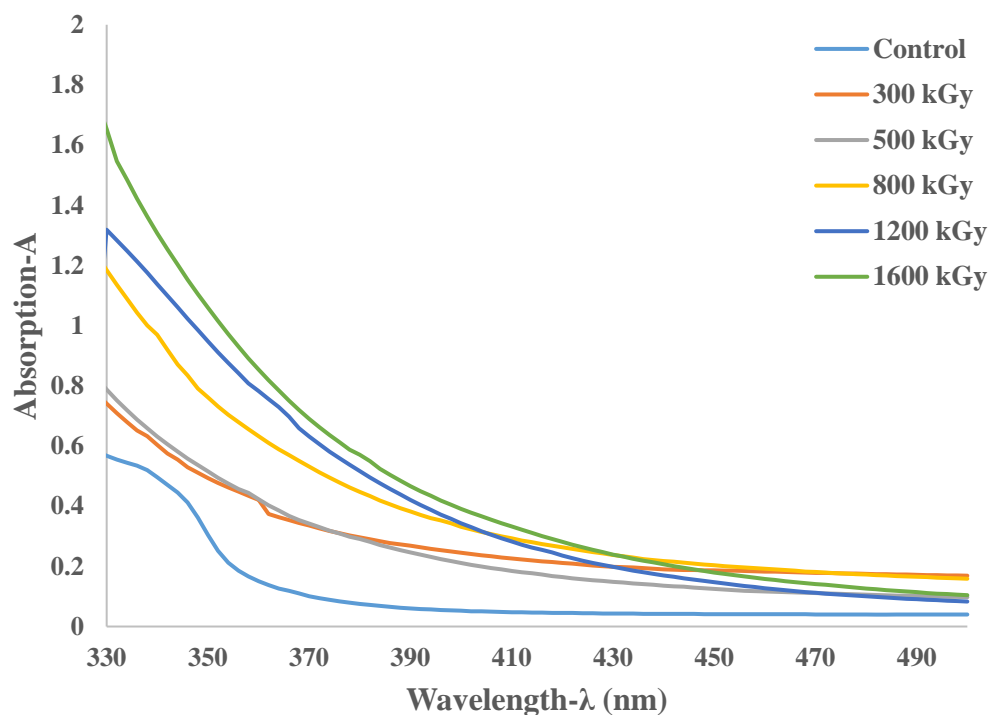


Figure (4-17) UV-Vis. at range (330-500 nm) for detector irradiated by gamma radiation at doses (300, 500, 800, 1200 and 1600 kGy), compared with un-irradiated detector control.

Figure (4-18) represents the relation between the absorbance and the wavelength at range (330-530 nm) for detector un-irradiated (control) and irradiated with gamma ray with doses of (300, 500, 800, 1200 and 1600 kGy) then exposed to laser beam for 15 min at 10 mW power, the results show that the absorbance were increased with increase in the radiation dose of gamma ray. Ultraviolet absorption in detector is due to breaking in bands and displacement of electrons and atoms. The displacement of electrons and ions migrate through the material until they are trapped in the lattice, thus leaving deficient regions. The electronic and ionic configurations thus formed may cause preferential light absorption at particular wavelength. The interaction also produces organic species which play a significant role in the absorption of ultraviolet light.

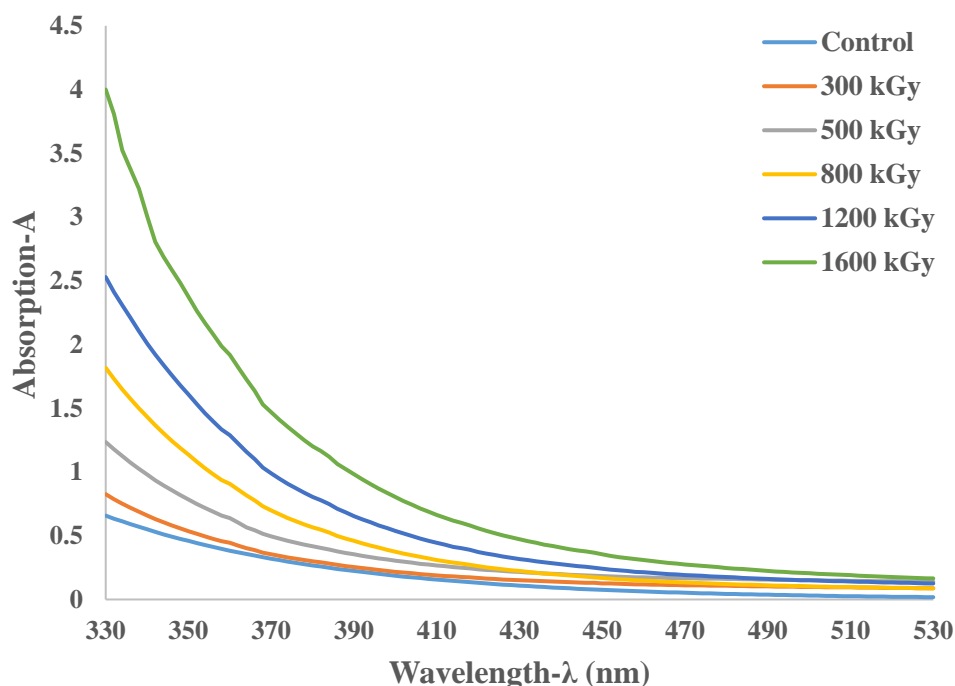


Figure (4-18) UV-Vis. at range (330-500 nm) for detector irradiated with gamma ray for various dose (300, 500, 800, 1200 and 1600 kGy) then exposed for laser beam of 10 mW power at time 15 min, compared with un-irradiated detector control.

4.3.2 Band gap energy measurement

The optical band gap energy- E_g for detector were measured using equation (2-10), and for ($n = 1/2$) direct allowed and ($n = 2$) indirect allowed transitions.

The direct and indirect optical band gap energy- E_g for detector is calculated for un-irradiated and for detector exposed to laser beam for different times at different powers shown in figures (4-19) to (4-28), the results show that a decreasing in the energy gap with an increase in the exposure time of laser and for each case as shown in the figures (4-39) and (4-40), because of increase in the absorbance as we have declared earlier. The results shown in the table (4-4) confirms that the exposed to (He-Ne) laser created defects in the detector (polymers) (free radicals, etc.), which increases the electronic disorder inducing the creation of an allowed state in the forbidden gap or the deformation of the valance band. Moreover, the values of energy band gaps in the case of direct

transition are higher than in the indirect transition, due to existence of delocalized states between conducting band and valance band.

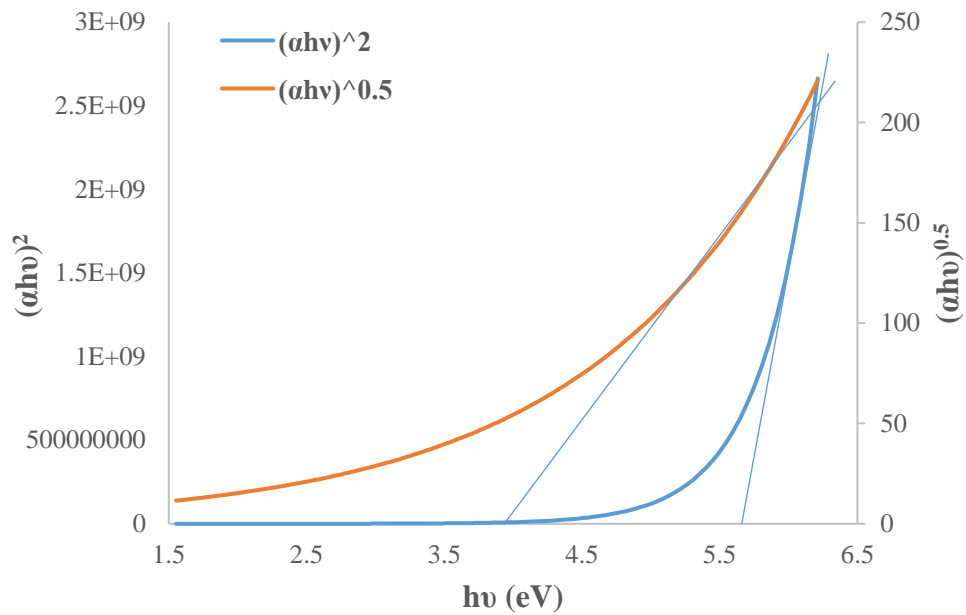


Figure (4-19) Behavior of $(\alpha hv)^2$ and $(\alpha hv)^{0.5}$ vs. Photon energy ($h\nu$) for un-irradiated detectors.

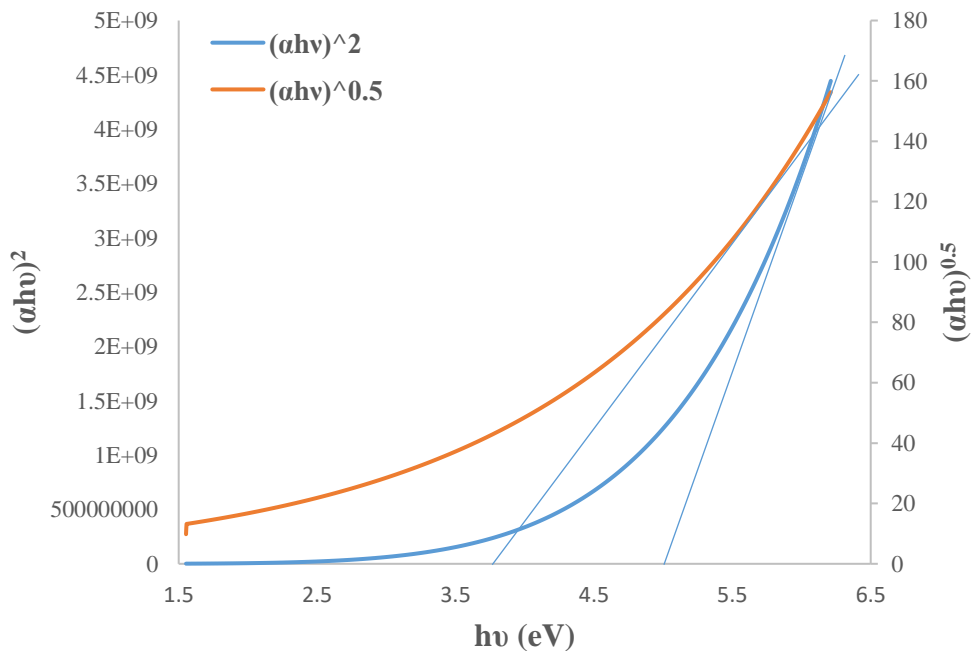


Figure (4-20) Behavior of $(\alpha hv)^2$ and $(\alpha hv)^{0.5}$ vs. Photon energy ($h\nu$) for CR-39 detectors exposed to 5 min of laser at 1 mW power.

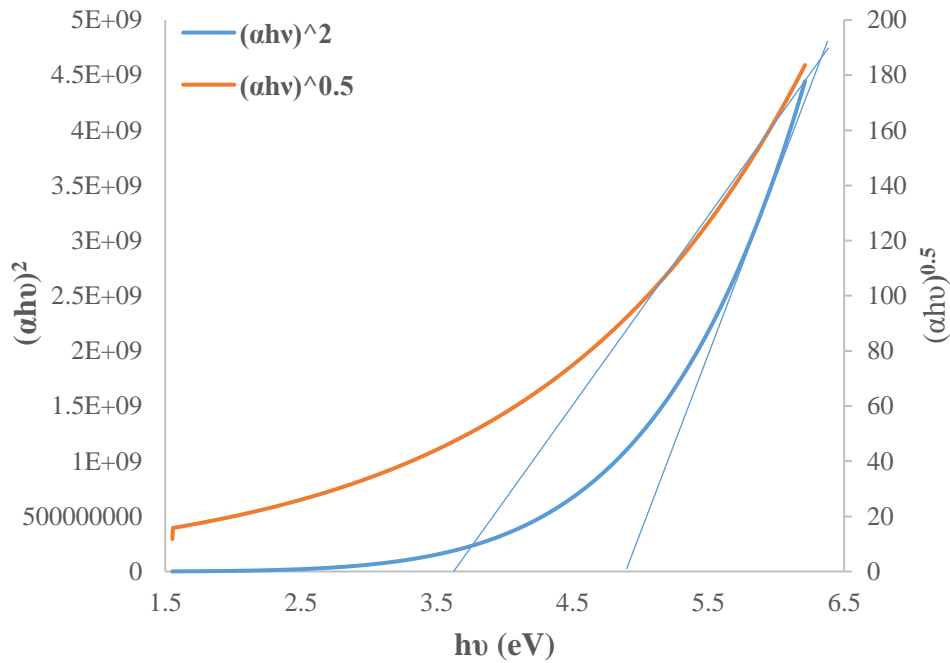


Figure (4-21) Behavior of $(\alpha h\nu)^2$ and $(\alpha h\nu)^{0.5}$ vs. Photon energy ($h\nu$) for detector exposed to 10 min of laser beam at 1 mW power.

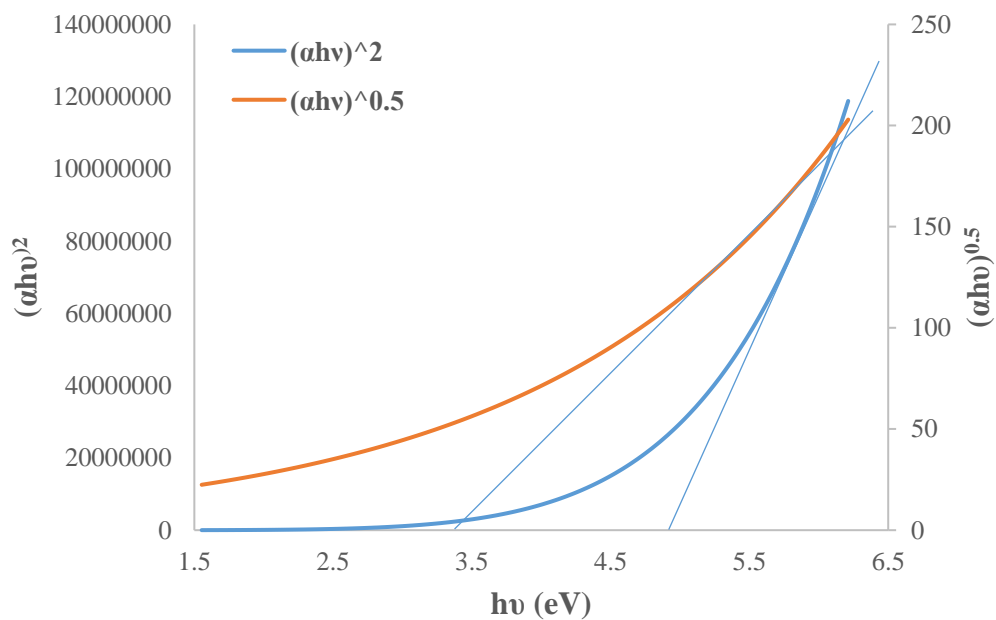


Figure (4-22) Behavior of $(\alpha h\nu)^2$ and $(\alpha h\nu)^{0.5}$ vs. Photon energy ($h\nu$) for detector exposed to 15 min of laser beam at 1 mW power.

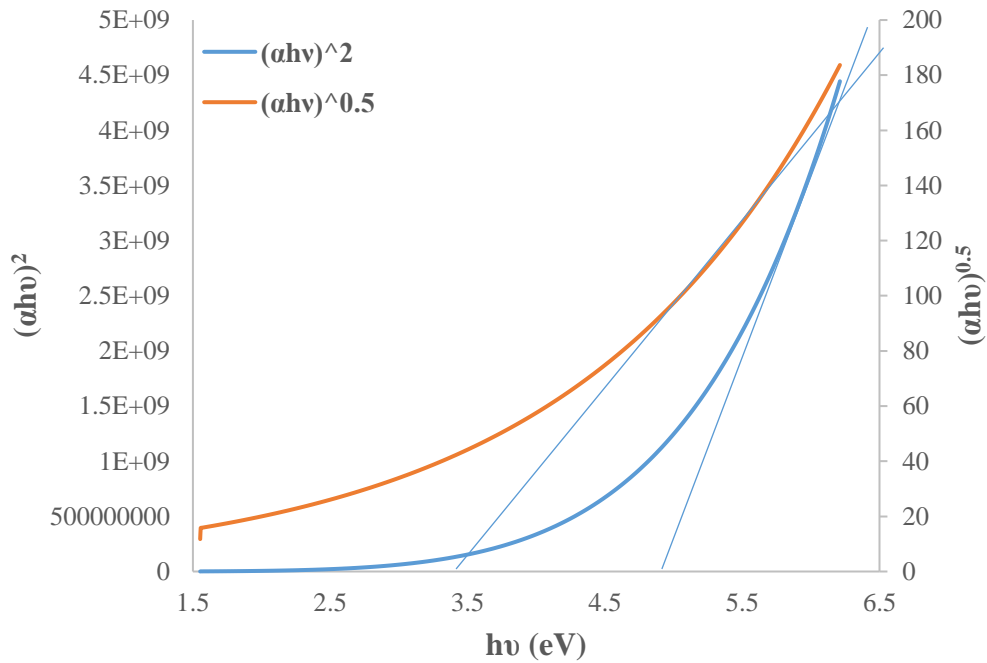


Figure (4-23) Behavior of $(\alpha h\nu)^2$ and $(\alpha h\nu)^{0.5}$ vs. Photon energy ($h\nu$) for detector exposed to 5 min of laser beam at 5 mW power.

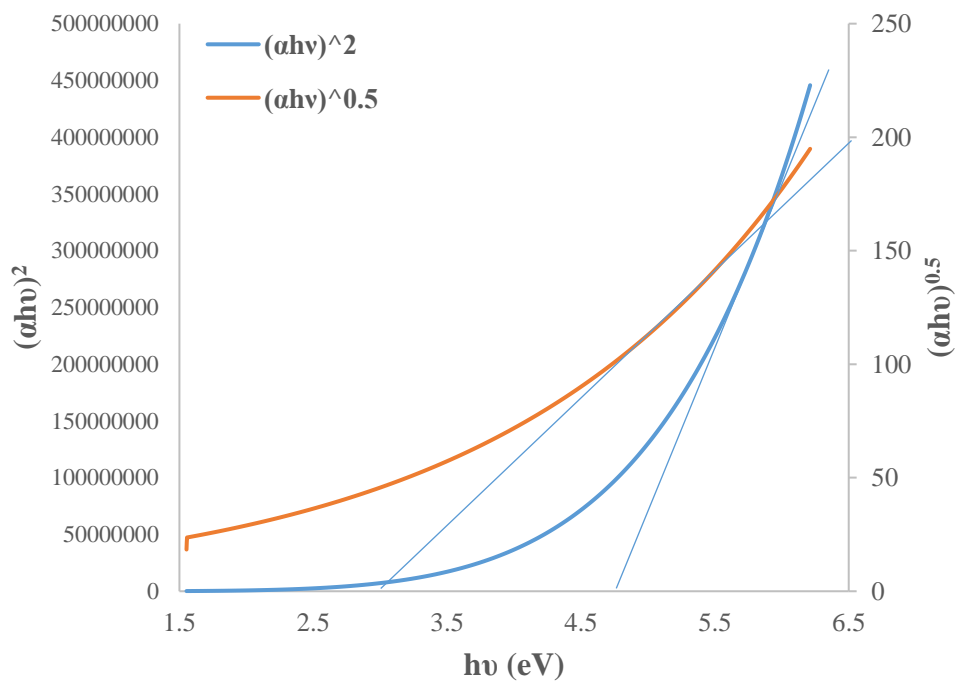


Figure (4-24) Behavior of $(\alpha h\nu)^2$ and $(\alpha h\nu)^{0.5}$ vs. Photon energy ($h\nu$) for detector exposed to 10 min of laser beam at 5 mW power.

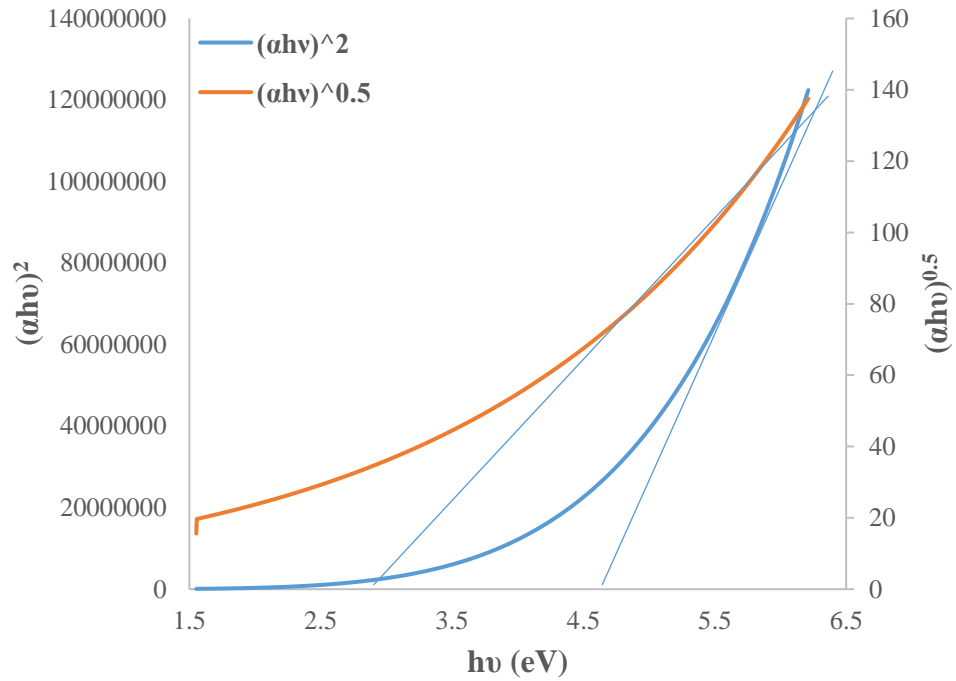


Figure (4-25) Behavior of $(\alpha h\nu)^2$ and $(\alpha h\nu)^{0.5}$ vs. Photon energy ($h\nu$) for detector exposed to 15 min of laser beam at 5 mW power.

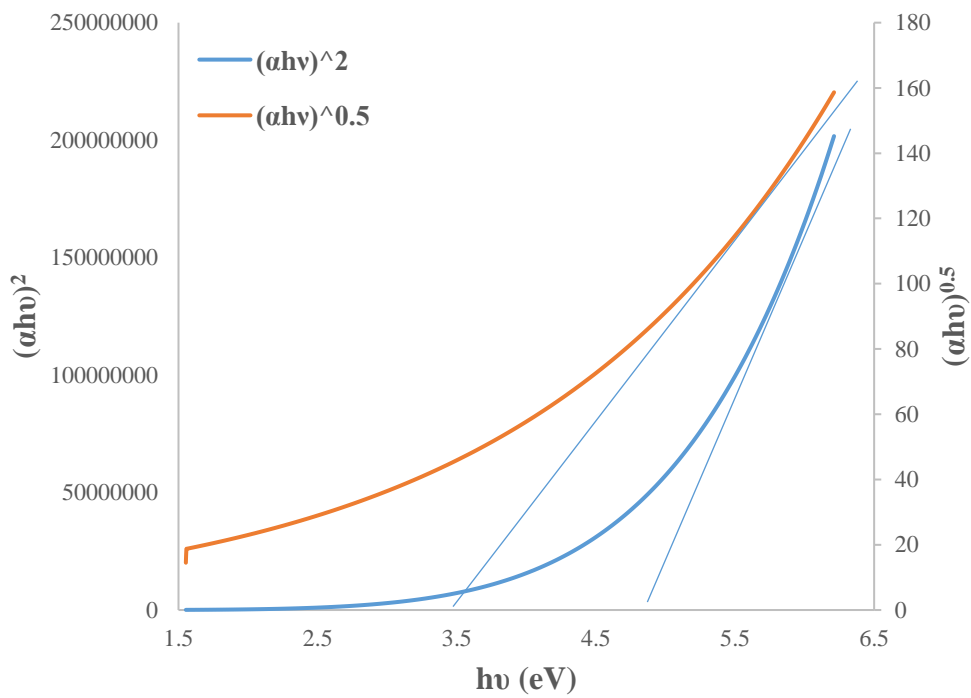


Figure (4-26) Behavior of $(\alpha h\nu)^2$ and $(\alpha h\nu)^{0.5}$ vs. Photon energy ($h\nu$) for detector exposed to 5 min of laser beam at 10 mW power.

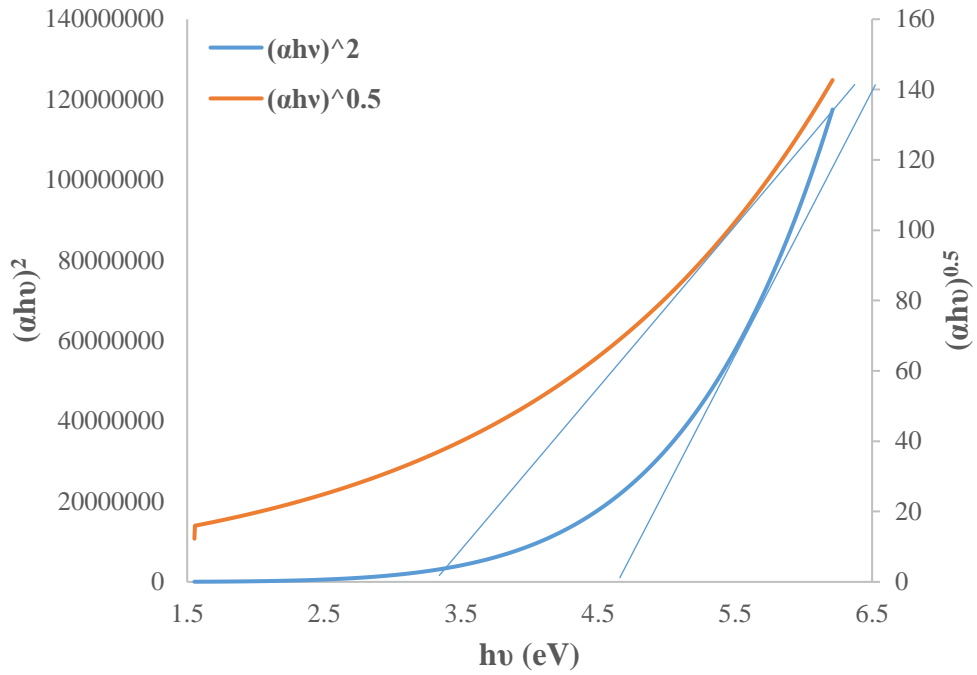


Figure (4-27) $(\alpha h\nu)^2$ and $(\alpha h\nu)^{0.5}$ vs. Photon energy ($h\nu$) for detector exposed to 10 min of laser beam at 10 mW power.

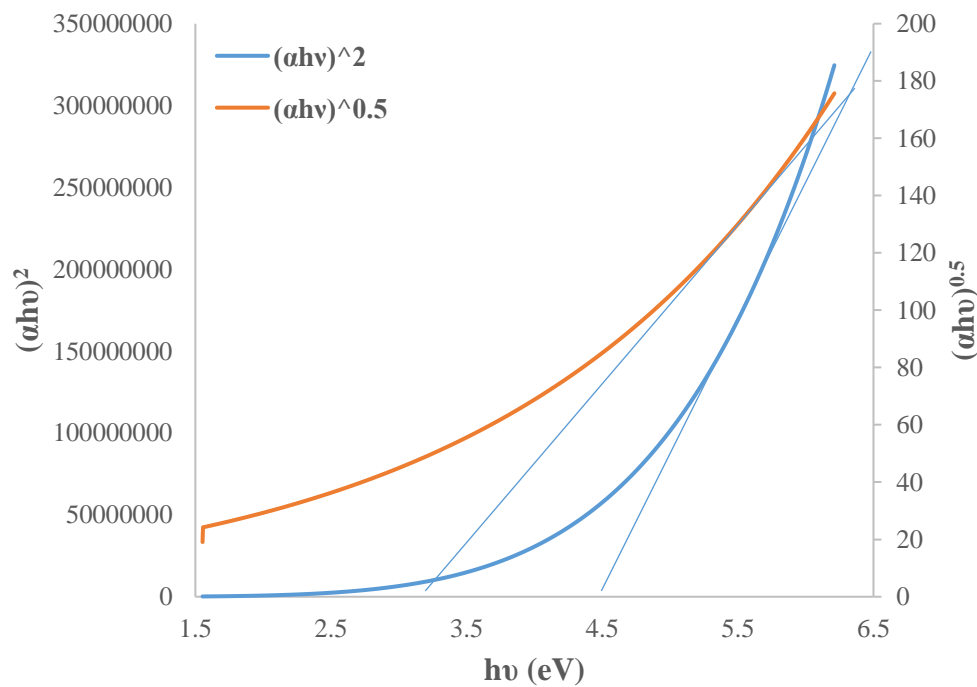


Figure (4-28) Behavior of $(\alpha h\nu)^2$ and $(\alpha h\nu)^{0.5}$ vs. Photon energy ($h\nu$) for detector exposed to 15 min of laser beam at 10 mW power.

The direct and indirect optical band gap energy- E_g were calculated for detector which irradiated by gamma ray at radiation dose (300, 500, 800, 1200 and 1600 kGy) as shown in figures (4-29) to (4-33). The results show that a decreasing in the energy gap with an increase in the exposure time of laser and for each case as shown in the figures (4-41) and (4-42), because of increase in the absorbance as we have declared earlier.

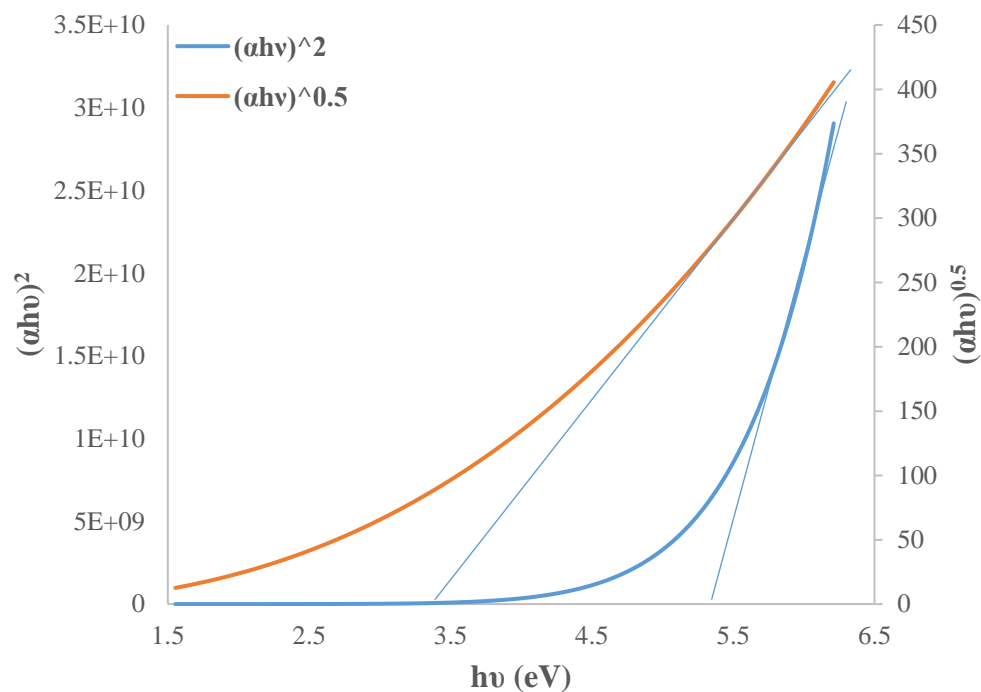


Figure (4-29) Behavior of $(\alpha hv)^2$ and $(\alpha hv)^{0.5}$ vs. Photon energy (hv) for detector irradiated with gamma ray at 300 kGy dose.

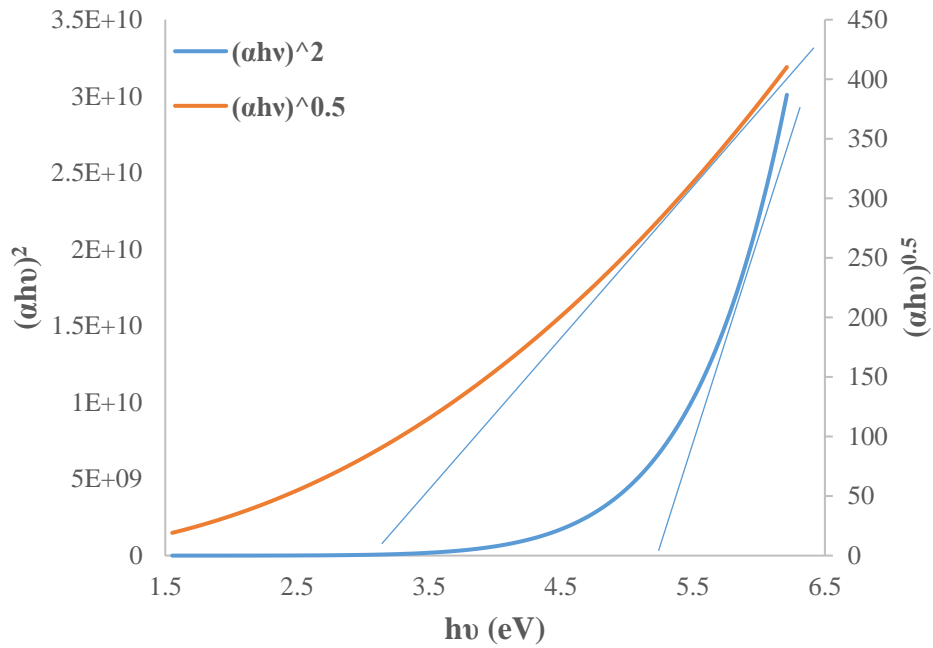


Figure (4-30) Behavior of $(\alpha hv)^2$ and $(\alpha hv)^{0.5}$ vs. Photon energy ($h\nu$) for detector irradiated with gamma ray at 500 kGy dose.

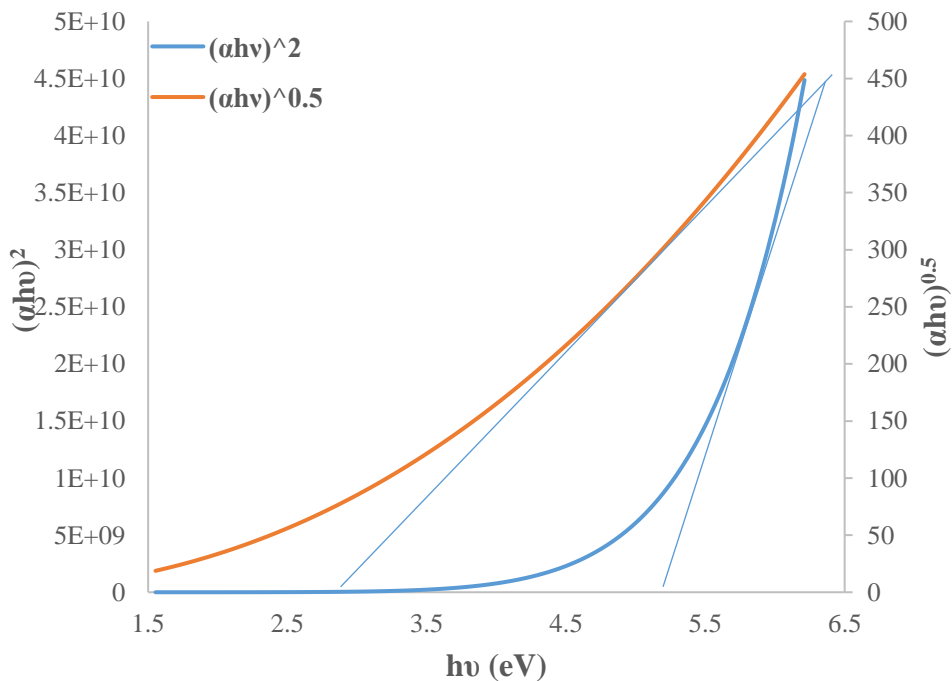


Figure (4-31) Behavior of $(\alpha hv)^2$ and $(\alpha hv)^{0.5}$ vs. Photon energy ($h\nu$) for detector irradiated with gamma ray at 800 kGy dose.

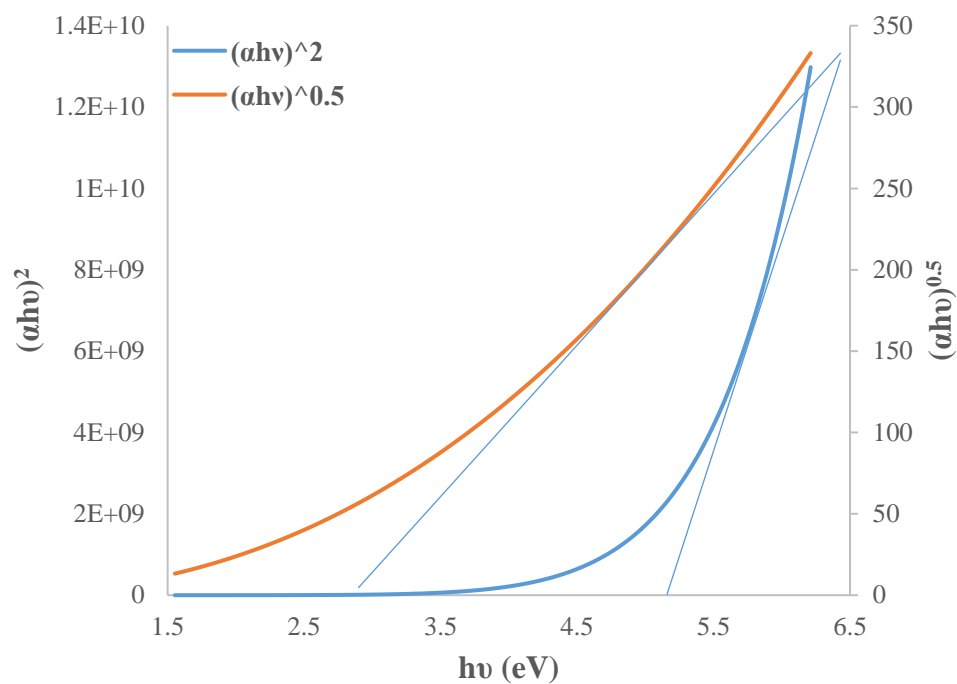


Figure (4-32) Behavior of $(\alpha hv)^2$ and $(\alpha hv)^{0.5}$ vs. Photon energy (hv) for detector irradiated with gamma ray at 1200 kGy dose.

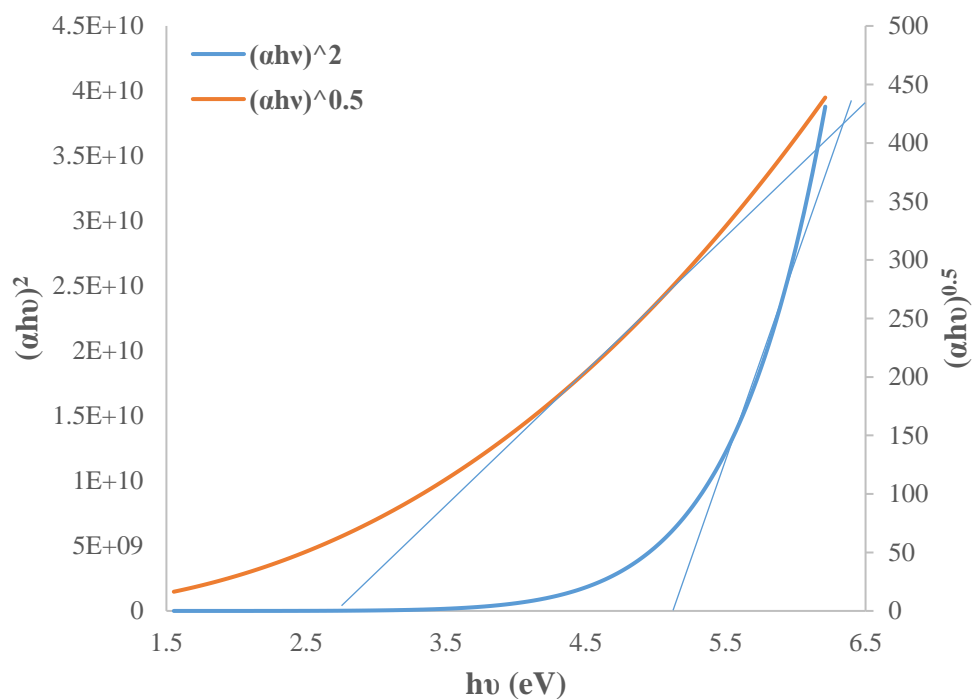


Figure (4-33) Behavior of $(\alpha hv)^2$ and $(\alpha hv)^{0.5}$ vs. Photon energy (hv) for detector irradiated with gamma ray at 1600 kGy dose.

The direct and indirect optical energy band gap- E_g were calculated for detector irradiate with various doses of gamma ray (300, 500, 800,1200 and 1600 kGy), then exposed to laser beam for-15 min at -10 mW power were shown in figures from (4-34) to (4-38), the results show that a decreasing in the energy gap with an increase in the dose of gamma ray and for each case as shown in the figures (4-43) and (4-44), because of increase in the absorbance as we have declared earlier.

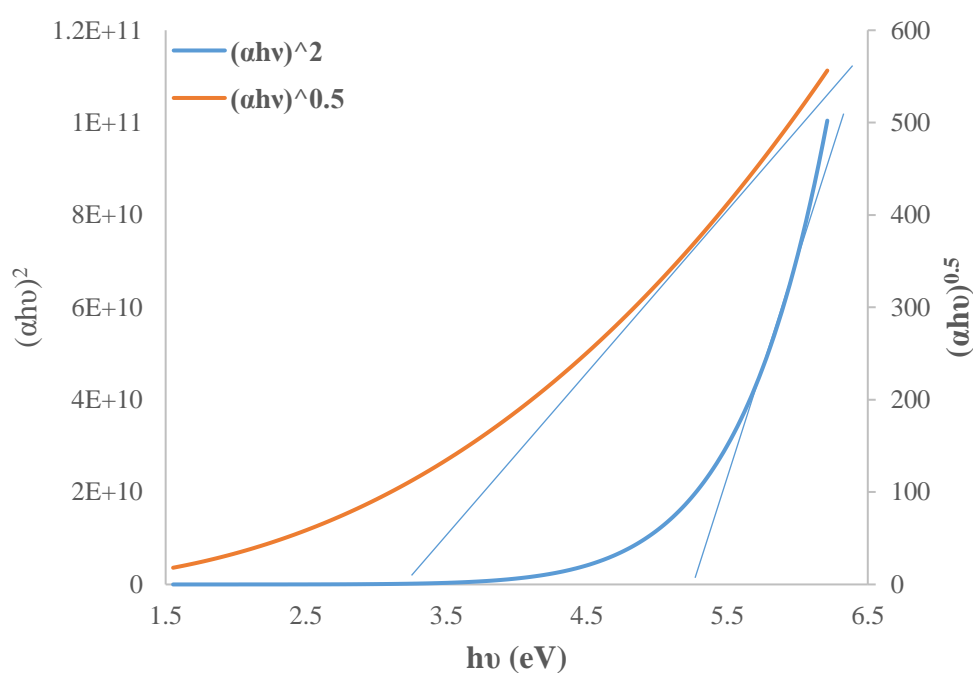


Figure (4-34) Behavior of $(\alpha hv)^2$ and $(\alpha hv)^{0.5}$ vs. Photon energy (hv) for detector irradiated with gamma ray dose 300 kGy, then exposed to 15 min of laser beam at 10 mW power.

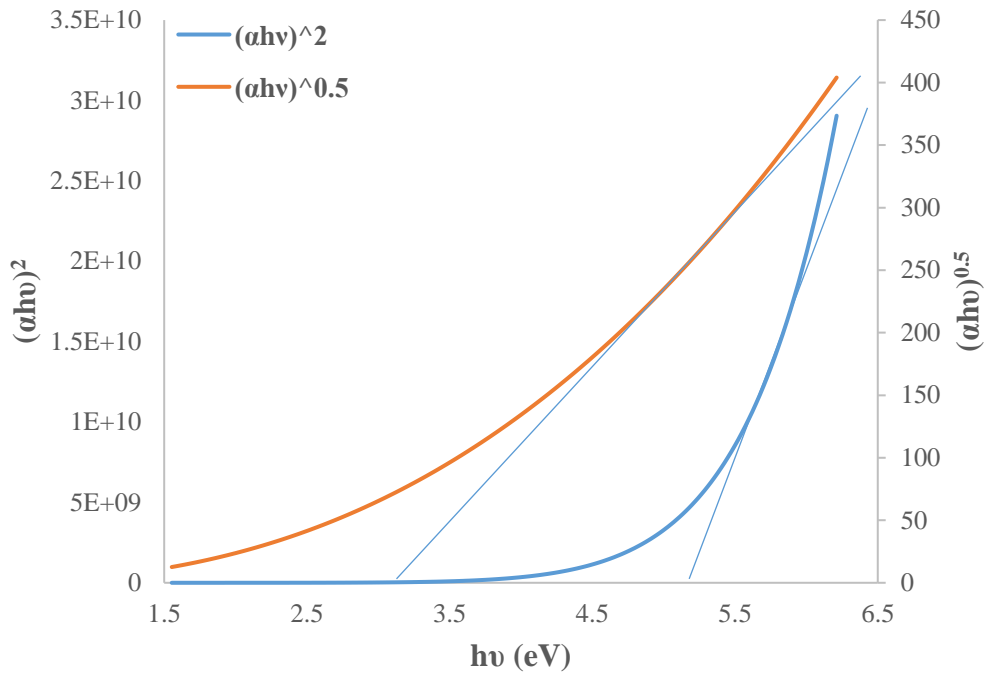


Figure (4-35) $(\alpha h\nu)^2$ and $(\alpha h\nu)^{0.5}$ vs. Photon energy ($h\nu$) for detector irradiated with gamma ray dose 500 kGy, then exposed to 15 min of laser beam of 10 mW power.

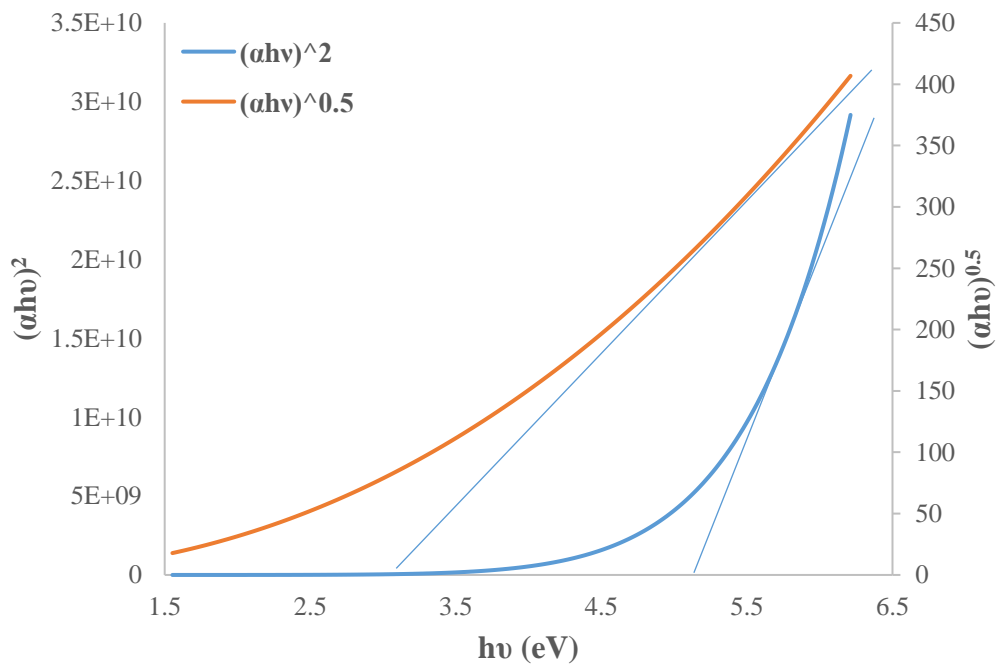


Figure (4-36) Behavior of $(\alpha h\nu)^2$ and $(\alpha h\nu)^{0.5}$ vs. Photon energy ($h\nu$) for CR-39 detector irradiated with gamma ray dose 800 kGy and exposed to 15 min of laser beam of 10 mW power.

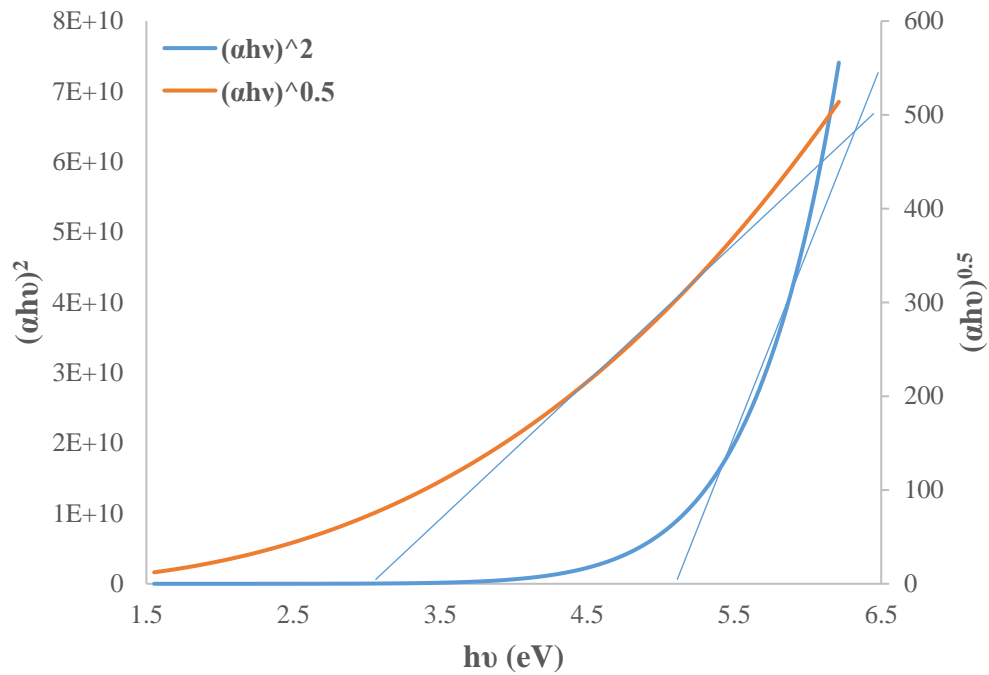


Figure (4-37) Behavior of $(\alpha hv)^2$ and $(\alpha hv)^{0.5}$ vs. Photon energy ($h\nu$) for detector irradiated with gamma ray dose 1200 kGy, then exposed to 15 min of laser beam of 10 mW power.

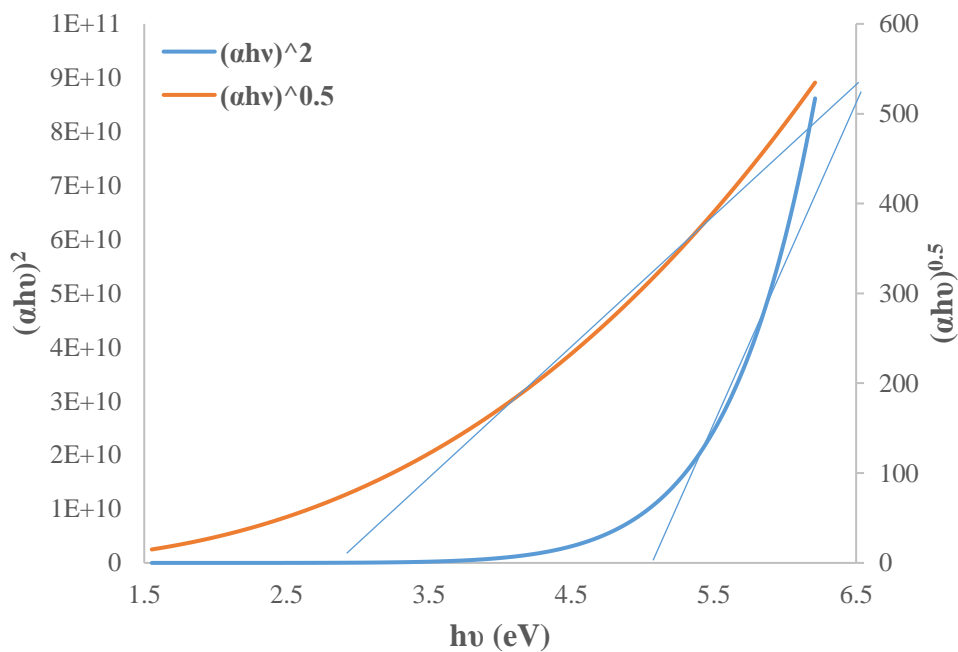


Figure (4-38) Behavior of $(\alpha hv)^2$ and $(\alpha hv)^{0.5}$ vs. Photon energy ($h\nu$) for detector irradiated with gamma ray dose 1600 kGy, then exposed to 15 min of laser beam of 10 mW power.

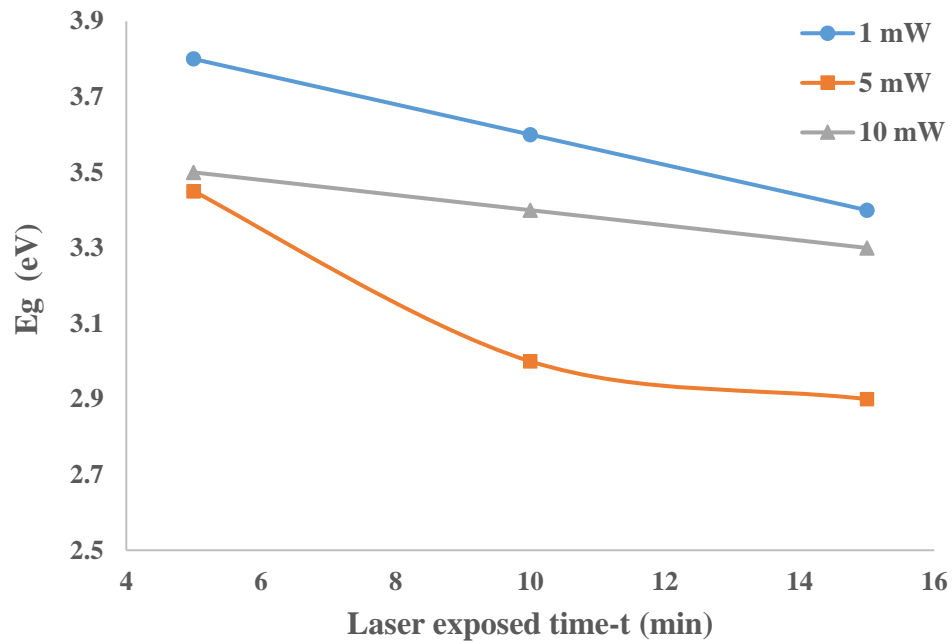


Figure (4-39) Indirect optical band gap energy vs. laser exposed time for detector exposed to laser beam at different powers.

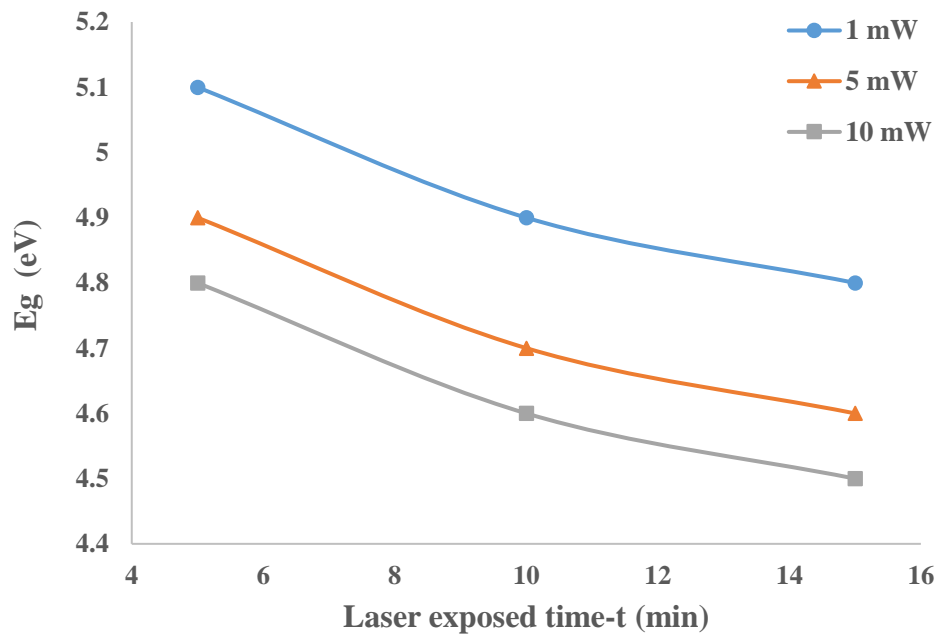


Figure (4-40) Direct optical band gap energy vs. laser exposed time for detector exposed to laser beam at different powers.

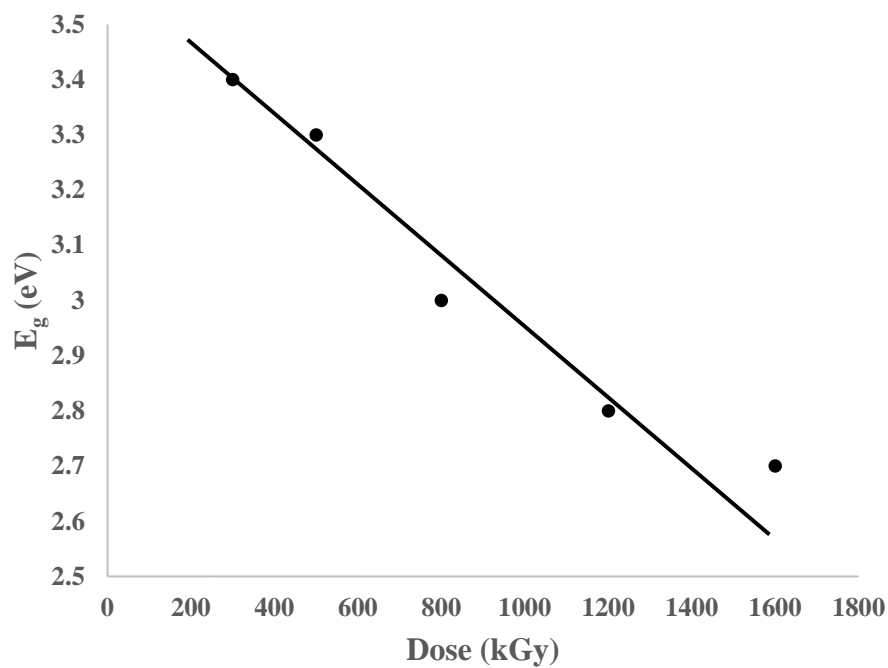


Figure (4-41) Indirect optical band gap energy vs. dose of gamma ray for detector irradiated with various doses of gamma ray.

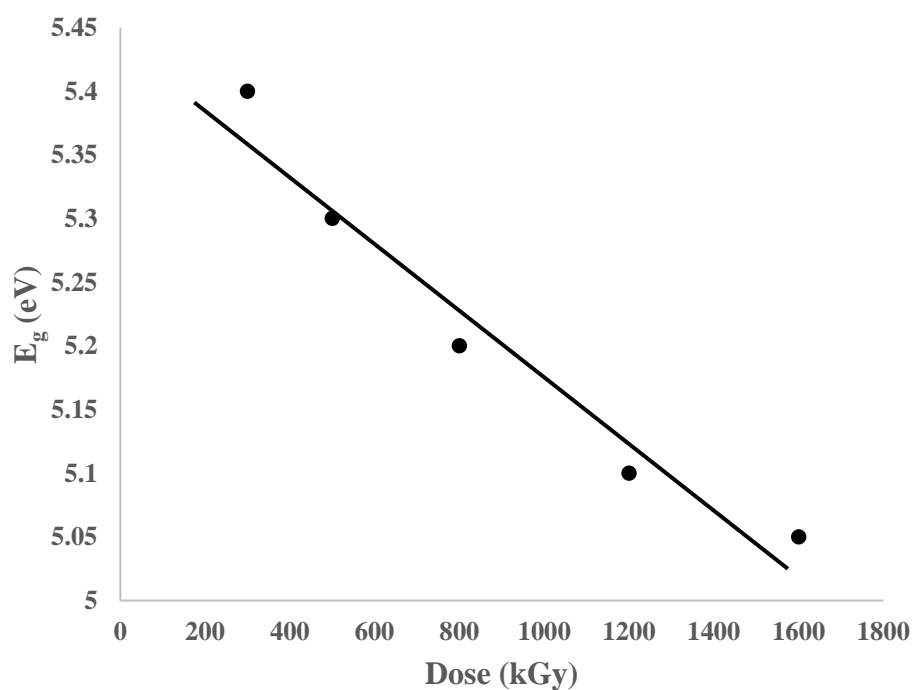


Figure (4-42) Direct optical band gap energy vs. dose of gamma ray for detector irradiated with various doses of gamma ray.

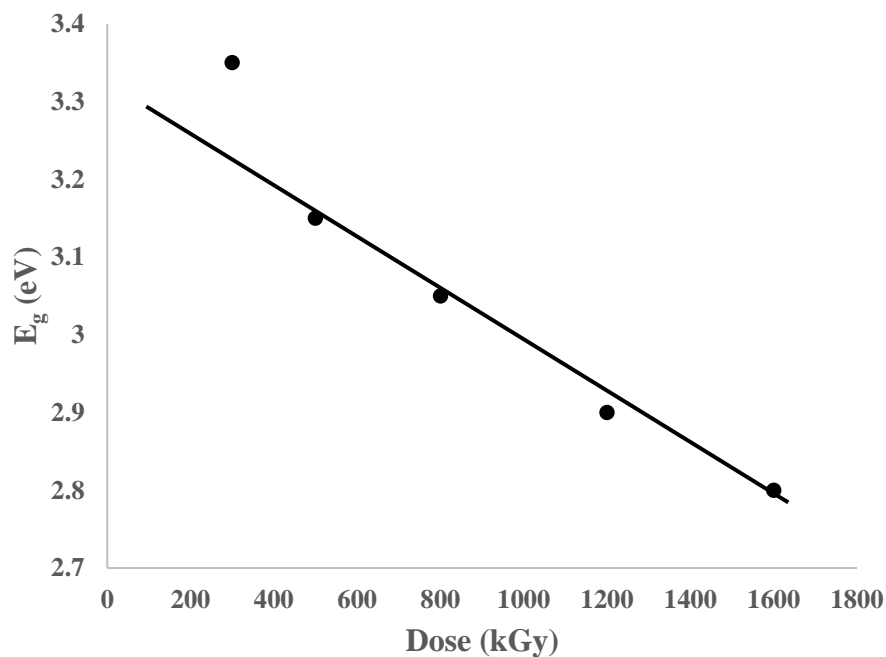


Figure (4-43) Indirect optical band gap energy vs. dose of gamma ray for detector irradiated with various doses of gamma ray, then exposed to laser beam for 15 min at 10 mW power.

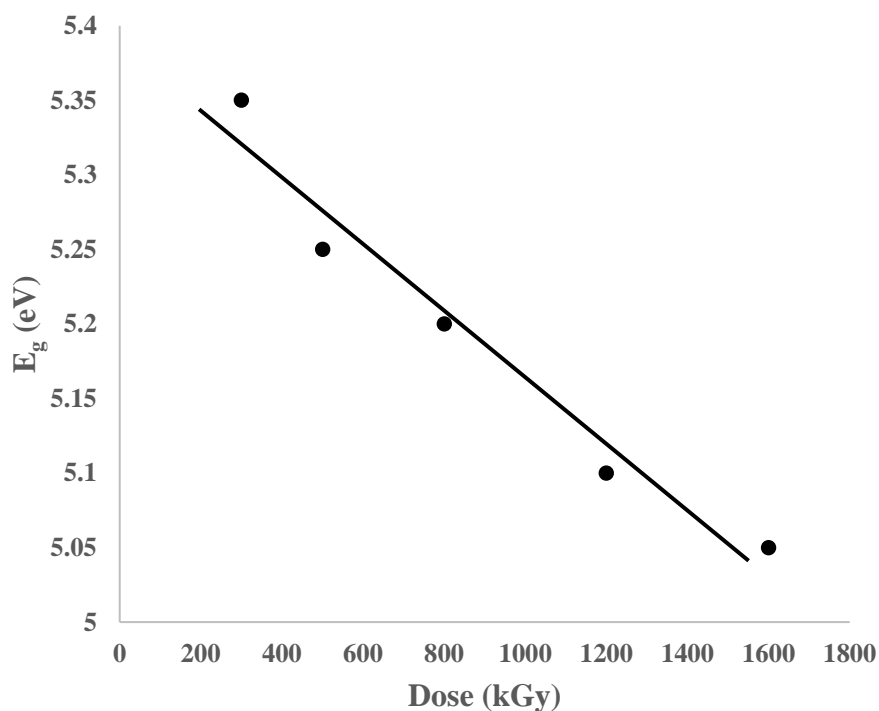


Figure (4-44) Direct optical band gap energy vs. dose of gamma ray for detector irradiated with various doses of gamma ray, then exposed to laser beam for 15 min at 10 mW power.

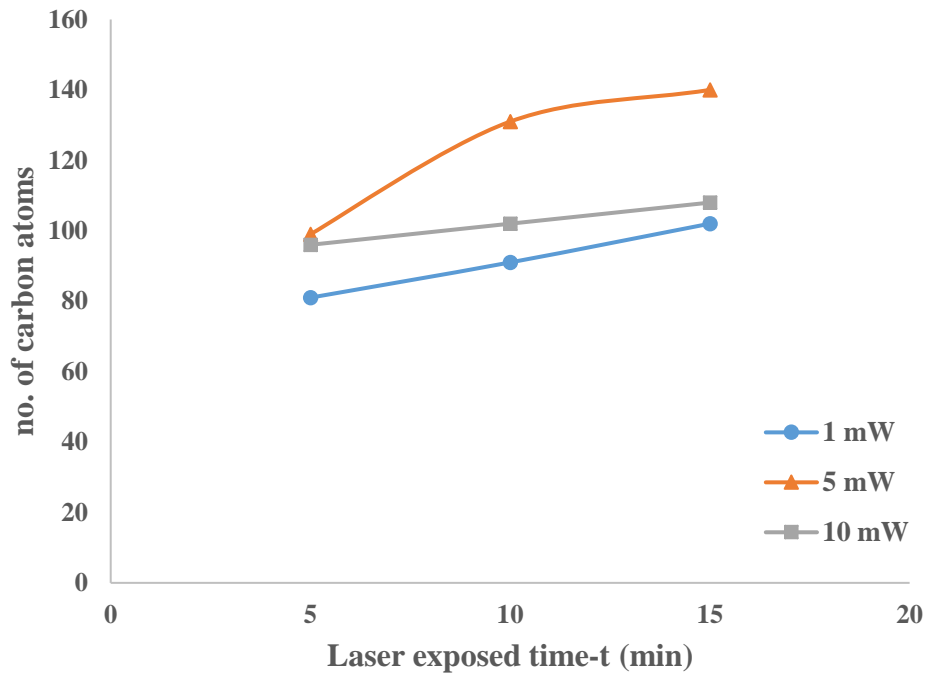


Figure (4-45) Number of carbon atoms vs. laser exposed time for detector exposed to laser beam at different powers, for indirect transition.

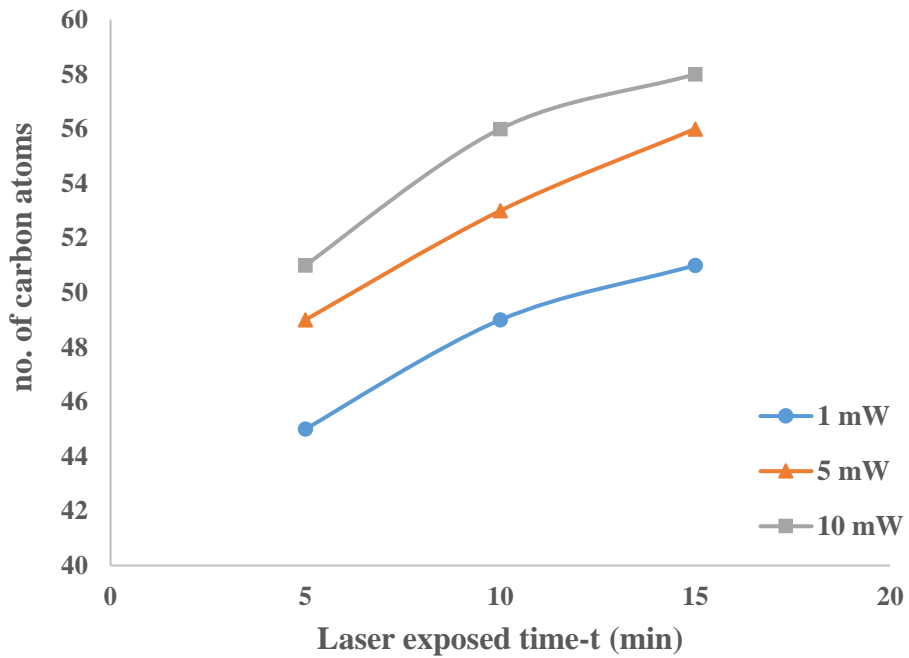


Figure (4-46) Number of carbon atoms vs. laser exposed time for detector exposed to laser beam at different powers, for direct transition.

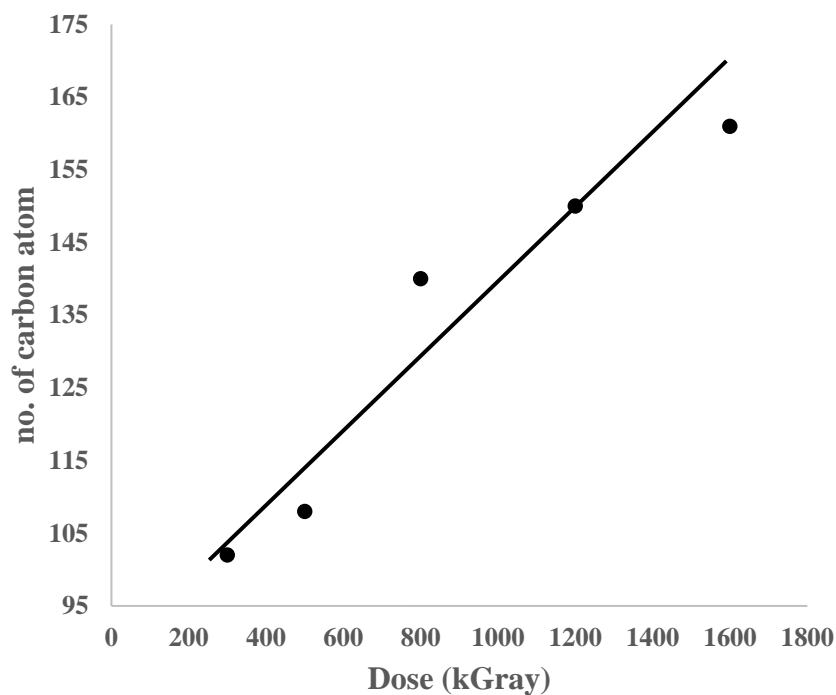


Figure (4-47) Number of carbon atoms vs. dose of gamma ray for detector irradiated with various doses of gamma ray, for indirect transition.

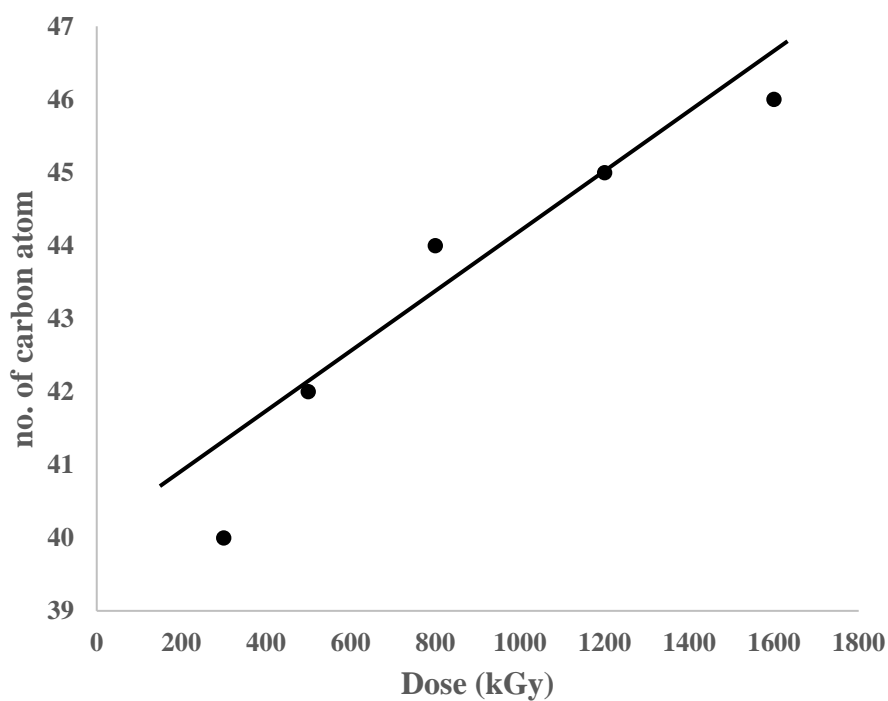


Figure (4-48) Number of carbon atoms vs. dose of gamma ray for detector irradiated with various doses of gamma ray, for direct transition.

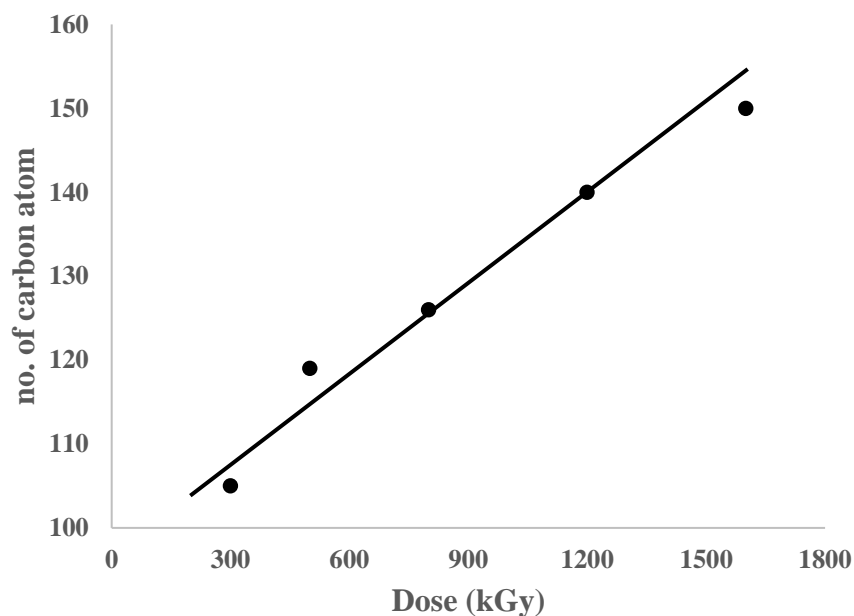


Figure (4-49) Number of carbon atoms vs. dose of gamma ray for detector irradiated with various doses of gamma ray, then exposed to laser beam for 15 min at 10 mW power, for indirect transition.

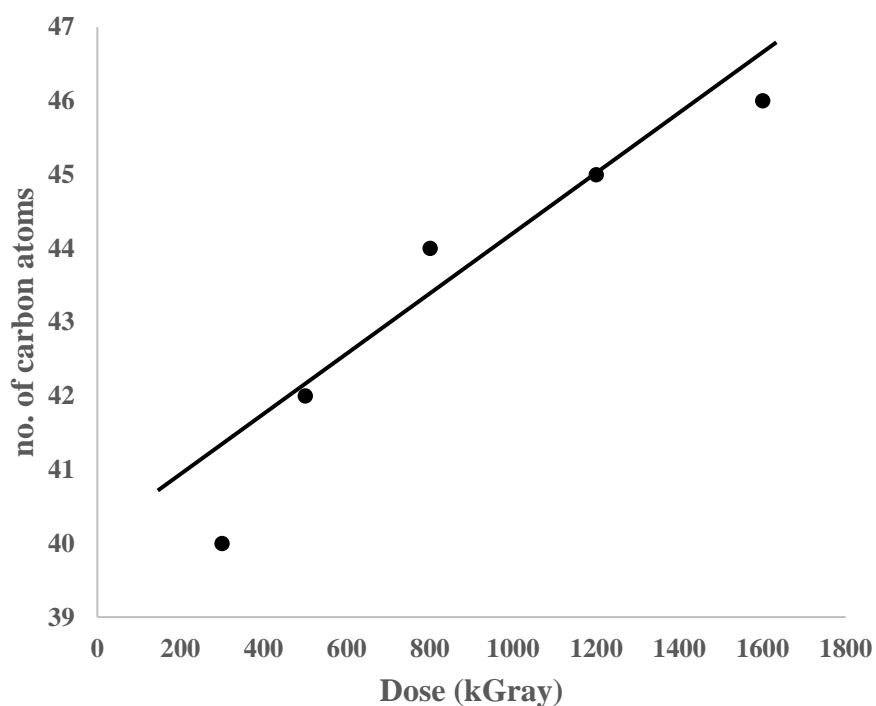


Figure (4-50) Number of carbon atoms with dose of gamma ray and for detector irradiated with different doses of gamma ray, then exposed to laser beam for 15 min at 10 mW power, for direct transition.

The optical band gap energy of un-irradiated CR-39 detector is very large as shown in table (4-2); because of the CR-39 is types of dielectric material. The direct and indirect optical energy band gap and number of carbon atoms have been determined for un-irradiated and irradiated detectors as shown in tables (4-2), (4-3) and (4-4), that result show increasing in the number of carbon atom at increase in the exposure time of laser beam or increase in the dose radiation of gamma ray as shown in figures (4-45) to (4-50), the decrease in the band gap energy lead to increase on number of carbon atom according to equation (2-13).

Table (4-2) Variations of the optical band gap energy and number of carbon atoms for detector un-irradiated and irradiated with various doses of gamma ray at range (300-1600 kGy).

Gamma				
Dose (kGy)	Indirect E_g (eV)	No. of carbon atom	Direct E_g (eV)	No. of carbon atom
Control	3.9	77	5.7	36
300	3.4	102	5.4	40
500	3.3	108	5.3	42
800	2.9	140	5.2	44
1200	2.8	150	5.1	45
1600	2.7	161	5.05	46

Table (4-3) Variations of the optical band gap energy and number of carbon atoms for detector irradiated with various doses of gamma ray, then exposed to laser beam for 15 min at 10 mW power.

Gamma + laser						
P(mW)	t(min)	Dose (kGy)	Indirect E_g (eV)	No. of carbon atom	Direct E_g (eV)	No. of carbon atom
10	15	300	3.35	105	5.35	41
		500	3.15	119	5.25	43
		800	3.05	126	5.2	44
		1200	2.9	140	5.1	45
		1600	2.8	150	5.05	46

Table (4-4) Variations of the optical band gap energy and number of carbon atoms for detector exposed to laser beam for 5, 10 and 15 min at different powers 1, 5 and 10 mW.

Laser					
P(mW)	t(min)	Indirect E_g (eV)	No. of carbon atom	Direct E_g (eV)	No. of carbon atom
1	5	3.8	81	5.1	45
	10	3.6	91	4.9	49
	15	3.4	102	4.8	51
5	5	3.45	99	4.9	49
	10	3	131	4.7	53
	15	2.9	140	4.6	56
10	5	3.5	96	4.8	51
	10	3.4	102	4.6	56
	15	3.3	108	4.5	58

4.3.4 FTIR spectroscopic

FTIR spectra of un-irradiated detector were shown in figure (4-51). A number of sharp intense bands at (783.03, 1234.14 and 1737.88 cm^{-1}) have been detected in the spectrum of un-irradiated CR-39 tracks detector. These bands correspond to $\text{CH}_2=\text{C-H}$ bending, O-C-O stretching and C=O stretching respectively. The other minor intensity bands at (1396.39 and 1452.53 cm^{-1}) originates from CH_2 deformation vibration modes while the bands in the region (1000-1200 cm^{-1}) are due to C-O stretching mode vibrations whereas the band at (871.81 cm^{-1} and 954.94 cm^{-1}) corresponds to C-H out of plane bending mode vibrations, and the bands at (2914.43 cm^{-1}) corresponds to CH_2 stretching vibrations. The occurrence of these bands confirms the monomer structure of detector (polymer).

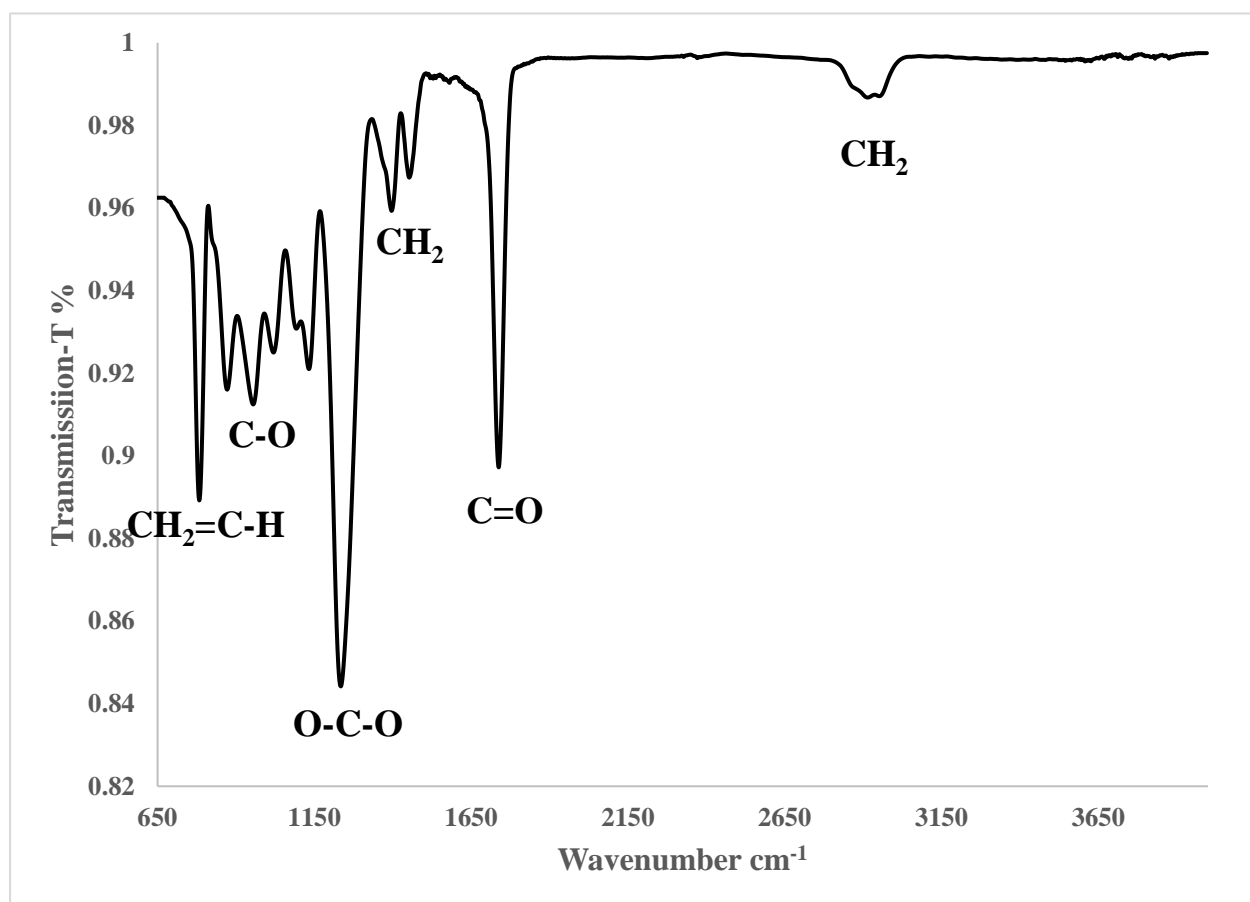


Figure (4-51) FTIR spectra for detector un-irradiated (control).

4.3.4.1 Effect of gamma radiation

FTIR spectra for detector un-irradiated (control) and irradiated with various doses of gamma ray (300, 500, 800, 1200 and 1600 kGy) were shown in figure (4-52). In table (4-5), at (300 kGy), the band at (783.03, 871.81 and 954.94 cm^{-1}) is shifted towards (785.94, 874.62 and 958.67 cm^{-1}) respectively, the bands at (1019 and 1132.14 cm^{-1}) is shifted towards (1082.71 and 1133.27 cm^{-1}) respectively due to plane bending mode vibrations of C-O, the band at (1234.18 cm^{-1}) are shifted toward (1237.08 cm^{-1}), the band at (1396.9 cm^{-1}) are shifted toward (1399.18 cm^{-1}), the band at (1737.88 cm^{-1}) is shifted towards (1736.28 cm^{-1}). New band at (2880.21 cm^{-1}) appears due to CH_2 stretching vibration; the bands at (2914.34 cm^{-1}) are shifted toward (2954.09 cm^{-1}). And new band appears at (3525.01 cm^{-1}), which are refers to formation of the O-H groups at (300 kGy). At (500 kGy), new band appears at (668.36 cm^{-1}) due to C-H out of phase bending, the bands at (783.03, 871.81 and 954.94 cm^{-1}) is shifted towards (786.36, 875.81 and 956.93 cm^{-1}) respectively due to C-H out of phase bending, the bands at (1019 and 1132.14 cm^{-1}) is shifted towards (1022.24 and 1133.51 cm^{-1}) respectively due to plane bending mode vibrations of C-O, the bands at (1396.9 and 1452.53 cm^{-1}) is shifted toward (1399.18 and 1450.93 cm^{-1}) respectively, the band at (1737.88 cm^{-1}) is shifted towards (1736.77 cm^{-1}). The bands at (2914.34 cm^{-1}) are shifted toward (2934.69 cm^{-1}). At (800 kGy), also the most bands in the range of (650-4000 cm^{-1}) show shifted in wavenumber due the gamma radiation dose, but new bands appearance at (668.18 and 677.17 cm^{-1}) due to C-H out phase bending, while a new band at (3436.67 cm^{-1}) due to O-H groups. At (1200 kGy), show that the bands at ranges (650-4000 cm^{-1}) shifted in wavenumber. Appearance of band at (719.22 cm^{-1}) is due to C-H out phase bending, and new bands at (3331.64 cm^{-1}) appear due to O-H groups, at (1600 kGy), the bands at (871.81 and 954.94 cm^{-1}) is shifted toward (876.28 and 955.89 cm^{-1})

respectively, the band at (1019.68 cm^{-1}) is shifted towards (1015.44 cm^{-1}) and disappear band at (1132.14 cm^{-1}), the bands at (1396.39 and 1452.53 cm^{-1}) shifted toward (1394.72 and 1448.8 cm^{-1}) due to CH_2 deformation vibration, and the band at (1737 cm^{-1}) is shifted toward (1734.79 cm^{-1}), the band at (2914.34 cm^{-1}) is shifted toward (2924.23 cm^{-1}), and new band at (3364.88 cm^{-1}) appear due to O-H groups.

It is stated that changes refer to change in detector configuration and structure, and on irradiated the detectors with differences dose of gamma ray.

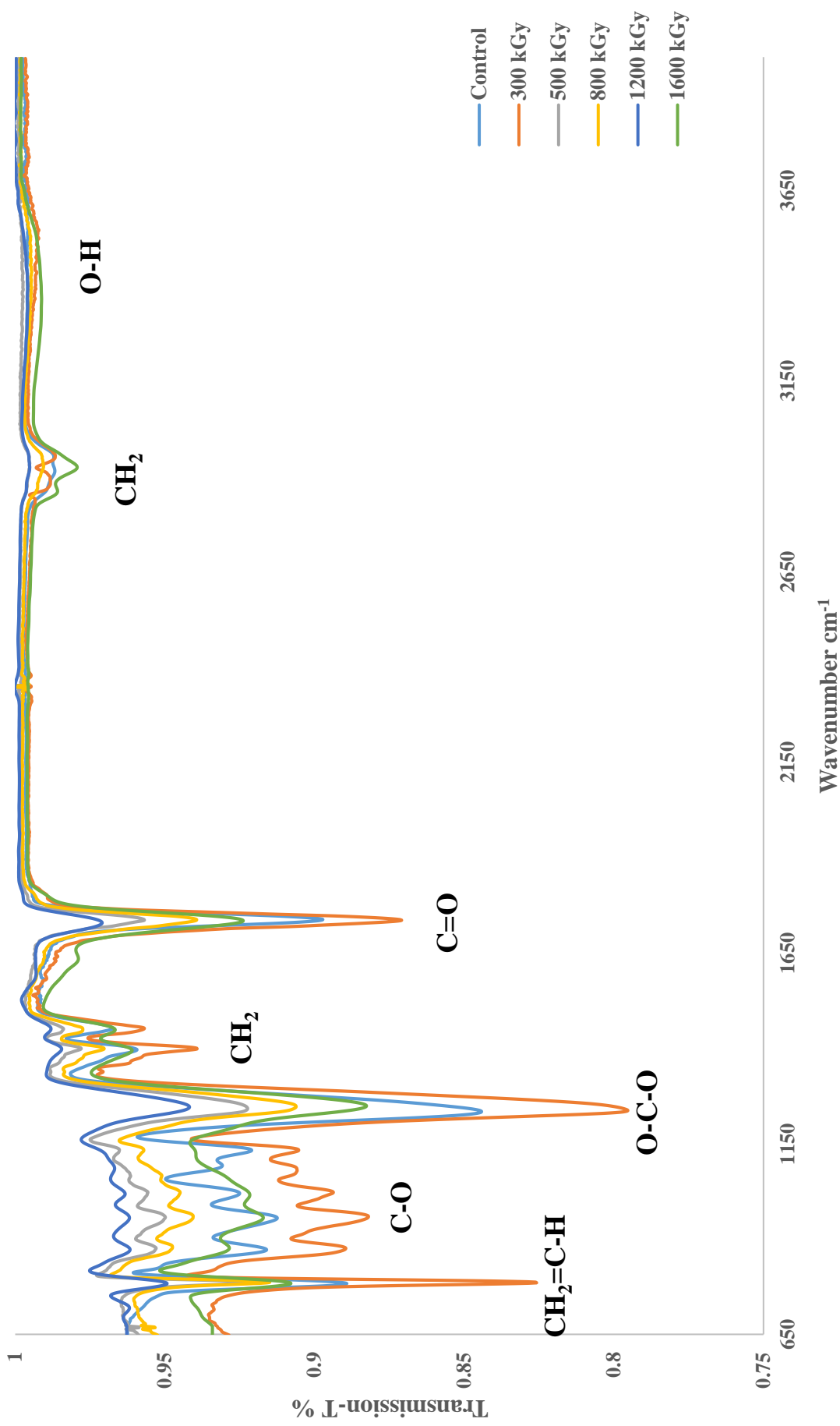


Figure (4-52) FTIR spectra for detector un-irradiated and irradiated with various doses of gamma ray.

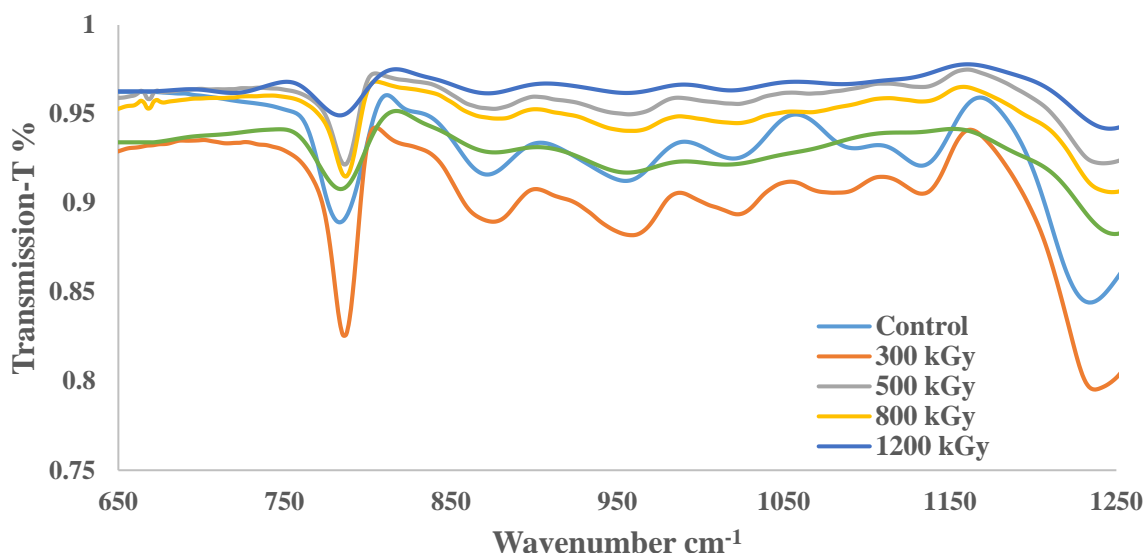


Figure (4-53) FTIR spectra at range (650-1250) for detector un-irradiated and irradiated with various doses of gamma ray.

Table (4-5) Wavenumbers for detector un-irradiated and irradiated with various doses of gamma ray.

State	Contoal	300 (kGy)	500 (kGy)	800 (kGy)	1200 (kGy)	1600 (kGy)
CH ₂ =C-H out phase bending 650-970	783.03	785.94	668.36	668.18	719.22	783.68
	871.81	874.62	786.36	677.17	783.14	876.28
	954.94	958.67	875.81	786.57	872.14	955.89
			956.93	878.33	955.5	
				959.9		
C-O Stretching vibration 1000-1200	1019.68	1082.71	1022.24	1021.78	1018.15	1015.44
	1324.14	1133.27	1133.51	1132.8	1084.98	
O-C-O stretching 1200-1400	1234.14	1237.08	1242.11	1247.4	1246.15	1249.11
CH ₂ deformation vibration 1200-1600	1396.39	1399.18	1399.51	1399.27	1398.2	1394.72
	1452.53	1452.81	1450.93	1449.38	1451.2	1448.8
C=O Stretching 1550-1750	1737.88	1736.28	1736.77	1737.16	1729.37	1734.79
CH ₂ Stretching 2800-3000	2914.34	2880.21 2954.09	2934.69	2926.55	2932.28	2924.23
O-H 3300-3800	—	3525.01	—	3436.67	3397.23	3364.88

4.3.4.2 Effect of (He-Ne) laser

FTIR spectra for detector un-irradiated (control) and exposed to laser beam for different times at 1 mW power was shown in figure (4-53). In the table (4-6), at (5 min), the most bands on range (650-4000 cm^{-1}) shifted, the band at (783.03, 871.81 and 954.94 cm^{-1}) is shifted towards (785.44, 873.04 and 955.53 cm^{-1}) respectively, the bands at (1019 and 1324.14 cm^{-1}) is shifted towards (1090.49 and 1134.41 cm^{-1}) respectively due to plane bending mode vibrations of C-O, the band at (1234.18 cm^{-1}) are shifted toward (1232.12 cm^{-1}), the band at (1396.9 cm^{-1}) are shifted toward (1399.58 cm^{-1}), the band at (1737.88 cm^{-1}) is shifted towards (1736.28 cm^{-1}) .New band at(2880.21 cm^{-1}) appears due to CH₂ stretching vibration; the bands at (2914.34 cm^{-1}) are shifted toward (2955.15 cm^{-1}). At (10 min), the most bands on range (650-4000 cm^{-1}) show a little shifted, the bands at (2914.34 cm^{-1}) are shifted toward (2919.97 cm^{-1}). At (15 min), also the most bands in the range of (650-4000 cm^{-1}) show a little shifted in wavenumber due increase in time exposure, the bands at (2914.34 cm^{-1}) are shifted toward (2953.07 cm^{-1}).

In Figure (4-53) is shown an increase in intensity absorption with increasing of the time exposure of laser, it is referring to infrared-laser interactions with detector made thermal effects and lead to increase in the absorbance due to increase in the exposure time, that lead to changes in the structure and configuration of detector.

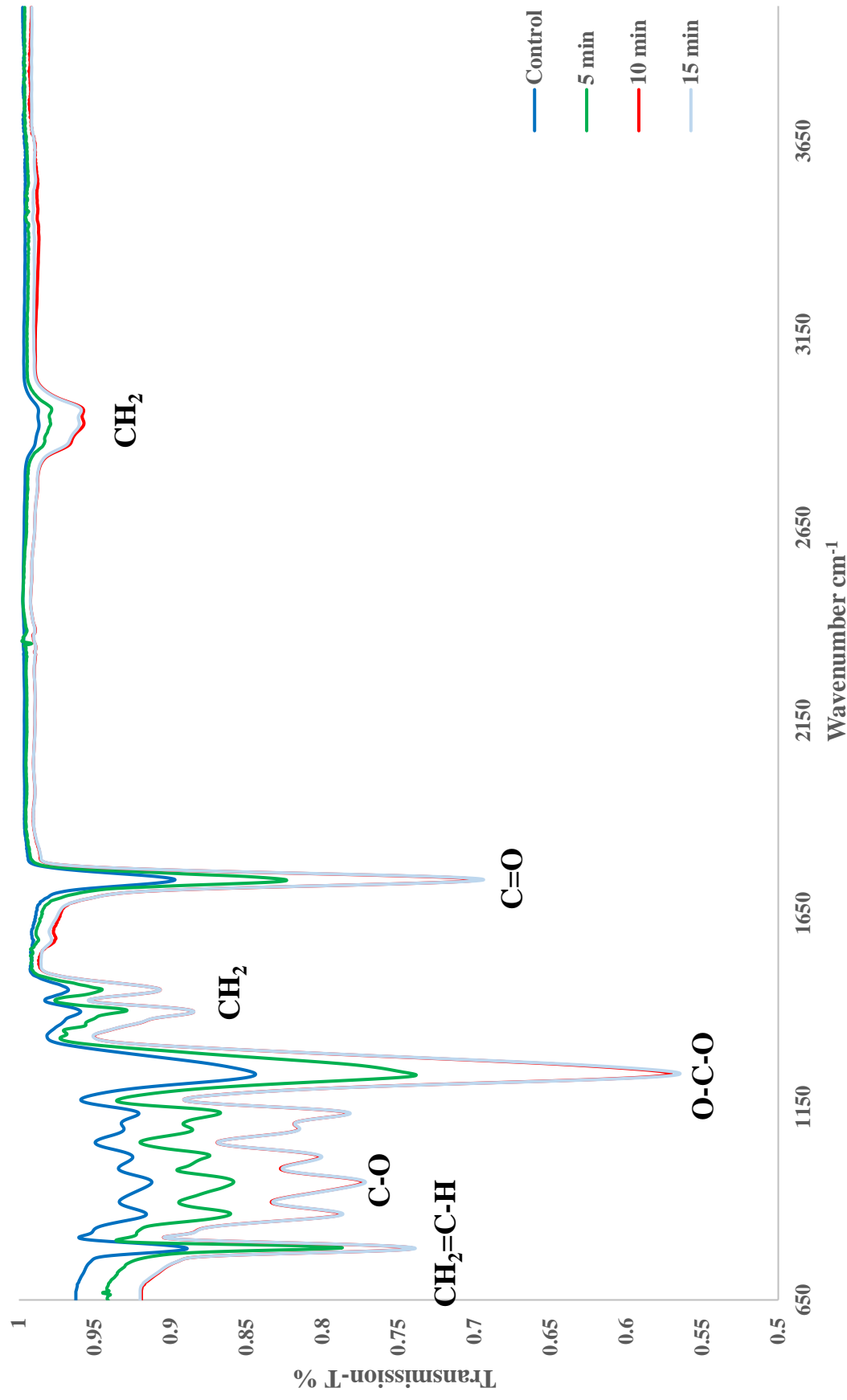


Figure (4-54) FTIR spectra for detector un-irradiated and exposed to laser beam for different times at 1 mW power.

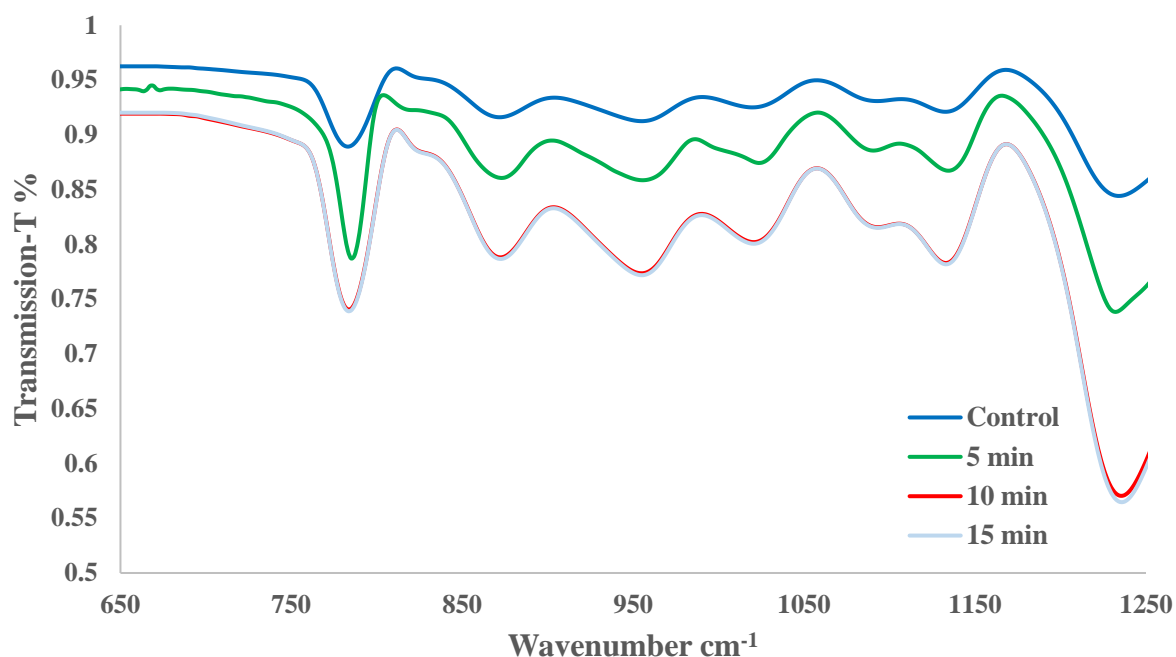


Figure (4-55) FTIR spectra at range (650-1250) for detector un-irradiated and exposed to laser beam for different times at 1 mW power.

Table (4-6) Wavenumbers for detector un-irradiated and exposed to laser beam for different times at 1 mW power.

State	Control	5 min	10 min	15 min
CH ₂ =C-H out phase bending 650-970	783.03	785.44	783.64	783.67
	871.81	873.04	872.31	872.41
	954.94	955.53	954.82	954.98
C-O Stretching vibration 1000-1200	1019.68	1090.49	1020.47	1020.51
	1324.14	1134.41	1132.91	1133.02
O-C-O stretching 1200-1400	1234.14	1232.12	1235.58	1235.79
CH ₂ deformation vibration 1200-1600	1396.39	1399.58	1396.13	1396.22
	1452.53	1453.56	1453.12	1452.88
C=O Stretching 1550-1750	1737.88	1736.69	1737.78	1738.88
CH ₂ Stretching 2800-3000	2914.34	2955.16	2919.97	2953.07

FTIR spectra for detector un-irradiated (control) and exposed to laser beam for different times at 5 mW power were shown in figure (4-54). In the table (4-7), at (5 min), the most bands on range (650-4000 cm^{-1}) shifted, the band at (783.03, 871.81 and 954.94 cm^{-1}) is shifted towards (785.4, 873.1 and 955.49 cm^{-1}) respectively, the bands at (1019 and 1324.14 cm^{-1}) is shifted towards (1023.75 and 1134.35 cm^{-1}) respectively, new band at (1090.69 cm^{-1}) appears due to plane bending mode vibrations of C-O, the band at (1234.18 cm^{-1}) are shifted toward (1232.13 cm^{-1}), the band at (1396.9 cm^{-1}) are shifted toward (1399.89 cm^{-1}), the band at (1737.88 cm^{-1}) is shifted towards (1736.28 cm^{-1}), the bands at (2914.34 cm^{-1}) are shifted toward (2955.81 cm^{-1}). At (10 min), the most bands on range (650-4000 cm^{-1}) show a little shifted, the bands at (2914.34 cm^{-1}) are shifted toward (2952.85 cm^{-1}). At (15 min), also the most bands in the range of (650-4000 cm^{-1}) show a little shifted in wavenumber due increase in time exposure, new band at (1090.69 cm^{-1}) appears due to plane bending mode vibrations of C-O, the bands at (2914.34 cm^{-1}) are shifted toward (2919.53 cm^{-1}).

Figure (4-54) shows an increase in intensity absorption with increasing of the time exposure of laser, it is referring to infrared-laser interactions with detector made thermal effects and lead to increase in the absorbance due to increase in the exposure time, that lead to changes in the structure and configuration of detector.

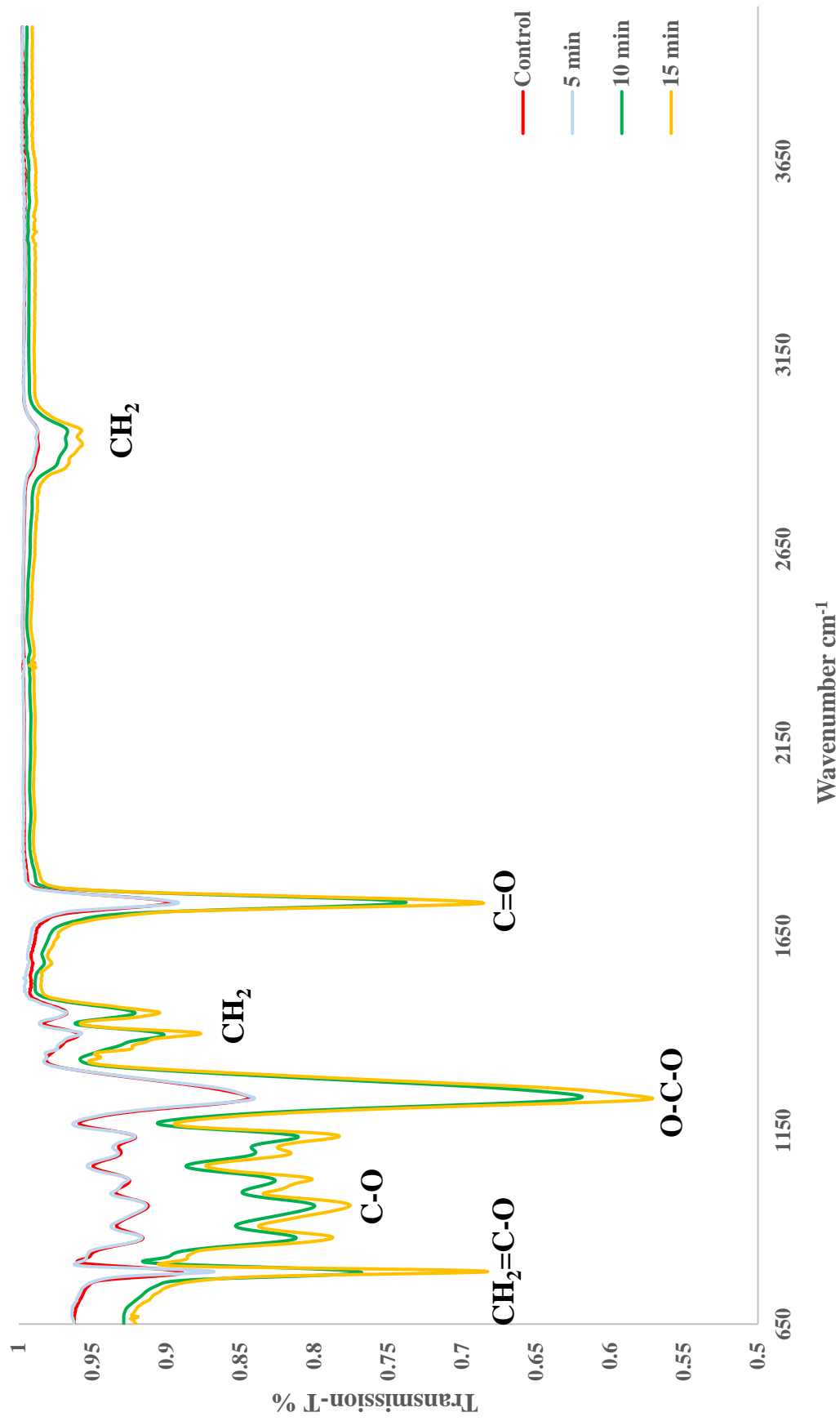


Figure (4-56) FTIR spectra for detector un-irradiated and exposed to laser beam for different times at 5 mW power.

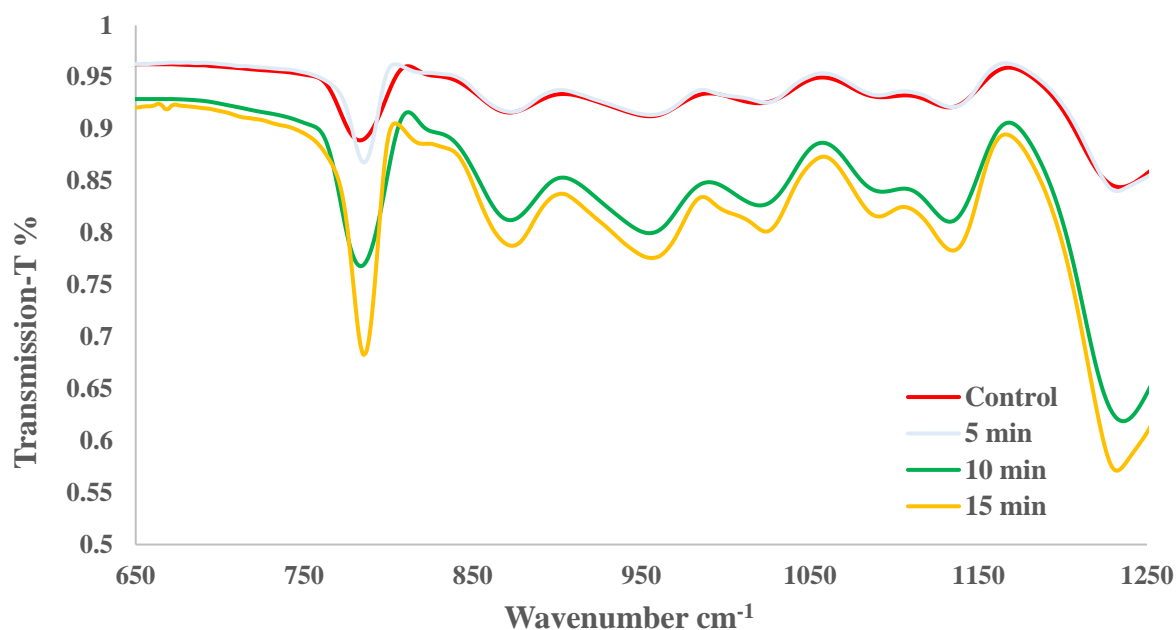


Figure (4-57) FTIR spectra at range (650-1250) for detector un-irradiated and exposed to laser beam for different times at 5 mW power.

Table (4-7) Wavenumbers for detector un-irradiated and exposed to laser beam for different times at 5 mW power.

State	Control	5 min	10 min	15 min
CH ₂ =C-H out phase bending 650-970	783.03	785.4	783.54	785.54
	871.81	873.1	872.24	873.32
	954.94	955.49	954.8	956.15
C-O Stretching vibration 1000-1200	1019.68	1023.75	1020.39	1023.87
	1324.14	1090.69	1132.96	1090.95
		1134.35		1134.76
O-C-O stretching 1200-1400	1234.14	1232.13	1235.86	1232.12
CH ₂ deformation vibration 1200-1600	1396.39	1399.89	1396.22	1399.33
	1452.53	1453.53	1452.9	1453.5
C=O Stretching 1550-1750	1737.88	1737.09	1738.25	1736.38
CH ₂ Stretching 2800-3000	2914.34	2955.81	2952.85	2919.53

FTIR spectra for detector un-irradiated (control) and exposed to laser beam for different times at 10 mW power were shown in figure (4-55). In the table (4-8), at (5 min), the most bands on range (650-4000 cm^{-1}) shifted, the band at (783.03, 871.81 and 954.94 cm^{-1}) is shifted towards (785.41, 872.87 and 956.51 cm^{-1}) respectively, the bands at (1019 and 1324.14 cm^{-1}) is shifted towards (1024.49 and 1134.41 cm^{-1}) respectively, new band at (1091.02 cm^{-1}) due to plane bending mode vibrations of C-O, the band at (1234.18 cm^{-1}) are shifted toward (1231.91 cm^{-1}), the bands at (1396.9 and 1452.53 cm^{-1}) are shifted toward (1399.58 and 1453.1 cm^{-1}), the band at (1737.88 cm^{-1}) is shifted towards (1736.51 cm^{-1}); the bands at (2914.34 cm^{-1}) are shifted toward (2992.05 cm^{-1}). New band at (3350.73 cm^{-1}) appears due to O-H groups. At (10 min), the most bands on range (650-4000 cm^{-1}) show a little shifted, new band at (1090.41 cm^{-1}) due to plane bending mode vibrations of C-O, the bands at (2914.34 cm^{-1}) are shifted toward (2954.72 cm^{-1}). At (15 min), also the most bands in the range of (650-4000 cm^{-1}) show a little shifted in wavenumber due increase in time exposure, the bands at (2914.34 cm^{-1}) are shifted toward (2920.31 cm^{-1}).

Figure (4-55) shows an increase in intensity absorption with increasing of the time exposure of laser, it is referring to infrared-laser interactions with detector made thermal effects and lead to increase in the absorbance due to increase in the exposure time, that lead to changes in the structure and configuration of detector.

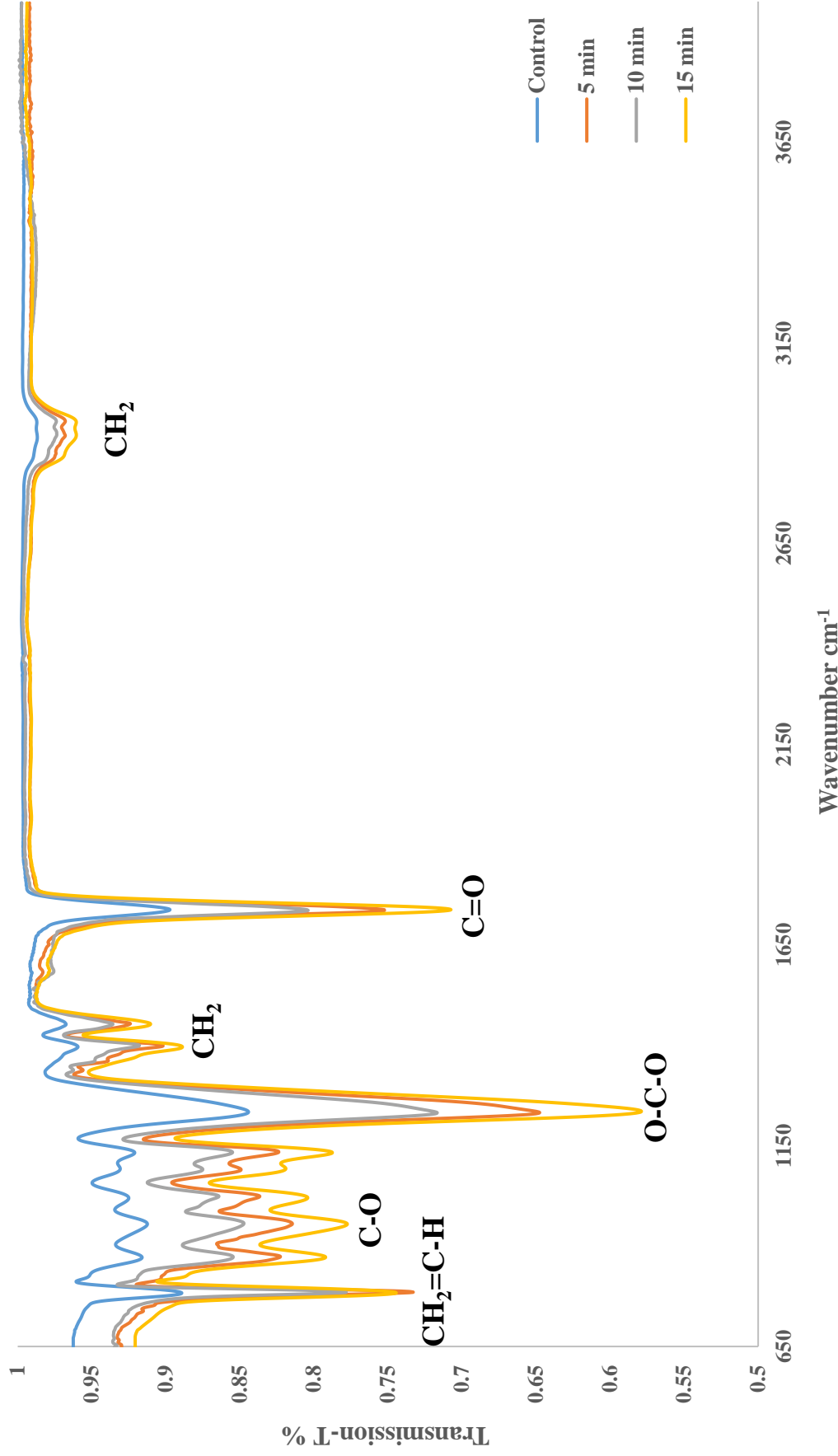


Figure (4-58) FTIR spectra for detector un-irradiated and exposed to laser beam for different times at 10 mW power.

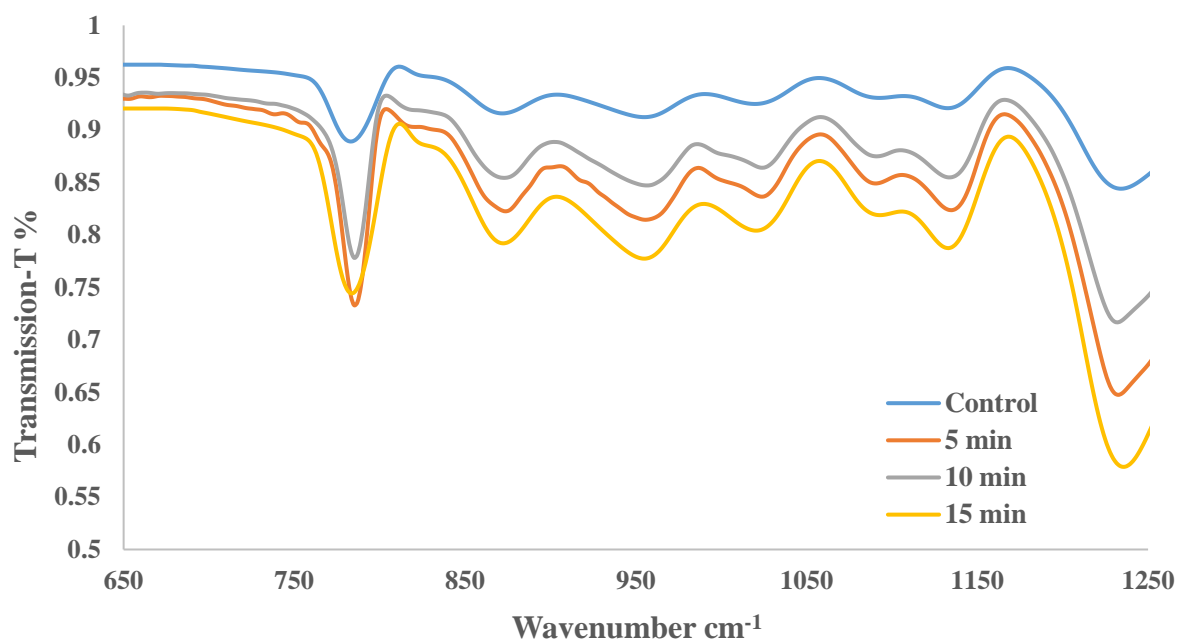


Figure (4-59) FTIR spectra at range (650-1250) for detector un-irradiated and exposed to laser beam for different times at 10 mW power.

Table (4-8) Wavenumbers for detector un-irradiated and exposed to laser beam for different times at 10 mW power.

State	Control	5 min	10 min	15 min
CH ₂ =C-H out phase bending 650-970	783.03 871.81 954.94	785.41 872.87 956.51	785.51 873.74 955.76	783.62 872.33 954.9
C-O Stretching vibration 1000-1200	1019.68 1324.14	1024.02 1091.02 1133.63	1023.86 1090.41 1134.67	1020.46 1132.87
O-C-O stretching 1200-1400	1234.14	1231.91	1232.51	1235.64
CH ₂ deformation vibration 1200-1600	1396.39 1452.53	1399.57 1453.1	1399.06 1454.05	1396.07 1453.15
C=O Stretching 1550-1750	1737.88	1736.51	1736.88	1738.01
CH ₂ Stretching 2800- 3000	2914.34	2921.05	2954.72	2920.31
O-H 3300-3800	—	3350.73	—	—

4.3.4.2 Effect of gamma ray and (He-Ne) laser

FTIR spectra for detector un-irradiated (control) and irradiated with gamma ray with various doses, then exposed to laser beam for 15 min at 10 mW power were shown in figure (4-56). In the table (4-9), at (300 kGy), the bands at (783.03, 871.81 and 954.94 cm^{-1}) is shifted towards (782.03, 872.11 and 956.32 cm^{-1}) respectively, the band at (1132.14 cm^{-1}) is shifted towards (1129.38 cm^{-1}), appearance of new band at (1080.52 cm^{-1}) due to plane bending mode vibrations of C-O, the band at (1234.18 cm^{-1}) are shifted toward (1240.82 cm^{-1}), the band at (1452.53 cm^{-1}) are shifted toward (1451.96 cm^{-1}), the band at (1737.88 cm^{-1}) is shifted towards (1736.91 cm^{-1}). The bands at (2914.34 cm^{-1}) are shifted toward (2922.86 cm^{-1}). And new band appears at (3397.98 cm^{-1}) which are refers to formation of the O-H groups at (300 kGy). At (500 kGy), the band at (783.03 cm^{-1}) is shifted towards (782.42 cm^{-1}) respectively due to C-H out of phase bending, the bands at (1019 and 1132.14 cm^{-1}) is shifted towards (1071.01 and 1128.11 cm^{-1}) respectively due to plane bending mode vibrations of C-O, the band at (1452.53 cm^{-1}) is shifted toward (1450.73 cm^{-1}), the band at (1737.88 cm^{-1}) is shifted towards (1735.27 cm^{-1}). The bands at (2914.34 cm^{-1}) are shifted toward (2919.93 cm^{-1}). At (800 kGy), the bands at (783.03, 871.81 and 954.94 cm^{-1}) is shifted towards (786.57, 878.98 and 961.37 cm^{-1}) respectively, the band at (1019.68 cm^{-1}) is shifted towards (1022.29 cm^{-1}), disappearance the band at (1123.14 cm^{-1}), the band at (1234.18 cm^{-1}) are shifted toward (1246.26 cm^{-1}), the bands at (1396.39 and 1452.53 cm^{-1}) are shifted toward (1399.35 and 1451.96 cm^{-1}), the band at (1737.88 cm^{-1}) is shifted towards (1736.47 cm^{-1}). The bands at (2914.34 cm^{-1}) are shifted toward (2924.08 cm^{-1}). And new band appears at (3361.54 cm^{-1}) which are refers to formation of the O-H groups. At (1200 kGy), the bands at (871.81 and 954.94 cm^{-1}) is shifted towards (877.22 and 956.72 cm^{-1}) respectively, the band at (1019.68 cm^{-1}) is shifted towards (1018.36 cm^{-1}), disappearance the band at (1132.21 cm^{-1}), the band at (1234.14 cm^{-1}) are shifted toward (1248.78 cm^{-1}), the bands at (1396.39 and 1452.53 cm^{-1}) are shifted

toward (1394.24 and 1447.3 cm^{-1}), the band at (1737.88 cm^{-1}) is shifted towards (1735.1 cm^{-1}). The bands at (2914.34 cm^{-1}) are shifted toward (2924.85 cm^{-1}). And new band appears at (3358.91 cm^{-1}) which are refers to formation of the O-H groups, at (1600 kGy), the band at (954.94 cm^{-1}) is shifted toward (956.16 cm^{-1}), disappearance band at (871.81 cm^{-1}), the band at (1019.68 and 1132.14 cm^{-1}) disappear, the band at (1234.14 cm^{-1}) shifted towards (1249.55 cm^{-1}), the bands at (1396.39 and 1452.53 cm^{-1}) shifted toward (1394.34 and 1448.87 cm^{-1}), appearance band at (1527.96 cm^{-1}) due to CH_2 deformation vibration, and the band at (1737 cm^{-1}) is shifted toward (1735.24 cm^{-1}), the band at (2914.34 cm^{-1}) is shifted toward (2932.28 cm^{-1}), and new bands at (3613.85, 3740.41 and 3828.74 cm^{-1}) appear due to O-H groups.

It is stated that changes refer to change in detector configuration and structure, and on irradiated the detectors with differences dose of gamma radiation then expos with laser.

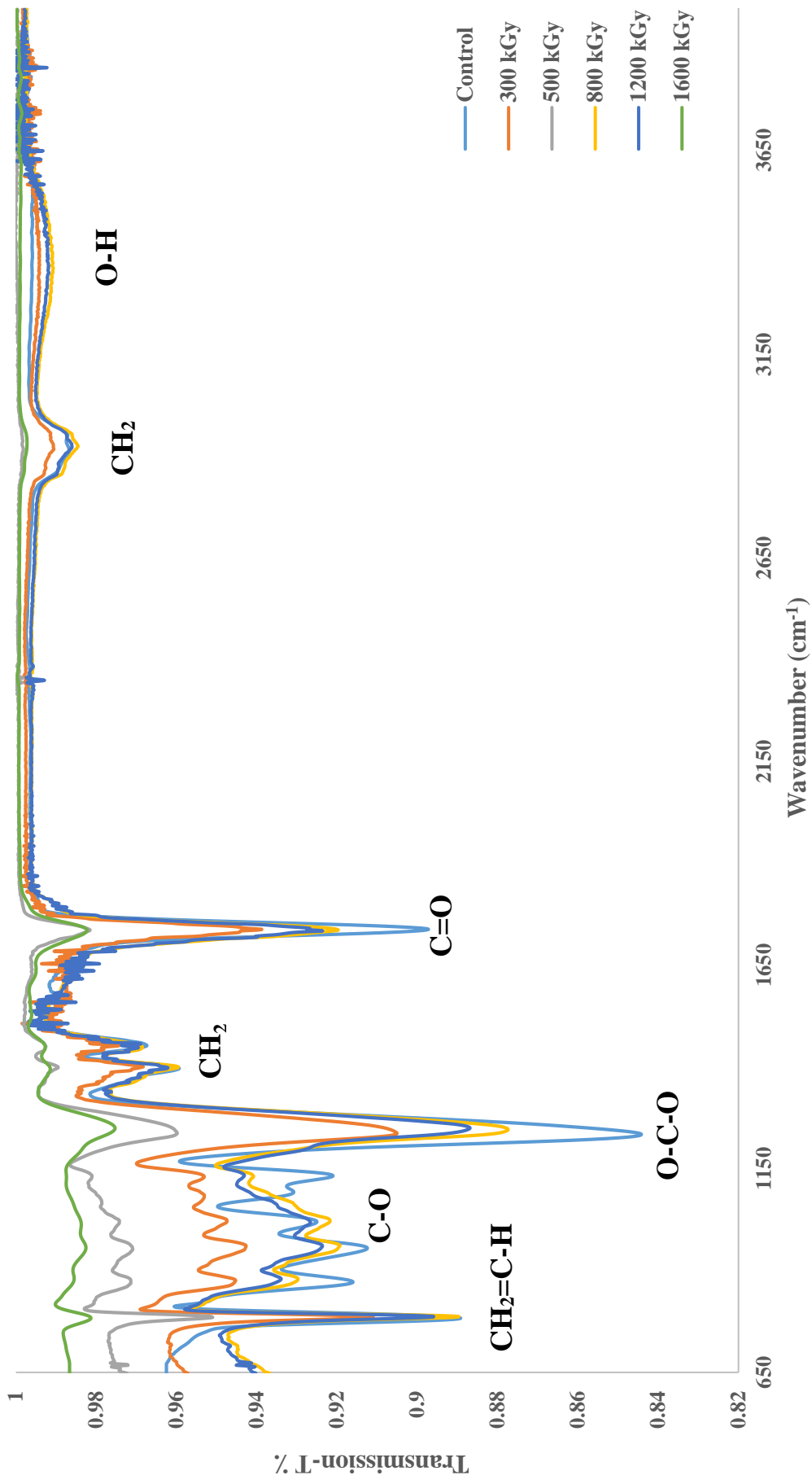


Figure (4-60) FTIR spectra for detector un-irradiated and irradiated with various doses of gamma ray, then exposed to laser beam for 15 min at 10 mW power.

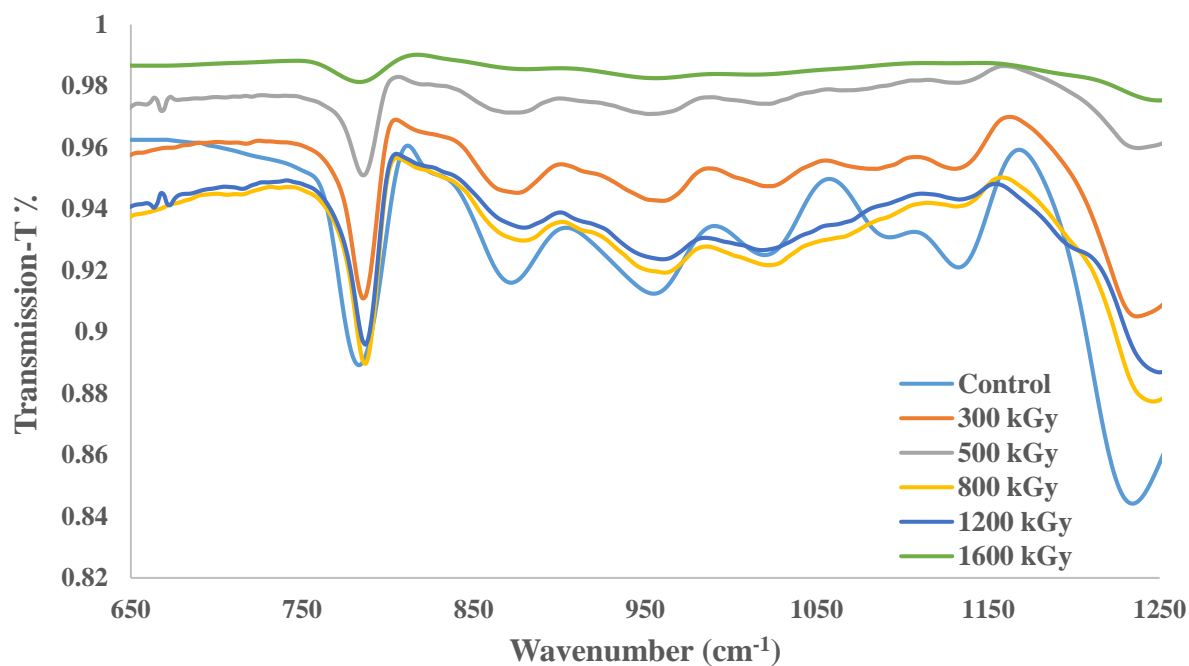


Figure (4-61) FTIR spectra at range (650-1250) for detector un-irradiated and irradiated with various doses of gamma ray, then exposed to laser beam for 15 min at 10 mW power.

Table (4-9) Wavenumbers for detector un-irradiated and irradiated with various doses of gamma ray, then exposed to laser beam for 15 min at 10 mW power.

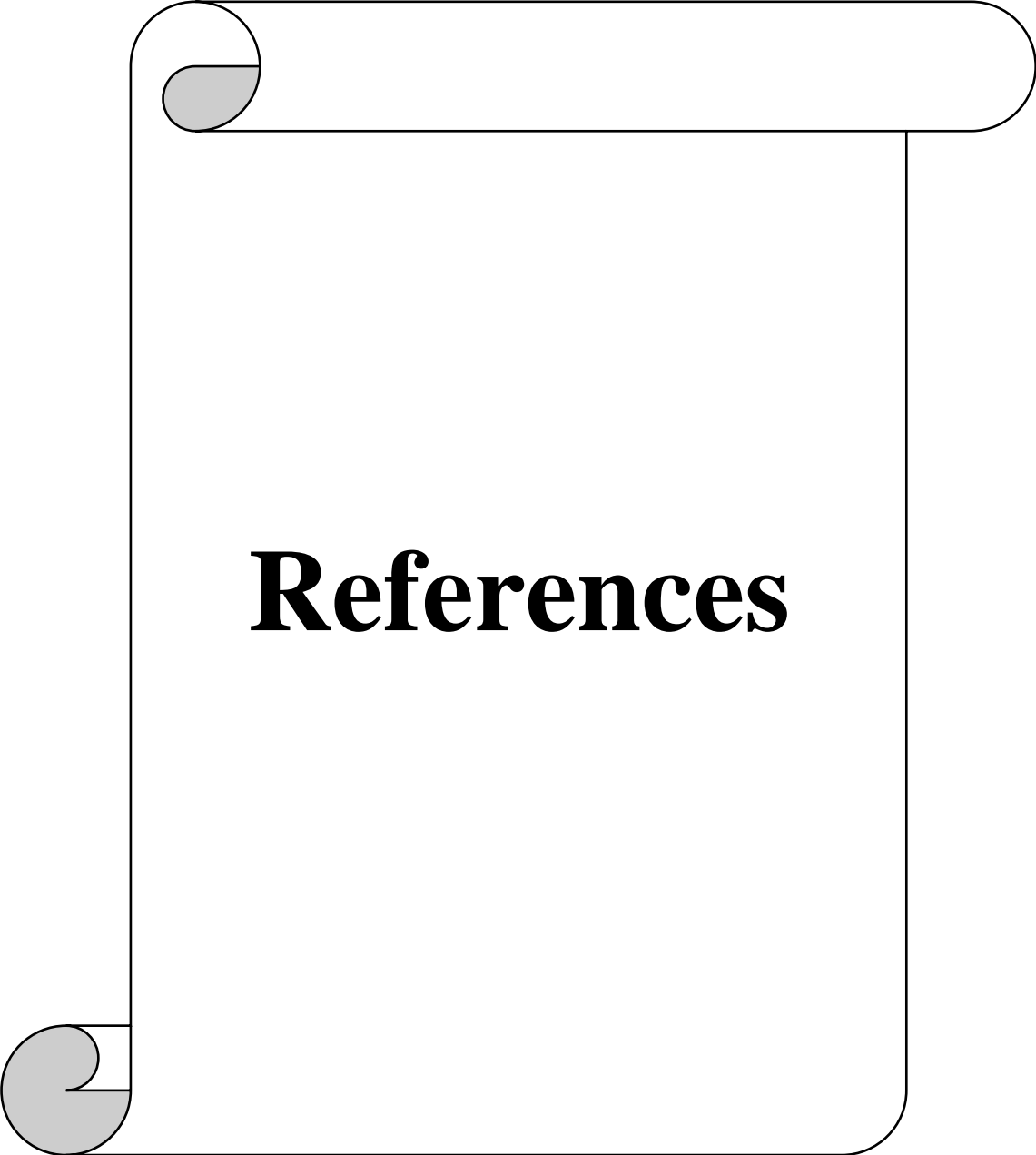
State	Control	300 kGy	500 kGy	800 kGy	1200 kGy	1600 kGy
CH ₂ =C-H out phase bending 650-970	783.03	782.94	782.42	786.57	783.26	783.39
	871.81	872.11	871.22	878.98	877.22	956.16
	954.94	956.32	954.23	961.37	956.72	
C-O Stretching 1000-1200	1019.68	1019.41	1071.01	1022.29	1018.36	
	1324.14	1080.52	1128.81			
		1129.38				
O-C-O stretching 1200-1400	1234.14	1240.82	1241.11	1246.26	1248.78	1249.55
CH ₂ deformation vibration 1200-1600	1396.39	1397.01	1396.461	1399.35	1394.24	1394.34
	1452.53	1451.96	450.73	1448.49	1447.3	1448.87 1527.96
C=O Stretch 1550-1750	1737.88	1736.91	1735.27	1736.47	1735.1	1735.24
CH ₂ Stretching 2800-3000	2914.34	2922.86	2919.93	2924.08	2292.85	2932.28
O-H 3300-3800	—	3397.98	—	3361.54	3358.91	3613.85 3740.41 3828.74

4.4 Conclusions

- 1- The increasing in the exposure times of laser at different powers lead to increasing in the track density and track diameter and the best case its seen to detector exposed to laser beam for 15 min at 10 mW power because they recorded maximum values compared with other cases.
- 2- The increasing in the exposure times of laser at different powers lead to increasing in the etch rate parameter (V_B and V_T), critical angle and sensitivity, the recorded the maximum value for detector exposed to laser beam for 15 min at 10 mW.
- 3- The UV-Vis spectra show increasing in the absorbance with in increasing the exposure times of laser at different powers and increase gamma ray, the high absorbance recorded for detector irradiated with gamma dose of 1600 kGy then exposed to laser beam for 15 min at 10 mW power.
- 4- The increasing with absorbance lead to decreasing in the optical band gab energy (directed and indirect allow transitions) that cause increasing in the number of carbon atom, the lowers value of energy gap recorded for direct allowed transition was (2.7 eV) for detector irradiated with gamma ray of dose (1600 kGy), and for indirect allowed transition was (4.5 eV) for detector exposed to laser beam for 15 min at 10 mW power.
- 5- FTIR spectra for detector exposed to gamma, laser and gamma+laser show shifting in the bands, appearance and disappearance in the some bands, due to changes in CR-39 detector structure and configuration.

4.5 Suggestion and future works

1. Use another types of nuclear track detectors and compare the results with the present study.
2. Studying the effect of the CO₂ laser and alpha particles on the CR-39 and other types of nuclear track detectors by using UV-Vis and FTIR spectroscopy.
3. The effect of the UV and gamma irradiation on CR-39 using different technique.
4. Studying the electrical properties of CR-39 and other types of nuclear track detectors.
5. The effect of (He-Ne) laser and alpha particles for nuclear track detectors with existence of heat treatment and determine the activation energy of the heating treatment (E_a) and track etchant energies (E_B and E_T).



References

References

- [1] Ford, J. International Atomic Energy Agency, IAEA, "Radiation, People and the Environment", Austria, (2004).
- [2] Ng, Kwan-Hoong. "Non-ionizing radiations—sources, biological effects, emissions and exposures." Proceedings of the international conference on non-ionizing radiation at UNITEN. (2003).
- [3] ATSDR. Toxicological Profile for Ionizing Radiation. Agency for Toxic Substances and Disease Registry, (1999).
- [4] Canada's Nuclear Regulator, "Introduction to Radiation" December, (2012).
- [5] Barish, Robert J. "Radiation Oncology Physics: A Handbook for Teachers and Students." 501, (2006).
- [6] Waseda, Yoshio, Eiichiro Matsubara, and Kozo Shinoda. "Fundamental Properties of X-rays." X-Ray Diffraction Crystallography. Springer Berlin Heidelberg, 1-20, (2011).
- [7] Siegman, A. E. "Lasers (University Science, Mill Valley, Calif.)." Chap 13: 663, (1986).
- [8] Wilson, John, and J. F. B. Hawkes. "Lasers, Principles and applications". Prentice Hall, (1987).
- [9] Chang, William SC. Principles of lasers and optics. Cambridge University Press, (2005).
- [10] Sinha, D., Ghosh, S., Srivastava, A., Dedgaonkar, V. G., & Dwivedi, K. K. . "Effect of gamma rays on PADC detectors." Radiation Measurements 28.1: 145-148, (1997).
- [11] Sinha, D., Mishra, R., Tripathy, S. P., & Dwivedi, K. K. "Effect of high gamma doses on the etching behaviour of different types of PADC detectors." Radiation Measurements 33.1: 139-143, (2001).

References

- [12] Abdullah, Ahmed K. "The effect of high irradiation energy (Gamma, UV–light) radiation on the energy gap of polymers doped with anthracene." *Iraqi Journal of Science* 47.1: 99-103, (2006).
- [13] Zaki, M. F. "Gamma-induced modification on optical band gap of CR-39 SSNTD." *Brazilian Journal of Physics* 38.4: 558-562, (2008).
- [14] Kalsi, P. C., V. S. Nadkarni, and V. K. Manchanda. "Effect of gamma irradiation on the etching and optical properties of a newly developed nuclear track detector called (PNADAC) homopolymer." *Radiation Physics and Chemistry* 77.9: 1002-1004, (2008).
- [15] Sapkal, Jyotsna A., Kalsi, P. C., Agarwal, C., Thanamani, M., & Murali, S. "The etching and optical response of Tuffak polycarbonate nuclear track detector to gamma irradiation." *Radiation Physics and Chemistry* PP: 81-84, (2009).
- [16] Amer H. Ali," Effect of Laser Radiation on the Nuclear Track Detector LR-115", Tikrit University, Tikrit Journal of Pure Science, Volume: 15, PP. 302-305, (2009).
- [17] Eissa, Mostafa Fawzy. "Optical Properties of CR-39 Track Etch Detectors Irradiated by Alpha Particles with Different Energies." *Journal of Materials Science and Engineering* 5.1: 26, (2011).
- [18] Gupta, R., Kumara, V., Goyala, P. K., Kumara, S., Kalsib, P. C., & Goyal, S.L. "Effect of γ - irradiation on thermal stability of CR-39 polymer" *Pelagia Research Library Advances in Applied Science Research*, 2 (1): 248-254, (2011).
- [19] Zaki, M. F., Tarek M. Hegazy, and Doaa H. Taha. "Investigation of the Effect of a He-Ne Laser on the Optical Properties through Etched CN-85 and CR-39 Containing Alpha Tracks." *Arab Journal of Nuclear Science and Applications*, 46(3), (201-210), (2012).
- [20] Abdel Raouf, Kh M. "Study of CR-39 SSNTDs Irradiated with Different Types of Radiation by FTIR Spectroscopy and α -Range

References

- Determination." American Journal of Environmental Protection 2: 53-57, (2013).
- [21] Kumar, A., Jain, R. K., Chakraborty, R. N., Pandit, T., & Singh, B. K."FTIR Analysis of UV Irradiated CR-39 Solid State Nuclear Track Detector." Proceedings of the DAE Symp. on Nucl. Phys. Vol. 59. (2014).
- [22] Saad, Emad N., M. F. Eissa, Emad A. Badawi, M. A. K. El-Fayoumi"Investigation of the physical properties of polymeric materials induced by alpha radiation." International Journal 2.12: 694-702, (2014).
- [23] Meenakshi Choudhary, Sangeeta Prasher, Mukesh kumar," Structural Analysis of Gamma Induced Modification in Cr-39 Polymers", International Journal of Innovative Research in Science, Engineering and Technology, July (2014).
- [24] Abdul-Kader, A. M., M. F. Zaki, and Basma A. El-Badry. "Modified the optical and electrical properties of CR-39 by gamma ray irradiation." Journal of Radiation Research and Applied Sciences 7.3: 286-291, (2014).
- [25] Fala Hatem Taha, "Radiation Dose Assessment for Ionizing and Ultraviolet Radiations Using CR-39, Lexan and LR-115 Nuclear Track Detectors", (2014).
- [26] Ahmed A. Ibrahim Sozan Bhaa-al-deen "Laser Effect on the Activation Energies, Bulk Etch Rate and Track Etch Rate of CR-39 Polymeric Detector", International Journal of Physics, Science and Education Publishing, Vol. 4, No. 1, 1-4, (2016).
- [27] Young, D. A. "Etching of radiation damage in lithium fluoride." Nature 182, (1958).

References

- [28] Silk, E. C. H., and R. S. Barnes. "Examination of fission fragment tracks with an electron microscope." *Philosophical Magazine* 4.44: 970-972, (1959).
- [29] Fleischer, R.L., Price, P.B., "Tracks of charged particles in high polymers". *Science* 140, 1221-1222, (1963).
- [30] Fleischer, R.L., Price, P.B., "Charge particle tracks in glass. *J. Appl. Phys*". 34, 2903-2904, (1963).
- [31] R.L. Fleischer, P.B. Price and R.M. Walker, "Nuclear Tracks in Solids: 'Principles and Applications'" (Berkeley: Univ. of California Press), (1975).
- [32] D. Velickovic, I. Miric, P. Miric, P. Bojovic. Proc. of the 11th International Conference in SSNTD, Bristol, England, pp. 583–586, (1981).
- [33] Gohn C.E. & Golden R., " *Rev. Sci. Inst.* ", p 13-43, (1972).
- [34] Fleischer, R. L., Price, P. B., Walker, R. M., & Hubbard, E. L. "Track registration in various solid-state nuclear track detectors." *Physical Review* 133.5A: A1443, (1964).
- [35] Hepburn C. & Windle A.H., "*J. Material Science* ", p 15-24, (1980).
- [36] S. A. DURRANI, R. K. BULL, "Solid State Nuclear Track Detection Principles, Methods and Applications", (1983).
- [37] Tsuruta, T., Koguchi, Y., Yasuda, N., "Discrimination of heavy ions using copolymers of CR-39 and DAP". *Radiation Measurement* 43, S48-S51, (2008).
- [38] Durrani, S.A., Bull, R.K., "Solid State Nuclear Track Detection". Pergamon Press, Oxford, p. 1, (1987).
- [39] Michael F. L'Annunziata, "Handbook of Radioactivity Analysis", Academic Press.(2012)

References

- [40] Benton, E.V. "On latent track formation in organic nuclear charged particle track detectors, Radiation Effect." 2, 273, 1970.
- [41] Fleischer, R. L., P. B. Price, and R. M. Walker. "Solid-state track detectors: applications to nuclear science and geophysics." Annual Review of Nuclear Science 15.1: 1-28, (1965).
- [42] Fleischer, R. L., P. B. Price, and R. M. Walker. "Ion explosion spike mechanism for formation of charged-particle tracks in solids." Journal of Applied Physics 36.11:3645-3652, (1965).
- [43] Fleischer, R. L., and P. B. Price. "Charged particle tracks in glass." Journal of Applied Physics 34.9: 2903-2904, (1963).
- [44] Hashemi-Nezhad, S. R., and S. A. Durrani. "Registration of alpha-recoil tracks in mica: the prospects for alpha-recoil dating method." Nuclear Tracks 5.1-2: 189-205, (1981).
- [45] Fremlin, J. H., and C. R. Wilson. "Alpha-emitters in the environment II: Man-made activity." Nuclear Instruments and Methods 173.1: 201-204, (1980).
- [46] Hepburn, C., and A. H. Windle. "Solid state nuclear track detectors." Journal of Materials Science 15.2: 279-301, (1980).
- [47] Price, P. B., Lal, D., Tamhane, A. S., & Perelygin, V. P."Characteristics of tracks of ions of $14 \leq Z \leq 36$ in common rock silicates." Earth and Planetary Science Letters 19.3: 377-395, (1973).
- [48] Fleischer, R. L., P. B. Price, and R. T. Woods. "Nuclear-particle-track identification in inorganic solids." Physical Review 188.2: 563, (1969).
- [49] Yamamoto, M., Yasuda, N., Kaizuka, Y., Yamagishi, M., Kanai, T., Ishigure, N., & Doke, T. "CR-39 sensitivity analysis on heavy ion beam with atomic force microscope." Radiation Measurements 28.1: 227-230, (1997).

References

- [50] Blanford Jr, G. E., R. M. Walker, and J. P. Wefel. "Track etching parameters for plastics." *Radiation Effects* 3.2: 267-270, (1970).
- [51] Durrani, S.A. "Nuclear Track Detection", Pergammon Press, London (1976).
- [52] Durrani, Saeed A., and Richard K. Bull. *Solid state nuclear track detection: principles, methods and applications*. Vol. 111. Elsevier, (2013).
- [53] Phukan, T., Kanjilal, D., Goswami, T. D., & Das, H. L. "Study of optical properties of swift heavy ion irradiated PADC polymer." *Radiation Measurements* 36.1: 611-614, (2003).
- [54] Calcagno, L., G. Compagnini, and G. Foti. "Structural modification of polymer films by ion irradiation." *Nuclear Instruments and Methods in Physics Research Section B: Beam Interactions with Materials and Atoms* 65.1-4: 413-422, (1992).
- [55] Hazarika, Jayanta, Chandrani Nath, and A. Kumar. "Swift heavy ion irradiation-induced enhancement in structural, conformational and electrical properties of polyaniline nanofibers." *Radiation Effects and Defects in Solids* 169.1: 30-40, (2014).
- [56] Tauc J. In: Ables A, editor. "Optical properties of solids", Amsterdam: North-Holland; (1970).
- [57] Robertson J, O'Reilly EP. "Electronic and atomic structure of amorphous carbon", *Phys Rev B*; 35:2946–57, 1987.
- [58] Ramola, R. C., Chandra, S., Rana, J. M. S., Sonkawade, R. G., Kulriya, P. K., Singh, F., ... & Annapoorni, S. "A comparative study of the effect of O^+ ion beam on polypyrrole and CR-39 (DOP) polymers." *Journal of Physics D: Applied Physics* 41.11: 115411, (2008).

References

- [59] C. Darrand, B. Bennamane, C. Gagnadr, J. L. Decossas, J .C. Vareille,"Optical modification of polymers by ion beam irradiation ".Polymer, 35,2447-2451(1994).
- [60] C. Gagndre, J. L. Decossas, J. C. Varcille," IR Spectroscopy Studies of Polycarbonate irradiated by H⁺ and Li⁺ ions .Nucl. Inst. Meth. B73, 48-52 (1993).
- [61] M. A. Malek, C. S. Chong, "FTIR study of H₂O in polyallyldiglycol carbonate". Vibration Spectroscopy, 24,181-184 (2000).
- [62] Tse Chun Chun," Investigations of The Effects of UV Irradiation on The Etching Behavior of CR-39 Solid State Nuclear Track", Master of Phiolosophy City University of Hong Kong march (2007).



جمهورية العراق
وزارة التعليم العالي والبحث العلمي
جامعة النهرين
كلية العلوم
قسم الفيزياء

دراسة تأثيرات حزمة ليزر (هيليوم-نيون) و أشعة كاما على كاشف CR-39 المشع بجسيمات ألفا بأستعمال بعض التقنيات المطيافية

رسالة

مقدمه إلى كلية العلوم / جامعة النهرين
كجزء من متطلبات نيل درجة الماجستير في علوم الفيزياء

من قبل

محمد محسن نعمة

بكالوريوس 2014

إشراف

الاستاذ الدكتور

ندى فاضل توفيق

المستخلص:

تهدف الدراسة الحالية الى دراسة تأثير كل من دقائق الفا, أشعة كاما و حزمة ليزر هيليوم- نيون (He-Ne) على خصائص القشط و الخصائص البصرية لكاشف CR-39. اربعة و عشرون كاشف تم تصنيفها الى خمسة مجموعات للعمل. المجموعة الاولى: تضم تسع كواشف من كاشف CR-39 تم تعريضها لقدرات مختلفة (1, 5 & 10 mW) من ليزر (هيليوم-نيون) و عند أزمان تعريض مختلفة (5, 10 & 15 min) ثم بعد ذلك تم تشيعها بدقائق ألفا من مصدر الراديوم (^{226}Ra) بفعالية (10 μCi). وتم قياس قطر الأثر-D, كثافة الأثر- ρ , و حساب معدل قشط الأثر- V_B , معدل القشط على طول الأثر- V_T , الزاوية الحرجة- Θ_C , كفاءة الأثر- η , حساسيته-S و نسبة معدل القشط-V. النتائج أوضحت بأن هناك زيادة في قيم كل من ($\Theta_C, V_T, V_B, \rho, D$) عند زيادة زمن التعرض لحزمة الليزر عند القدرات (1, 5 & 10 mW), و انخفاض في قيم (η, S, V) بزيادة زمن التعرض لحزمة الليزر عند قدرة - 1 mW بينما تزداد مع ازدياد زمن التعرض لحزمة الليزر عند (5 & 10 mW). و تم أيجاد زمن القشط الملائم للكاشف عند زمن القشط (4 hr) و معيارية (6.25 N) مع محلول القشط NaOH و عند (60 °C). المجموعة الثانية: تضم كاشف CR-39 غير مشع (control). المجموعة الثالثة: تضم خمسة كواشف تم تشيعها بأشعة كاما من مصدر كوبلت (^{60}Co) (300, 500, 800, 1200 & 1600 kGy). المجموعة الرابعة: تشيع المجموعة الثالثة لحزمة الليزر هيليوم نيون و بقدرة (10 mW) لزمن تعرض (15 min). المجموعة الخامسة: تضم تسعة كواشف تم تعريضها لقدرات مختلفة (1, 5 & 10 mW) من حزمة الليزر هيليوم-نيون و عند لفترات زمنية مختلفة (5, 10 & 15 min).

تم دراسة الخصائص البصرية لكاشف الأثر CR-39 باستخدام مطيافية الأشعة فوق البنفسجية و مطيافية تحويل فورير للأشعة تحت الحمراء, حيث تم حساب فجوة الطاقة البصرية و عدد ذرات الكربون للمجاميع (الثانية, الثالثة, الرابعة و الخامسة), و أوضحت نتائج طيف الأشعة فوق البنفسجية زيادة بالامتصاصية لكاشف مع زيادة كل من زمن التعرض لحزم الليزر هيليوم نيون عند قدر مختلفة و جرعة أشعة كاما, و أيضا انخفاض في قيم فجوة الطاقة البصرية و زيادة بعدد ذرات الكربون لكاشف بزيادة في كل من زمن التعرض لليزر هيليوم-نيون عند قدر مختلفة و جرعة أشعة كاما. أما بالنسبة لطيف تحويلات فورير للأشعة تحت الحمراء أوضحت النتائج تغير بمواقع الاواصر لكاشف للمجاميع (الثانية, الثالثة و الرابعة).